AD-A122 960 CRACK TIP PLASTICITY ASSOCIATED WITH CORROSION ASSISTED 1/2
FATIGUE(U) SOUTHWEST RESEARCH INST SAN ANTONIO TX
D L DAVIDSON ET AL. 15 NOV 82 N00014-75-C-1038

UNCLASSIFIED F/G 11/6 NL

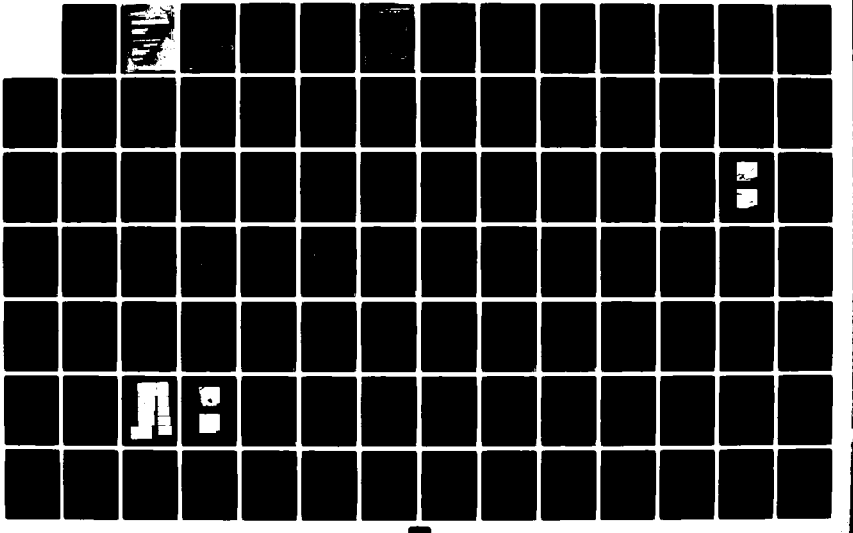

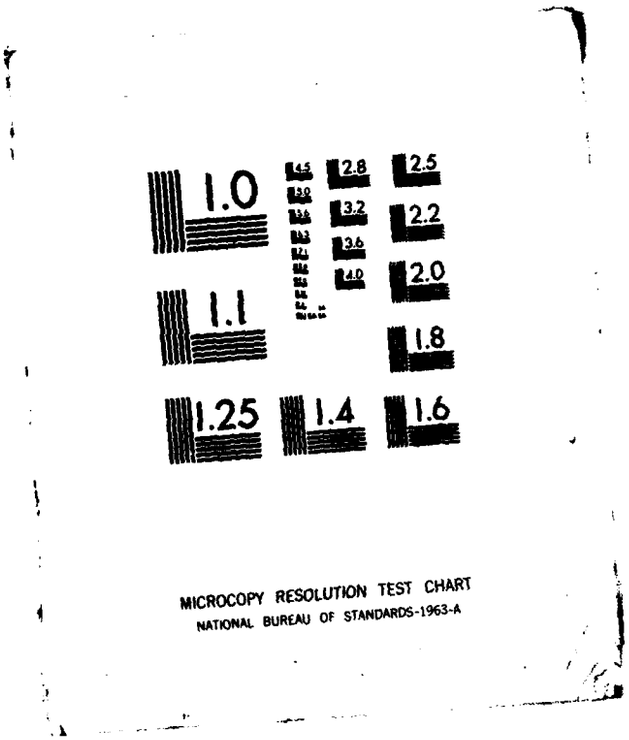

SOUTHWEST RESEARCH INSTITUTE

POST OFFICE DRAWER 28510 · 6220 CULEBRA ROAD · SAN ANTONIO, TEXAS 78284 · (512) 684-5111

(9)

CRACK TIP PLASTICITY ASSOCIATED WITH CORROSION ASSISTED FATIGUE

INTERIM REPORT FOR PERIOD JUNE 1981 - SEPTEMBER 1982

by

D. L. Davidson
J. Lankford

Prepared for

Office of Naval Research
800 North Quincy Street
Arlington, Virginia 22217

November 15, 1982

SUMMARY

This is the seventh and final Annual Report on this research project entitled, "Crack Tip Plasticity Associated with Corrosion Assisted Fatigue." The objective of this program has been to examine the effect of environment on the deformation response of the material near the crack tip—the plastic zone—and from that response, determine the effect of environment on fatigue crack growth.

The results described in this report were obtained using essentially two techniques: the relatively new technique stereoimaging, coupled with the use of a cyclic loading stage for the scanning electron microscope, and the now standard technique of electron fractography, using the SEM. The effect of environment on aluminum and titanium alloys was determined by analyzing cracks grown in both moist and very dry environments.

The principal focus of this year's experiments has been on the aluminum alloy MA-87, which has about the same chemical composition as the ingot alloy 7075-T651, but is manufactured by powder metallurgical techniques.

The focus of the analytical effort this year has been on completing the analysis of the 7075-T651 data, begun last year, analyzing recent MA-87 data, and comparing the results for these two microstructurally different materials. Considerable emphasis has been placed on utilizing these analytical results in models for crack growth. While the modeling efforts were limited, some progress has been made. The analysis of the titanium alloy data is not yet complete; thus, it will be presented in the final summary report.

This report is a compilation of 4 manuscripts which are in review at various Journals, together with Appendices of some of the data from which the analyses were derived. Together they form a complete record of the work done on this project in the past year, and provide readers with both our interpretation of results and data from which other interpretations may be made.

TABLE OF CONTENTS

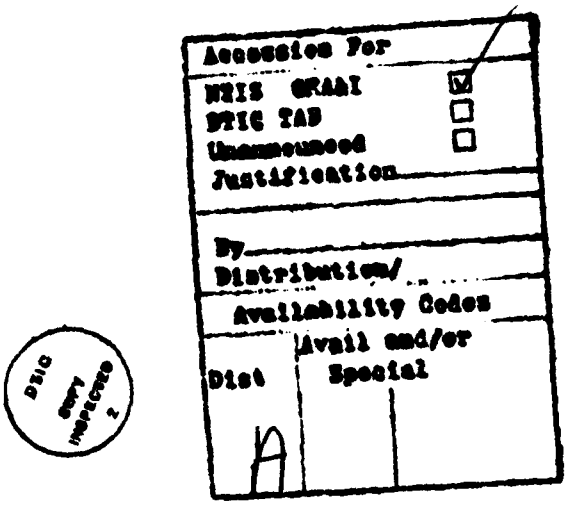

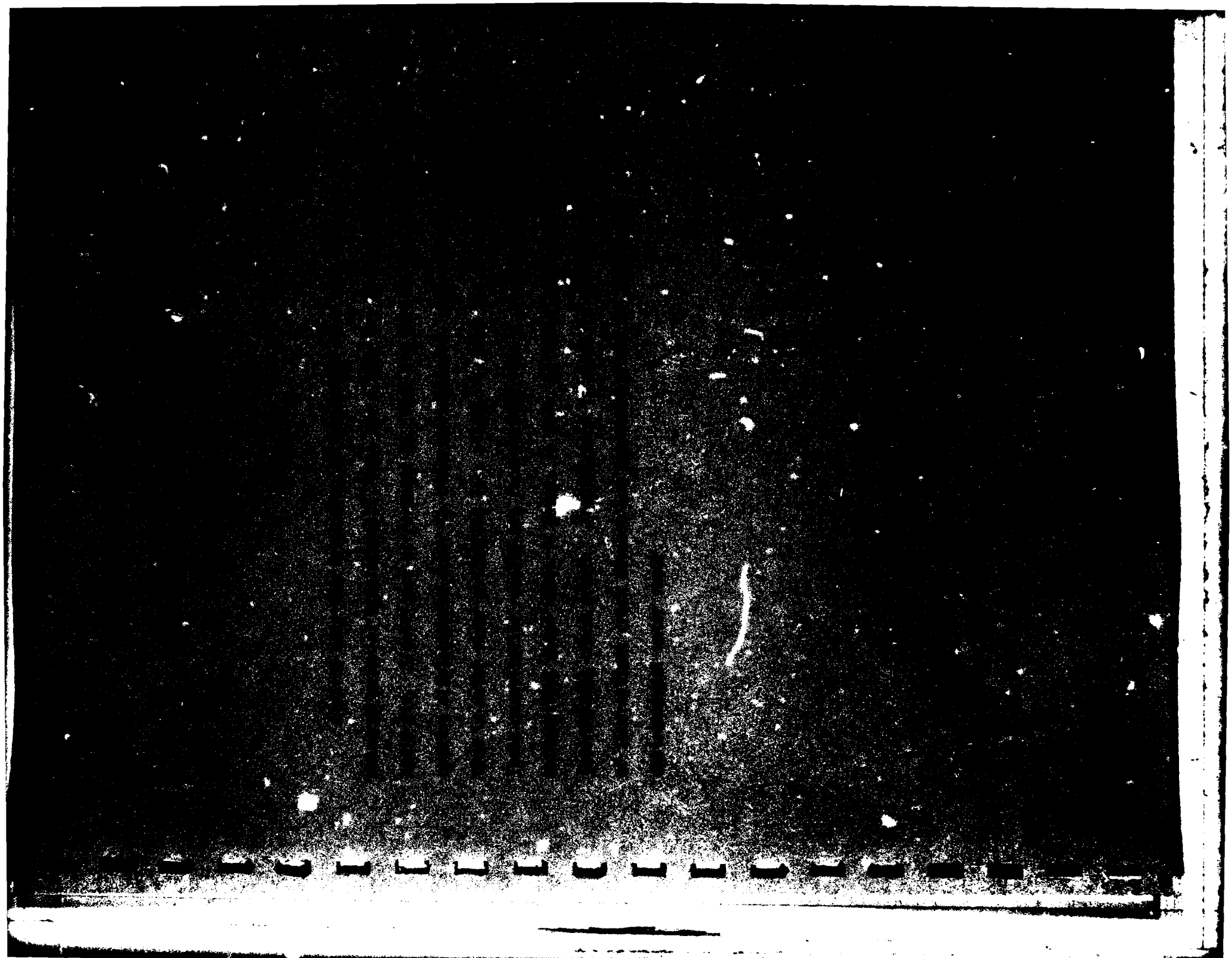

I. INTRODUCTION

Models for describing the rate of growth of fatigue cracks have been developed through either of two fundamental approaches. The first is empirical, and consists of modifying the correlation between crack growth rate and cyclic stress intensity factor to include factors such as the threshold stress intensity, mean stress, crack closure, and net section plastic strain.

The second, more basic, approach is the formulation of a cycle-dependent criterion for crack advance based on either hypothetical, or experimentally determined, crack tip micromechanics. Most current micromechanical models are theoretical, since it has been a difficult experimental task to measure the strains and crack opening displacements right at the crack tip. Measurement methods, typified by the Moire fringe[1] and strain gage[2] techniques, have been capable of measuring strains to within only about 100 μm of the crack tip. To make measurements at higher resolution, we have developed a technique which, for the first time, permits the assessment of local crack tip in-plane displacements,[3] as well as direct, high magnification observation of fatigue crack growth under dynamic cycling conditions.[4] This paper reports on observations and measurements made using these techniques, and then utilizes this information in a model for crack growth which excludes any environmental effect.

Although fatigue crack growth is known to be altered by environment, it has been impossible to include this factor in theoretical models because of a lack of information on how the parameters needed to describe

crack growth are changed. This paper examines how water vapor alters the micromechanics of fatigue cracks and incorporates this information into an analytical model. The more fundamental questions of how and why this environment affects these alterations remain unanswered.

Results from experiments with the ingot aluminum alloy 7075-T651 are presented here. Similar work was also carried out on a chemically similar, but microstructurally different, powder metallurgy alloy, and those results are presented in a companion paper.

II. APPROACH

A. Material

Commercially produced 7075-T6 aluminum alloy of thickness 6 mm was used as-received for this study. Grain shape in this material was very anisotropic, typical of wrought sheet aluminum products. Grains were approximately 130 x 60 x 18 μm (length, width, thickness), with the largest dimension oriented in the rolling direction. The material contained numerous large intermetallic inclusions. Tensile yield strength was 508 MPa.

B. Experimental Technique

Specimens 54-mm long, 20-mm wide and 3-mm thick were machined from the sheet, with the long dimension in the rolling direction. To create a surface texture, and reveal grain boundaries, modified Keller's reagent was used as an etch. Fatigue cracks were nucleated from a starting saw slit and grown at 5 Hz perpendicular to the rolling direction with a stress ratio of approximately 0.2. Both moist and dry environments were used: laboratory air, of approximately 50% relative humidity at 20°C (~12,000 ppm water vapor) and either very dry nitrogen (<10 ppm water vapor at 20°C) or vacuum (1 MPa/10^{-5} torr). Cracked specimens were subsequently transferred to a special cyclic loading stage within the scanning electron microscope,[5] where they could be loaded in a manner identical to that used in the laboratory. For cracks previously grown in water vapor, photographs were made only on the first few loading cycles, during which the crack tip plasticity was the same as in laboratory air. Two observations lead to

this conclusion: (1) Wanhill[6] noticed that striations on the fracture surface continued to be formed in vacuum for 10 to 20 cycles after transfer from a water vapor environment; (2) we observe that cracks transferred into the vacuum of the SEM become increasingly blunt after 10 to 20 additional cycles which is indicative of increased strain at the crack tip.

Cracks previously grown in vacuum or dry nitrogen could be observed as desired after transfer of the specimen to the SEM, and were on occasion loaded for hundreds of cycles, during which both videotapes of dynamic behavior and still photographs of the crack tip region were periodically obtained. Finally, fractography of typical fracture surfaces was carried out in the scanning electron microscope. Surfaces were paladium coated to enhance resolution.

C. Analytical Techniques

Crack tip regions were photographed at 1000 or 2000 magnification at minimum and maximum load. The stereoimaging technique was used to both observe and quantify[3] the near crack tip displacements in the plane of the specimen surface caused by material response to the change in load. These displacements were then used to compute[7] three elements of the symmetric strain tensor: $\Delta\varepsilon_{xx}$, $\Delta\varepsilon_{yy}$ and $\Delta\gamma_{xy}$. These are the in-plane strain increments parallel and perpendicular to the loading axis and the shear strain, respectively.

D. Model

The parameters measured during this experimental program have been brought together in an analytical model of crack growth previously presented by the authors. The model was designed to describe the physical

sequence of events which occurred as the crack advanced, in terms of crack tip mechanics, although it is not yet possible to factor directly into the model the fundamental metallurgical parameters which describe the behavior of the material through which the crack is growing. The model presented is very similar to those previously developed by Antolovich, Saxena and Chanani[8] and by Lanteigne and Bailon,[9] but there are several important differences, which will be discussed.

As a fatigue crack grows, material just ahead of it undergoes cyclic deformation, during which numerous dislocations move through the material away from and towards the crack tip, on multiple slip planes. This dislocation activity causes microstructural damage, which is quantified in this paper as very locally measured strain. Thus, strain measured on the scale of 1-5 μm is considered to characterize the damage caused by the advancing crack, which accumulates with each cycle.

Dynamic observations of the crack tip region indicated that crack growth did not occur on each cycle, at least in vacuum. Crack tip blunting was observed to occur, and increase in magnitude on each successive cycle, followed finally by crack advance. This extension sequance was observed consistently in several powder metallurgy aluminum alloys, but was more difficult to see directly in ingot alloys. The events accompanying microstructural failure and the associated formation of new surface, i.e., crack extension, are not yet understood, and are the subject of ongoing investigation.

Previously, a number of models of crack tip strain accumulation were examined by the authors.[10] The analysis to be described here is a variation of one previously shown to explain experimental observations most satisfactorily. The principal reasons for choosing this model are: (1) it postulates a specific failure criterion which is loading parameter-independent; (2) it describes in mathematical terms the physical events which were observed to accompany crack growth. The model is derived as follows.

The macroscopically measured crack growth rate $^{da}/_{dN}$ is actually the summation of a number of microscopic events of crack extension Δa which occur after a number of cycles ΔN_c, so that

$$\frac{da}{dN} = \frac{\Delta a}{\Delta N_c} \tag{1}$$

Damage (strain) is presumed to accumulate on each cycle, so that

$$\Delta N_c^{\beta} \Delta \varepsilon_p = \varepsilon_c \tag{2}$$

where $\Delta \varepsilon_p$ = the plastic strain range experienced on each cycle by the element Δa, ΔN_c = the number of cycles to fail the element, and ε_c = a ΔK-independent constant. The physical meaning of these parameters is shown in Fig. 1. The factor β in Eq. (2) is used as a weighting factor; e.g., $\beta<1$ results in considerably more cycles at a given value of crack tip strain than if $\beta \geq 1$. This equation is of the same form as the low-cycle fatigue, or Coffin-Manson, equation.

Substituting Eq. (2) into Eq. (1) gives

$$\frac{da}{dN} = \Delta a \left(\frac{\Delta \varepsilon_p}{\varepsilon_c} \right)^{1/\beta} \tag{3}$$

It is known experimentally that $\frac{da}{dN}$ increases with increasing ΔK; therefore, the dependence of Eq. (3) on ΔK must be through Δa and $\Delta \varepsilon_p$. The following assumptions provide the necessary ΔK dependent factors. The increment of crack growth, Δa, has been assumed to be dependent on ΔK, either directly, as

$$\Delta a = A_o \Delta K_{eff}^n \tag{4}$$

or indirectly, through the crack tip opening displacement, by the following equations

$$\Delta a = \alpha C_o \tag{5}$$

and

$$C_o = C \Delta K_{eff}^q \tag{6}$$

where C_o = the crack tip opening displacement (to be defined), and $\Delta K_{eff} = \Delta K - \Delta K_{TH}$, with ΔK = the geometrically dependent cyclic stress intensity factor, and ΔK_{TH} = the threshold ΔK. A method for computing ΔK_{TH} has not been derived, so a value determined from the measured crack growth rate curve must be used. Which of these concepts of crack advance best describes the experimental results will be determined after the data has been presented.

One additional assumption is required:

$$\Delta \varepsilon_p = K_o \Delta K_{eff}^r \tag{7}$$

By assuming that crack advance is directly ΔK_{eff} dependent, Eqs. (3), (4) and (7) may be combined to give:

$$\frac{da}{dN} = A_o\left(\frac{K_o}{\varepsilon_c}\right)^{1/\beta} \Delta K_{eff}^{(n + r/\beta)} \tag{8}$$

Alternatively, if Δa is assumed to be indirectly dependent on ΔK_{eff} through C_o, then combining Eqs. (3), (5) and (6) gives

$$\frac{da}{dN} = \alpha C\left(\frac{K_o}{\varepsilon_c}\right)^{1/\beta} \Delta K_{eff}^{(q + r/\beta)} \tag{9}$$

For both formulations, Eqs. (8) or (9), the parameters K_o, A_o, C, q, and r represent the response of the material just ahead of the crack tip. These can be experimentally determined by the techniques presently used, so if the weighting factor β could be determined, from low-cycle fatigue tests, for example, then measurement of da/dN at one value of ΔK should allow da/dN to be determined at another ΔK. However, in this paper, Eqs. (8) and (9) will be used to test the validity of the concepts outlined above against the experimental data.

Experimentally, it is known that

$$da/dN = B\Delta K_{eff}^{s} \tag{10}$$

By replacing $\frac{da}{dN}$ in Eq. (8) and rearranging

$$\varepsilon_c = \left(\frac{A_o}{B}\right)^{\beta} K_o \Delta K_{eff}^{(n + r/\beta - s)\beta} \tag{11}$$

The weighting factor β may be derived by invoking one of the original assumptions: ε_c is independent of ΔK_{eff}. Therefore

$$n + r/\beta - s = 0 \tag{12}$$

or

$$\beta = \frac{r}{s-n} \tag{13}$$

and

$$\varepsilon_c = \left(\frac{A_o}{B} \right)^{\beta} K_o \tag{14}$$

Alternatively, replacing da/dN in Eq. (9) gives

$$\beta = \frac{r}{s-q} \tag{15}$$

and

$$\varepsilon_c = \left(\frac{\alpha C}{B} \right)^{\beta} K_o \tag{16}$$

Thus, it will be possible to compute β and ε_c from the experimentally determined parameters, Eqs. (4)-(7) and (10), and examine the validity of the concepts described above.

III. EXPERIMENTAL RESULTS

A. Crack Tip Measurements

With the stereoimaging technique, the strains $\Delta\varepsilon_{xx}$, $\Delta\varepsilon_{yy}$ and $\Delta\gamma_{xy}$ are measured at several hundred locations within 25 to 50 μm of the crack tip.[7] Interpretation of the distribution of individual strain components is difficult; therefore, much of the analytical effort has been concentrated on utilizing the principal strain increments $\Delta\varepsilon_1$ and $\Delta\varepsilon_2$, the maximum shear strain $\Delta\gamma_{max}$, and the total effective strain increment

$$\Delta\varepsilon_t^{eff} = \frac{2}{\sqrt{3}} \left(\Delta\varepsilon_1^2 + \Delta\varepsilon_1\Delta\varepsilon_2 + \Delta\varepsilon_2^2 \right)^{1/2} \tag{17}$$

Distributions of shear strains, and the functional forms of the distribution functions, have previously been published,[10,11] and therefore are not repeated here.

The stereoimaging technique also allowed accurate measurement of the crack opening displacement (COD) as a function of the distance behind the crack tip. Components in both the in-plane coordinates x and y have been measured. The resultant value

$$COD = \left(COD_x^2 + COD_y^2 \right)^{1/2} \tag{18}$$

is used here as the measure of crack opening. Typical results for both environments are shown in Fig. 2; a relation of the form

$$COD = C_o |y|^p \tag{19}$$

is implied by this correlation. Values of the crack opening parameters C_o and p in Eq. (19), and of the plastic strain increment at the crack tip, $\Delta\varepsilon_p(0)$, are reported in Table I. The value of $\Delta\varepsilon_p(0) = \Delta\varepsilon_t^{eff}(0) - .0065$, where .0065 is approximately twice the shear strain at yield.

The data listed in Table I are plotted in Figs. 3 through 5. The best correlation obtained between any of the parameters was that between crack tip opening and strain, Fig. 3:

$$\Delta\varepsilon_p(0) = AC_o^x \tag{20}$$

For the dry environment, this correlation was found to be best with crack tip opening displacement defined at 1 μm behind the crack tip; therefore CTOD is defined at this point. Values of CTOD are determined by extrapolating COD values from those measured 3 to 5 μm behind the tip to 1 μm using Eq. (19).

For the wet air environment, crack tip strain was correlated with crack opening displacement, defined at 1, 0.5, and 0.1 μm behind the tip. The best correlation was obtained for CTOD defined at 0.1 μm, Fig. 3b. This better correlation for CTOD defined nearer the crack tip occurs because the value of p has decreased to ≃ 0.5, the value expected for an elastic crack.

Values derived for the constants in Eqs. (4), (6), (7), (10) and (20) are listed in Table II. The data points for crack growth rate have been published elsewhere,[12] so only the analytical results are presented. All values of the constants given in the table were derived statistically, using a regression which minimized the sum of the squares of the deviations.

TABLE I

7075-T651
Crack Tip Opening and Strain Data

ΔK $MN/m^{3/2}$	Environment	C_o (μm)	p	$\Delta\epsilon_p(0)$	R	Data Set
6	Dry	.15	.67	.0335	.15	34
6	Dry	.18	.64	.0475	.15	35
6.2	Dry	.11	.60	.0415	.15	36
6	Wet	.24	.60	.0545	.15	37
6	Wet	.11	.45	.0151	.16	38
7	Dry	.155	.52	.0385	.19	52
7	Wet	.145	.59	.006	.20	53
8	Dry	.097	.72	.0335	.13	39
8	Dry	.064	.77	.0425	.13	40
8	Dry	.25	.81	.0875	.26	41
8	Wet	.20	.81	.0647	.23	42
10	Dry	1.59	.34	.2885	.30	43
10	Dry	.52	.60	.1565	.12	44
10	Wet	.44	.62	.1545	.23	45
11	Dry	.79	.41	.1335	.13	54
11	Wet	.28	.73	.1035	.13	55
12	Dry	1.66	.36	.334	.10	89B

TABLE II

7075-T651
Constants for Various Equations Derived by
Least-Squares-Fit Through the Data

$\Delta K = MN/m^{3/2}$ CTOD and Δa = m

Variable	Equation Number	Dry	Wet
ΔK_{TH}		0	0
B	10	1.6×10^{-14}	9.6×10^{-13}
s		6.4	5.6
A_o	4	2×10^{-7}	3×10^{-9}
n		0.27	2.15
K_o	7	1.3×10^{-4}	5.8×10^{-5}
r		3.0	3.2
C	6	1.4×10^{-10}	4×10^{-9}
q		3.6	1.4
A		2.2×10^{3}	2.6×10^{18}
x	20	0.68	2.7

Note: Dry: CTOD defined 1 μm behind the tip.
Wet: CTOD defined 0.1 μm behind the tip.

The best correlations were found for $\Delta K_{eff} = \Delta K$, meaning $\Delta K_{TH} = 0$ was used in this derivation.

It should be noted that Eq. (20) is redundant, and may be derived using Eqs. (4) and (6). When this is done, $A = K_o/C^x$ and $x = r/q$.

B. Fractography

Fractographic examination of specimens cracked in air and vacuum was performed. These results are reported in detail elsewhere,[12] but a few examples of relevant features are presented here as well.

Striations were found for both vacuum and wet air environments, and at almost all stress intensities. No shear lips were found at the specimen surfaces, and striations found in the interior of the specimen had the same appearance and average spacing as those found adjacent to the surface.

In wet air, striations were found to be sharp-edged and rather flat, Fig. 6; because of their flatness, they were difficult to see in the SEM. Their appearance was basically "brittle." At $\Delta K \leq 6.5$ MN/m$^{3/2}$, striations formed in wet air could not be resolved, although TEM replica work by Broek[13] indicates that they are present at stress intensities as low as 4 MN/m$^{3/2}$.

Striations generated in vacuum were much easier to see, since they were more rounded in profile. Their appearance is rougher than that of striations formed in wet air (Fig. 7), and suggests increased crack tip strain.

The relationships between striation spacing, crack growth rate, CTOD, and ΔK are shown for vacuum and wet air in Figs. 8 and 9, respectively. The CTOD shown is that defined 1 μm behind the crack tip for both environments, and is derived from the data in Table I.

The ΔK range over which striations in wet air were obtained was quite limited. Consequently, TEM replica data obtained by Broek,[13] for 7075-T6 tested in moist air, are included; it is evident that the present results are in good agreement. Striation spacing and CTOD nearly coincide over the entire range in ΔK, Fig. 8. Their dependence on stress intensity is less sensitive than is that of da/dN, which, for $\Delta K \tilde{<} 5$ MNm$^{-3/2}$ they exceed by more than an order of magnitude. This disagreement diminishes as ΔK increases, and the three curves basically coincide at $\Delta K \simeq 10$ MNm$^{-3/2}$.

The CTOD and striation spacing curves for vacuum are considerably different than for wet air, Fig. 9. Crack tip opening displacement is very sensitive to cyclic stress intensity magnitude, while over the same range, the average striation spacing is almost constant.

The relation between measured striation spacing and ΔK is given by

$$ss = A_o \Delta K^n \tag{21}$$

Values of the constants A_o and n for both environments were derived using a regression which minimized the sum of the squares of the deviations, and are listed in Table II. The striation spacing is thus assumed to be equal to the crack growth increment Δa, so that Eqs. (4) and (21) are identical.

IV. DISCUSSION

A. Interpretation of Crack Tip Measurements

Crack tip plastic strain correlates very well with crack tip opening displacement for both environments, Fig. 3. The scatter associated with this correlation is small, even though the range of CTOD is nearly two orders of magnitude, for the dry data. Therefore, this relationship appears to be fundamentally correct.

It is not surprising that CTOD for wet air when defined at 0.1 μm correlates better with $\Delta\varepsilon_p(0)$ than when it is defined at 1 μm, Fig. 3b, because the effect of water vapor is to decrease the plastic strain at the crack tip. This finding is of fundamental importance in the understanding of the effect of environment.

Although $\Delta\varepsilon_p(0)$ clearly increases with ΔK, there is considerable variation about the mean, Fig. 4. These variations arise because of the nature of the fatigue process, and not from errors in measurement of crack tip strains; if such errors were present, then less correlation between $\Delta\varepsilon_p(0)$ and CTOD would be expected than was found, Fig. 3. Variation in $\Delta\varepsilon_p(0)$ occurs because of the periodically varying nature of the change in deformation experienced by material just ahead of the crack tip, as was observed dynamically and shown schematically in Fig. 1. It must be assumed, for further analysis, that the regression lines on Fig. 4 represent average behavior. The variation of CTOD data with ΔK, Fig. 5, has the same origin as the variations in $\Delta\varepsilon_p(0)$. As Table II indicates, neither CTOD nor crack tip strain increases as rapidly with ΔK as does crack growth rate; therefore, neither of these factors relates directly to average $^{da}/_{dN}$.

B. Interpretation of Fractography

All of the correlations needed for examining the models have been developed and are quantified in Table II, with exception of deciding whether the increment of crack advance is directly dependent on ΔK, or indirectly dependent through the CTOD dependence on ΔK. The existence and spacing of striations on the fracture surface is considered to be evidence for, and measurement of, the increment of crack advance. The results shown in Figs. 8 and 9 will be considered together with the work of other investigators. Most of the relevant supplemental information pertains to crack growth in air, which will be examined first. For both environments, the range of investigation is $5 < \Delta K < 15$ MN/m$^{3/2}$.

1. Crack Growth in Air

Bowles and Broek[14] analyzed transmission electron diffraction patterns obtained from thin foils which included the striated fracture surface of 7075-T6 fatigued in air. Their results showed conclusively that the planes were {110}. Nix and Flowers[15] also examined the fracture surfaces of a 7010-T76 alloy using TEM techniques and likewise concluded that the fracture plane was {110}. In addition, for the same specimen, they were able to image the dislocation substructures underlying the striations and determined that they coincided with the leading edges of the striations, which were imaged in the SEM mode. The region of the striation near the trailing edge of the striations was found to contain a much lower dislocation density. They concluded that striations formed in two steps, the first involving plastic flow, and the second resulting from "brittle" microfracture on {110}.

Wanhill[6] examined thin foils of 7075-T6 made adjacent to the fracture surface by TEM, and showed an exact correspondence between striation spacing and periodic subsurface dislocation structure, in general agreement with the work of Nix and Flowers.[15] Since the present fractographic observations, Fig. 6, generally agree with those other investigators, it is concluded that their findings are applicable to the 7075-T651 used in the present work.

From Fig. 8, it is clear that striation spacing exceeds the rate of crack growth at low ΔK. But from the foregoing discussion, it is inferred that this means that the increment of crack advance is larger than the average rate of crack growth. This observation is consistent with the measurements of CTOD and crack tip strain, as well as the findings of Wanhill, and Nix and Flowers, through the following description of crack advance. Starting with a sharp crack, each succeeding cycle results in an increasingly blunt crack tip, with the associated increase in strain. This results in a region of high dislocation density, corresponding to the first step in striation formation, and is followed by an increment of crack advance requiring at most a few cycles, which is the "brittle" second step of striation formation. There is a very close coincidence between striation spacing and CTOD (defined at 1 μm from the crack tip), and we conclude that the crack growth increment is directly related to CTOD, as expressed by Eqs. (5) and (6).

2. Crack Growth in Vacuum

Striations have been observed for fatigue crack growth in vacuum in both 7075-T6[6] and 7075-T651,[16] in addition to those seen here, Fig. 7. The TEM work of Wanhill showed that the dislocation substructure just below the fracture surface was arranged into bands whose

periodic structure equaled the corresponding average striation spacing. This suggests that striations in both environments are the result of the same two-step process of formation. However, the non-crystallographic, rounded profile of the striations formed in vacuum implies that more plasticity accompanied their creation than did so in wet air. This inference agrees with the crack tip strain measurements, Fig. 4.

Recalling Fig. 9, striation spacing is unrelated to the magnitude of the CTOD, and is only slightly dependent on ΔK. We thus conclude that incremental crack advance is related directly to ΔK, rather than to CTOD, as expressed by Eq. (4).

C. Examination of the Models

By considering the ΔK dependence of CTOD and striation spacing, we conclude that the effect of the wet air environment is to fundamentally alter the relationship between Δa, the increment of crack advance, and ΔK. For the wet air environment, Eqs. (5) and (6) describe the dependence of Δa on ΔK, with $\alpha=1$, and Eqs. (15) and (16) are used to compute the parameters β and ε_c. Conversely, for the dry environment, Eq. (4) describes Δa, and Eqs. (13) and (14) are used to compute β and ε_c. Table III lists the values of β and ε_c as computed by the appropriate equations and using the constants given in Table II.

TABLE III

7075-T651

Derived Values of β and ε_c Using the Constants in Table II

Environment	β	ε_c
Dry	.49	.43
Wet	.74	.28

The derived values of β and ε_c are rather sensitive to the crack growth rate constants B and s; just how sensitive is shown by the analysis in Appendix A. Using the vacuum crack growth rates of other investigators gives, on average, $\beta \simeq 0.73$ and $\varepsilon_c \simeq 0.4$. Using the air data of other investigators results in a broad range of estimates for β and ε_c. The general trend of this data indicates that

1) $\beta < 1$ for both environments, probably between 0.4 and 0.7.

2) ε_c for wet air is less than or equal to that for the dry environments.

The latter finding supports the other evidence, already presented, which indicates that the effect of water vapor is to decrease the plasticity associated with fatigue crack growth. *The environmental specie thought to* be responsible for this alteration in material property is hydrogen. Water is catalytically separated into H^+ and OH^- at the newly created (and unoxidized) surface at the crack tip.[17] The free hydrogen atom then enters the metal and is moved into the region ahead of the crack tip by dislocation transport or by diffusion. In either case, this penetration need not be over a distance greater than Δa (0.1 to 0.5 μm), or at least it need only exceed some minimum concentration level over that distance.

Having computed β and ε_c, it is possible to calculate ΔN_c, the number of cycles required for an increment of crack growth, using Eq. (2) and the plastic strains listed in Table I; these values are given in Table IV.

TABLE IV

7075-T651
Calculated Number of Cycles Required for Crack Extension

Environment	ΔK	$\Delta\varepsilon_p$	ΔN_c	$\Delta a/(da/dN)$
Dry	6	.030	220	210
Dry	10	.14	10	9
Wet	6	.018	41	6
Wet	10	.092	5	1

Clearly, ΔN_c is large at low ΔK in vacuum, just as it was observed to be dynamically, but ΔN_c decreases rapidly as ΔK is increased. Wet air at low ΔK greatly diminishes the number of cycles required, as compared to that required in vacuum, which is another manifestation of the decrease in crack tip plasticity associated with environment.

The model used here is conceptually similar to those formulated by Antolovich, et al,[8] and by Lanteigne and Bailon,[9] in that the number of cycles required for an increment of crack advance is controlled by a low-cycle fatigue law. However, measured crack tip strain and crack growth increments have been found to be different from their theoretical assumptions, and it has been necessary to alter the models accordingly.

D. Relation of Results to Low-Cycle Fatigue Tests

The element Δa ahead of the crack tip is considered to be acting much the same as a low-cycle fatigue specimen, Eq. (2). As derived from the crack tip parameters, $.5 < \beta < .9$, which compares with $\beta = 0.56$ as given in Jablonski and Pelloux,[18] and $\beta = 0.83$ as given in Lanteigne

and Bailon[9] as derived from low-cycle fatigue tests. The parameter equivalent to ε_c cited by Jablonski and Pelloux is 0.3, which is between the values derived for the two environments. Thus, the results obtained here are compatible with low-cycle fatigue test data.

E. The Effect of Environment

The effects of a wet air environment on fatigue crack growth have been found to be as summarized below:

1) crack tip strains are decreased

2) the factor ε_c is reduced

3) the increment of crack growth Δa increases

The net results of all these changes is to decrease the number of cycles required to cause crack advance, and this, combined with the increase in increment of crack growth, causes the crack growth rate in water vapor to increase.

V. SUMMARY AND CONCLUSIONS

Crack tip strains and openings have been measured in both humid air and dry nitrogen or vacuum over the range $6 < \Delta K < 12$ MN/m$^{3/2}$. Dynamic observation of crack growth and fractographic examination have also been made. The results have been incorporated into a model, and are summarized below:

1. Both crack tip strain range and opening displacement are strong functions of ΔK, and dependent on environment.
2. Striation spacing in vacuum is almost ΔK independent, while in water vapor it is strongly ΔK dependent.
3. The correlation between crack tip strain range and crack tip opening displacement is dependent on environment.
4. Crack growth is noncontinuous, requiring hundreds of cycles between growth increments at low ΔK.
5. The effect of environment is to decrease the strain which the crack tip can support. Hydrogen is considered to act at the crack tip, causing this result.
6. The model used is based on considering an element ahead of the crack tip as a small, low-cycle fatigue specimen, and factors are derived which correlate well with the same parameters derived by low-cycle-fatigue experiments.

These results have been compared elsewhere[19] with similar work[20] in the compositionally similar powder metallurgy alloy MA-87.

APPENDIX A

Values of β and ε_c from Eq. (2) are computed using values of crack growth rate from other investigators, together with the crack tip parameters given in Table II.

TABLE A-1

Model Parameters Computed From the Growth Data of Other Investigators, 7075-T6 and -T651

Investigators	Environment	Crack Growth Parameters B	s	β	ε_c	Reference Number
Present	Dry	1.6×10^{-14}	6.4	.49	.43	-
Schijve and Vogelesang	Vac	2.6×10^{-11}	3.9	.83	.21	21
Kirby and Beevers	Vac	9.25×10^{-12}	3.84	.84	.56	16
Wanhill	Vac	1.5×10^{-11}	3.82	.84	.39	6
Present	Air	9.6×10^{-13}	5.6	.74	.28	-
Schijve and Vogelesang	Air	3.66×10^{-10}	2.88	2.1	.002	21
Kirby and Beevers	Air	2×10^{-12}	4.7	.96	.042	16

It should be noted that the material of the other investigators may be sufficiently different from that of the present study that the measured crack tip parameters are inapplicable. It is concluded from this comparison that for both environments $0.5 < \beta < 0.9$.

REFERENCES

1. Liu, H. W. and Ke, J. S. 'Moire Method' in "Experimental Techniques in Fracture Mechanics, V. 2," A. S. Kobayashi, ed., Iowa State Univ. Press, Ames, Iowa, 1975, pp. 111-165.
2. Ikeda, S., Izumi, Y., and Fine, M. E. 'Plastic Work During Fatigue Crack Propagation in a High Strength Low Alloy Steel and in 7050 Al-Alloy' Engng. Fract. Mech. 1977 9, 123-136.
3. Davidson, D. L. 'The Observation and Measurement of Displacements and Strain by Stereoimaging' Scanning Electron Microscopy/1979/II, 79-86.
4. Davidson, D. L. and Lankford, J. 'Dynamic, Real-Time Fatigue Crack Propagation at High Resolution as Observed in the Scanning Electron Microscope' in "Fatigue Mechanisms," J. Fong, ed. Am. Soc. Test. Mater. STP-675, 1979, pp. 277-284.
5. Davidson, D. L. and Nagy, A. 'A Low Frequency Cyclic Loading Stage for the SEM' Journ. of Physics E 1978 11, 207-210.
6. Wanhill, R. J. H. 'Fractography of Fatigue Crack Propagation in 2024-T3 and 7075-T6 Aluminum Alloys in Air and Vacuum' Met. Trans. A 1975 6A, 1587-1596.
7. Williams, D. R., Davidson, D. L., and Lankford, J. 'Fatigue-Crack-Tip Plastic Strains by the Stereoimaging Technique' Exp. Mech. 1980 20, 134-139.
8. Antolovich, S. D., Saxena, A., and Chanani, G. R. 'A Model for Fatigue Crack Propagation' Engng. Fract. Mech. 1975 7, 649-652.

9. Lanteigne, J. and Bailon, J-P. 'Theoretical Model for FCGR Near the Threshold' Met. Trans. A 1981 12A, 459-466.

10. Davidson, D. L. and Lankford, J. 'Fatigue Crack Tip Strains in 7075-T6 by Stereoimaging and Their Use in Crack Growth Models' ASTM, Dearborn 1982 (in press).

11. Davidson, D. L. and Lankford, J. 'Characterization of Crack Tip Plastic Zone Parameters and Their Interrelationship with NDE Techniques' in "Nondestructive Evaluation," O. Buck and S. M. Wolf eds., The Met. Soc. AIME, 1981, pp. 299-318.

12. Lankford, J. and Davidson D. L. 'Fatigue Crack Micromechanics in Ingot and Powder Metallurgy 7XXX Aluminum Alloys in Air and Vacuum' Acta Met. 1982 (submitted).

13. Broek, D. 'Some Contributions of Electron Fractography to the Theory of Fracture' Natl. Aerospace Lab. Report NLR TR 72029 U, The Netherlands, p. 47.

14. Bowles, C. Q. and Broek, D. 'On the Formation of Fatigue Striations' Inter. Journ. of Fracture Mech. 1972 8, 75-85.

15. Nix, K. J. and Flowers, H. M. 'The Micromechanisms of Fatigue Crack Growth in a Commercial Al-Zn-Mg-Cu Alloy' Acta Met. 1982 30, 1549-1559.

16. Kirby, B. R. and Beevers, C. J. 'Slow Fatigue Crack Growth and Threshold Behavior in Air and Vacuum of Commercial Aluminum Alloys' Fat. of Engng. Mater. and Struct. 1979 1, 203-215.

17. Wei, R. P., Pao, P. S., Hart, R. G., Weir, T. W. and Simmons, G. W. 'Fracture Mechanics and Surface Chemistry Studies of Fatigue Crack Growth in an Aluminum Alloy' Met. Trans. A 1980 11A, 151-158.

18. Jablonski, D. A. and Pelloux, R. M. 'An Evaluation of the Summation of Cyclic Plastic Strain Damage in Two High Strength Aluminum Alloys' Met. Trans. A 1979 10A, 63-66.

19. Davidson, D. L. and Lankford, J. 'The Effect of Metallurgical Structure, Environment, and Stress Intensity on Fatigue Crack Tip Plasticity in Al-Zn-Mg-Cu Alloys' Fat. of Engng. Mat. and Struct. (to appear).

20. Davidson, D. L. and Lankford, J. 'Fatigue Crack Tip Mechanics of a Powder Metallurgy Aluminum Alloy in Vacuum and Humid Air' Fat. of Engng. Mat. and Struct. (this volume).

21. Schijve, J. and Vogelesang, L. B. 'Environmental Effects on Fatigue Fracture Mode Transitions Observed in Aluminum Alloys' Delft University of Technology Report LR-289, The Netherlands, 1979, p. 17.

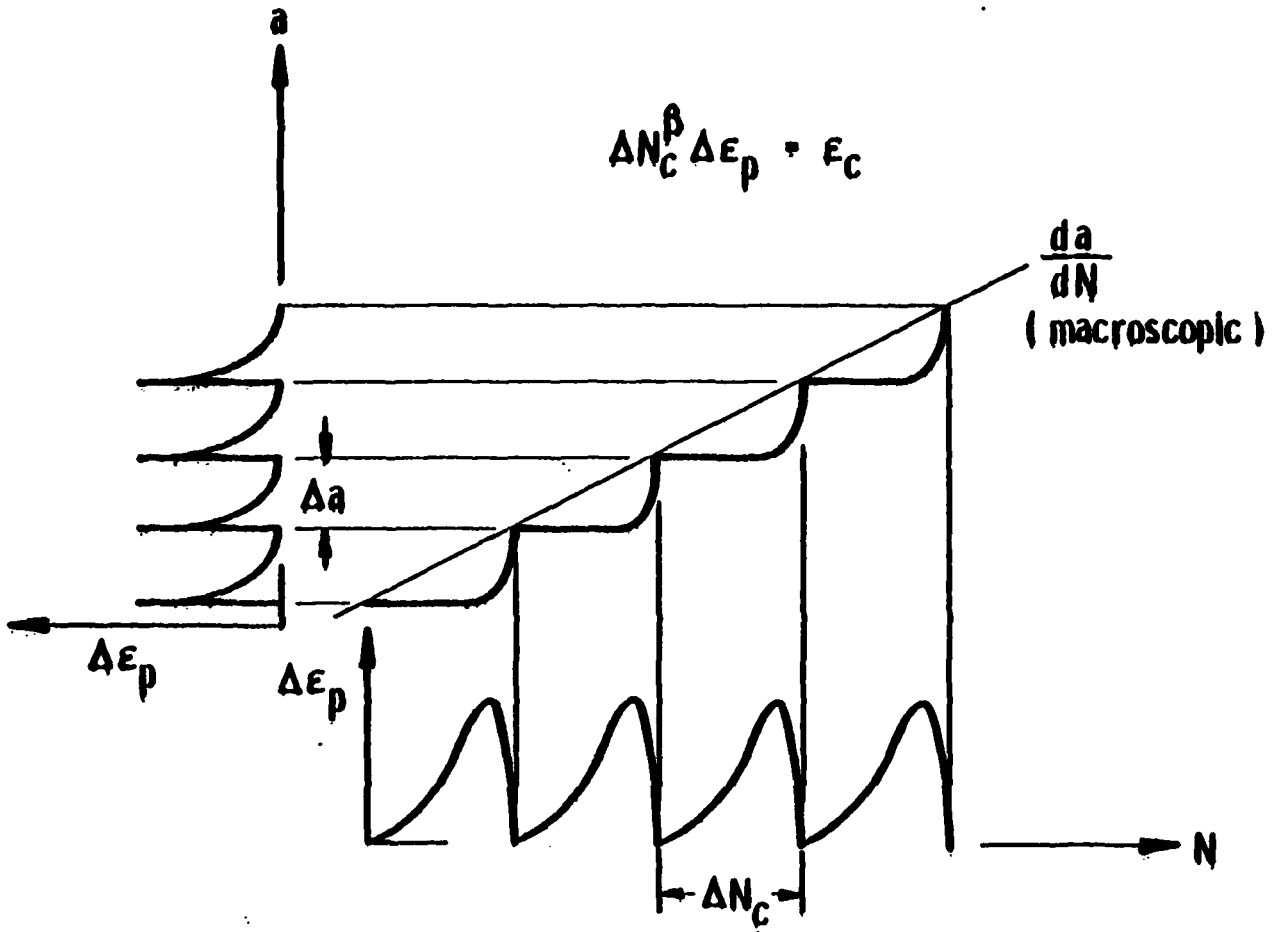

Figure 1. Diagram of the relationships embodied in Eq. (2), showing schematically how $\Delta\epsilon_p$ and Δa can change microscopically with N, leading to the macroscopic growth da/dN. Crack growth is microscopically intermittent: cycling increases $\Delta\epsilon_p$, while a remains constant. Upon reaching the critical condition given by the equation, the crack extends a distance Δa, which results in a decrease in the crack tip strain.

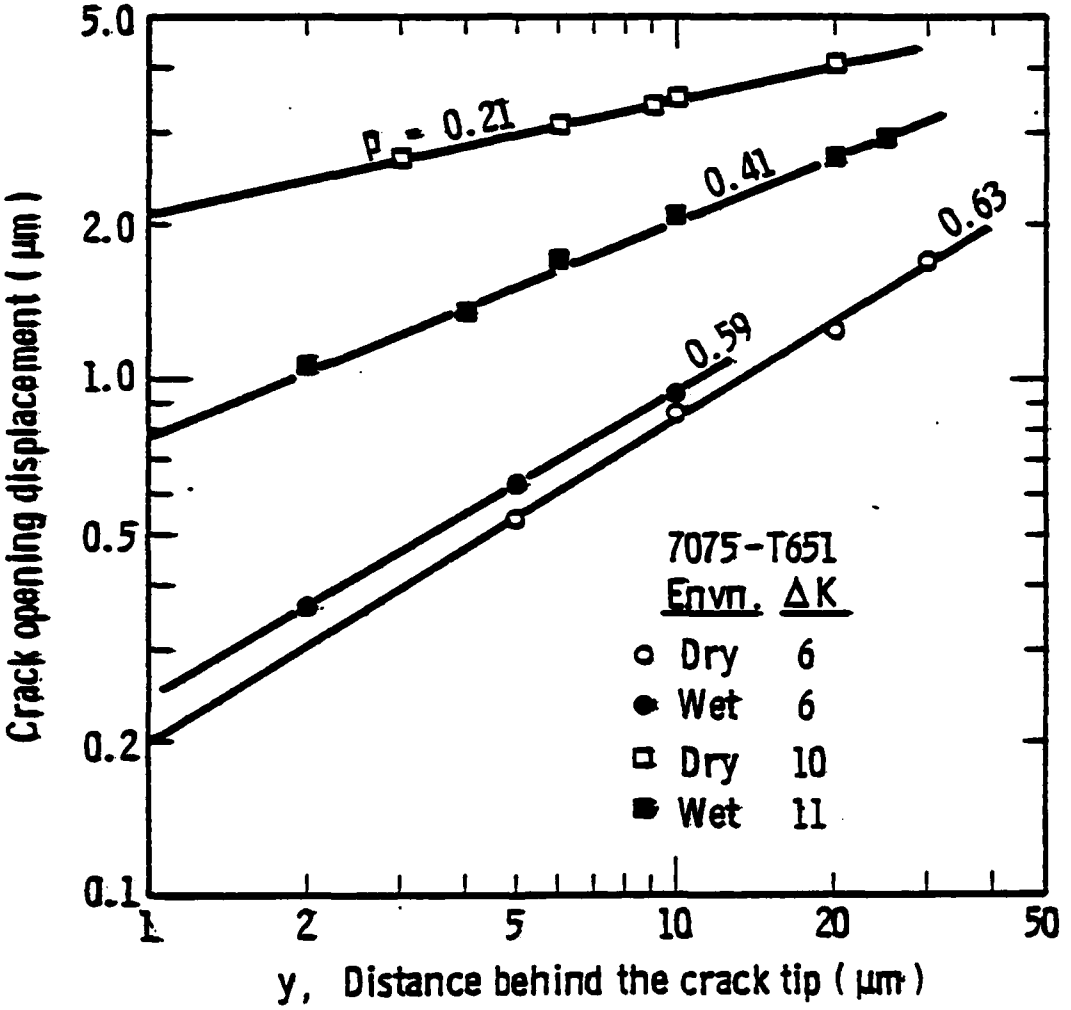

Figure 2. Total crack opening displacement vs distance behind the crack tip.

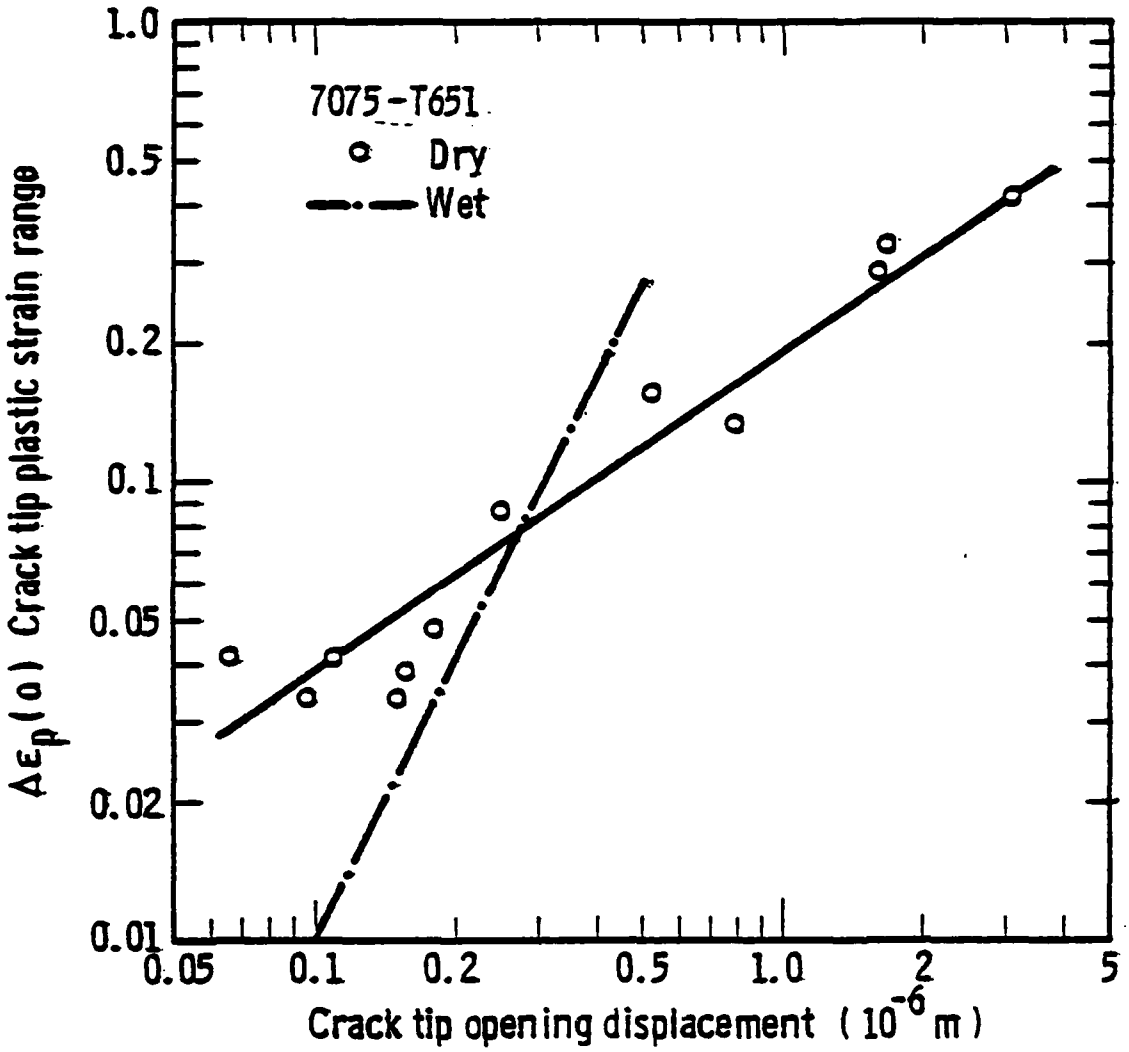

Figure 3a. Crack tip plastic strain increment vs crack opening displacement 1 μm behind the tip, dry environment. Also shown for comparison is the same line, by least-squares-fit, for the wet environment.

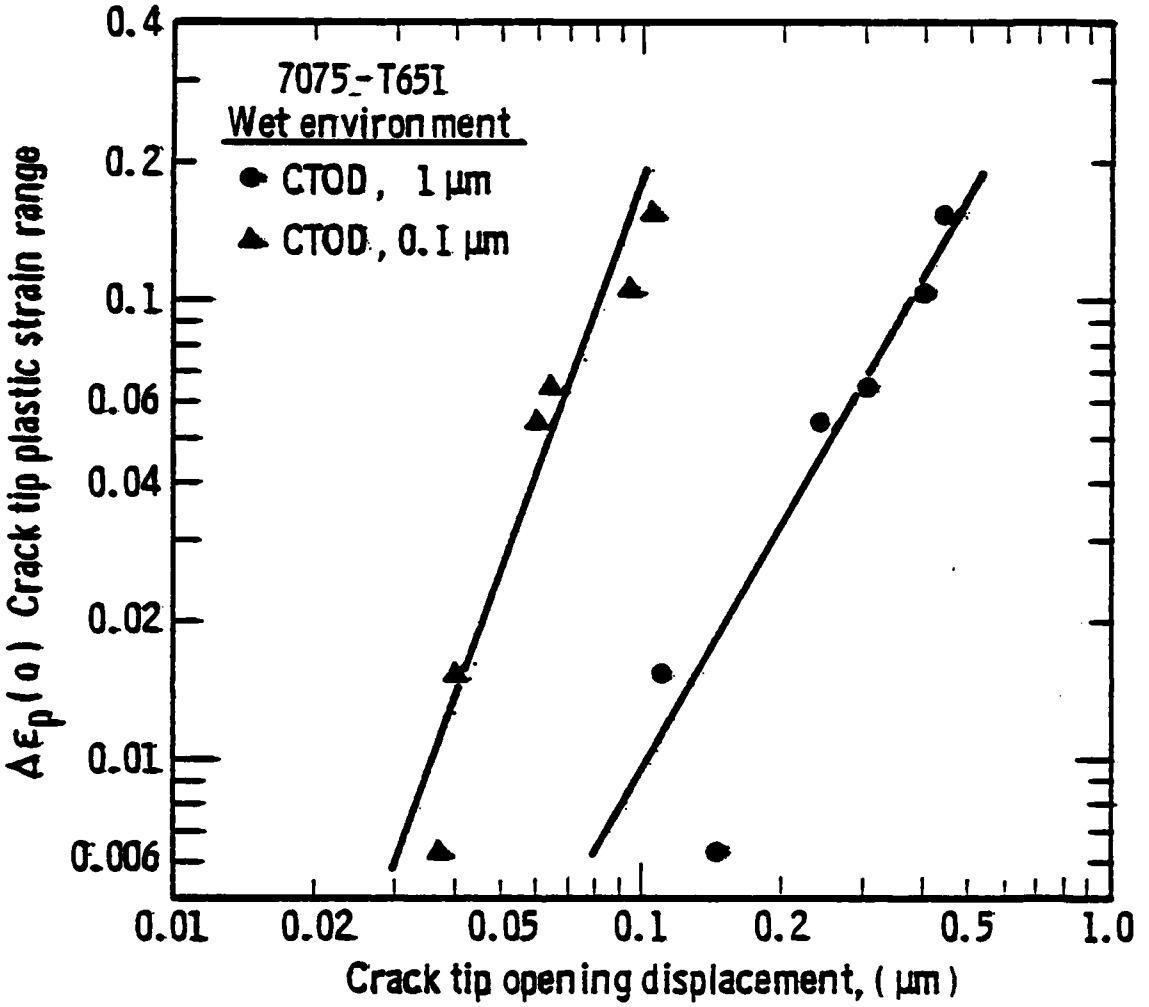

Figure 3b. Crack tip plastic strain increment vs crack opening displacement at 1 μm and at 0.1 μm behind the crack tip, wet air environment.

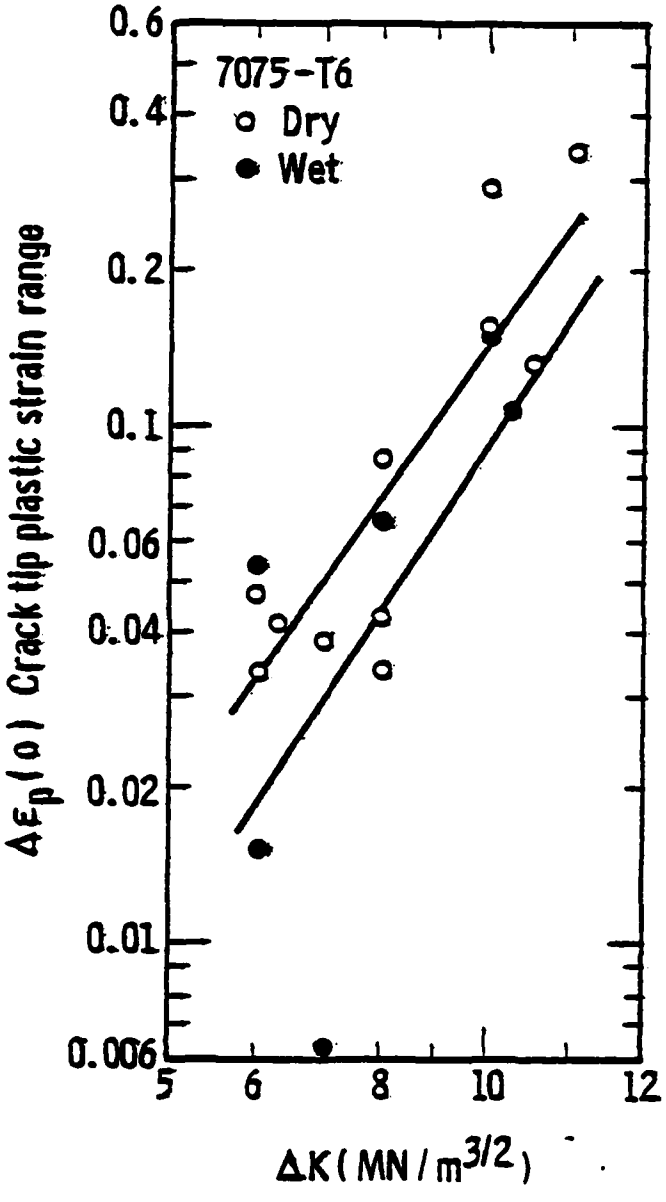

Figure 4. Crack tip plastic strain increment vs ΔK.

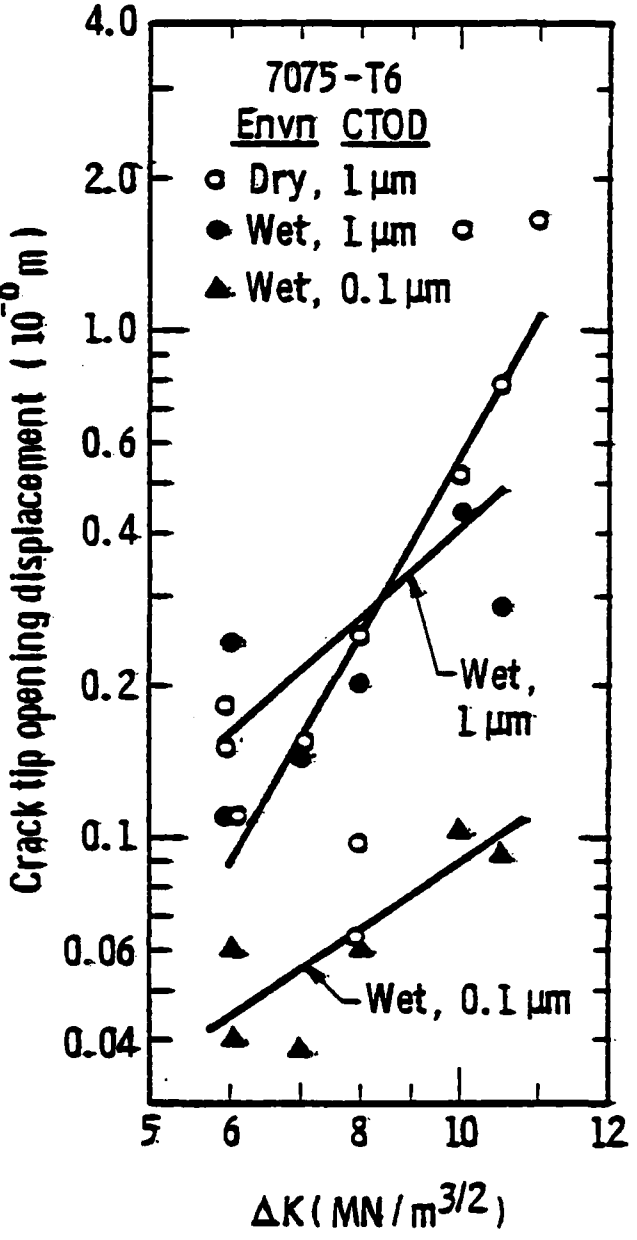

Figure 5. Crack tip opening displacement vs ΔK with CTOD defined 1 μm behind the tip for the dry environment and at both 1 μm and 0.1 μm for the wet environment.

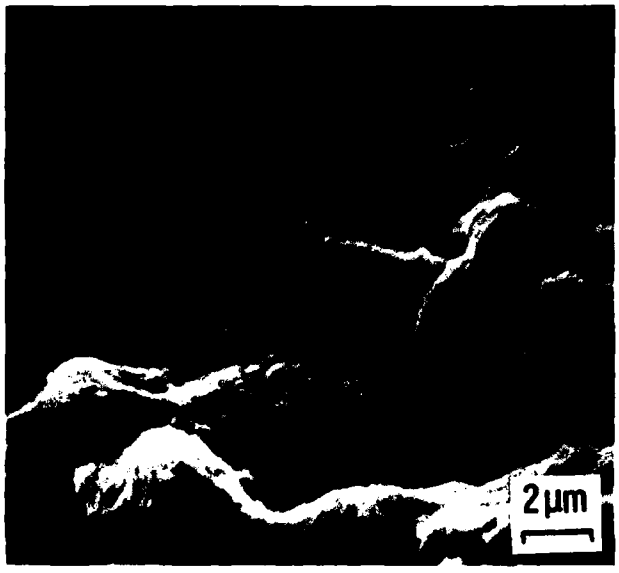

Figure 6. Fracture surface striations formed in moist air, ΔK = 10 $MN/m^{3/2}$.

Figure 7. Fracture surface striations formed in vacuum, ΔK = 6.5 $MN/m^{3/2}$.

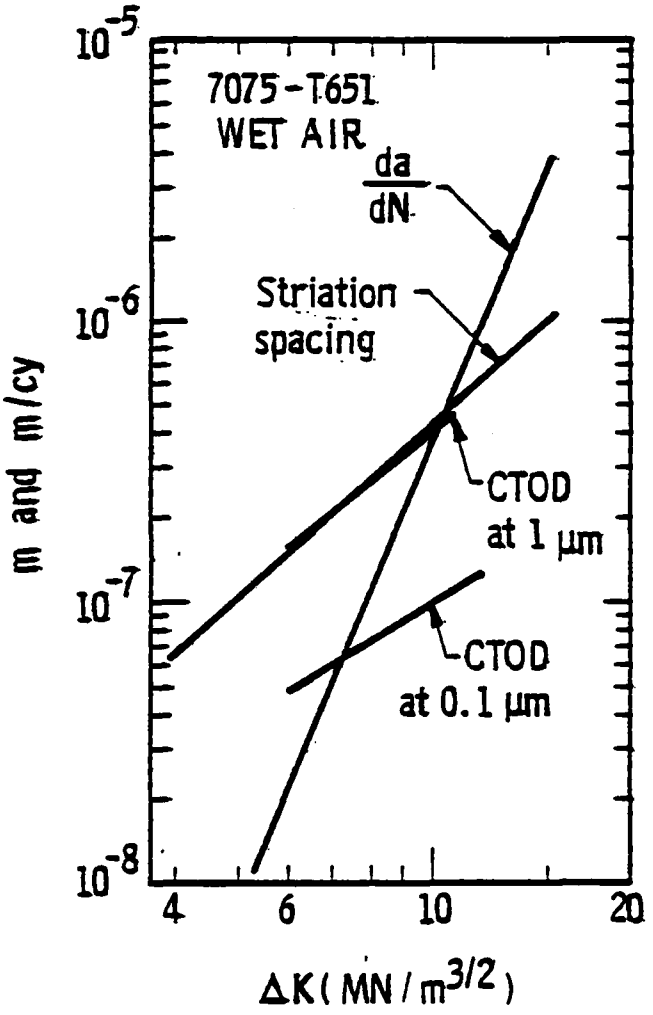

Figure 8. Comparison of crack growth, CTOD, and striation spacing for the wet air environment.

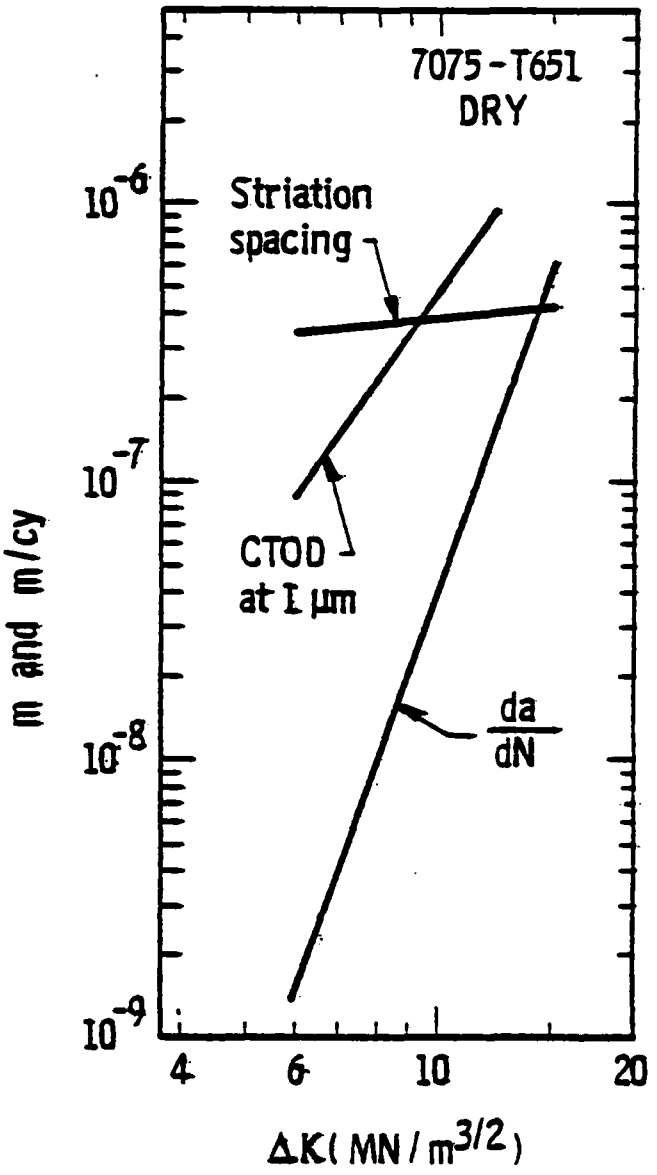

Figure 9. Comparison of crack growth, CTOD, and striation spacing for the dry environment.

APPENDIX A

7075-T651

The purpose of this appendix is to present additional information, not available in the manuscript. The plots presented show the distribution of strains near the crack; only crack tip values were used in the manuscript. The data set numbers correlate with those given in Table I. In each case, the crack is shown schematically on the zero strain plane. GMAX = the maximum shear strain range; x and y dimensions are in micrometers.

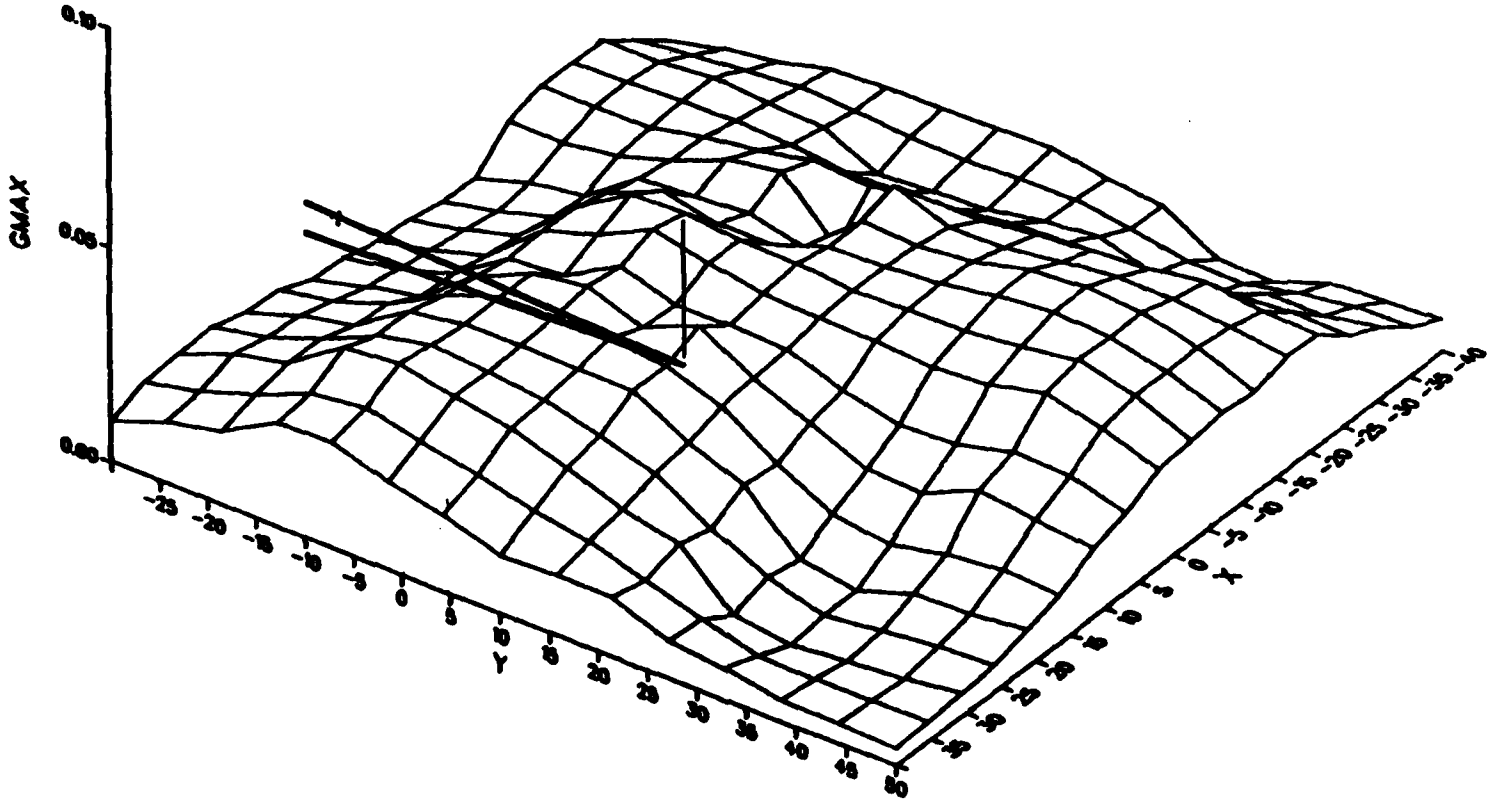

Figure A1. Set 34, ΔK = 6 $MN/m^{3/2}$, dry nitrogen environment.

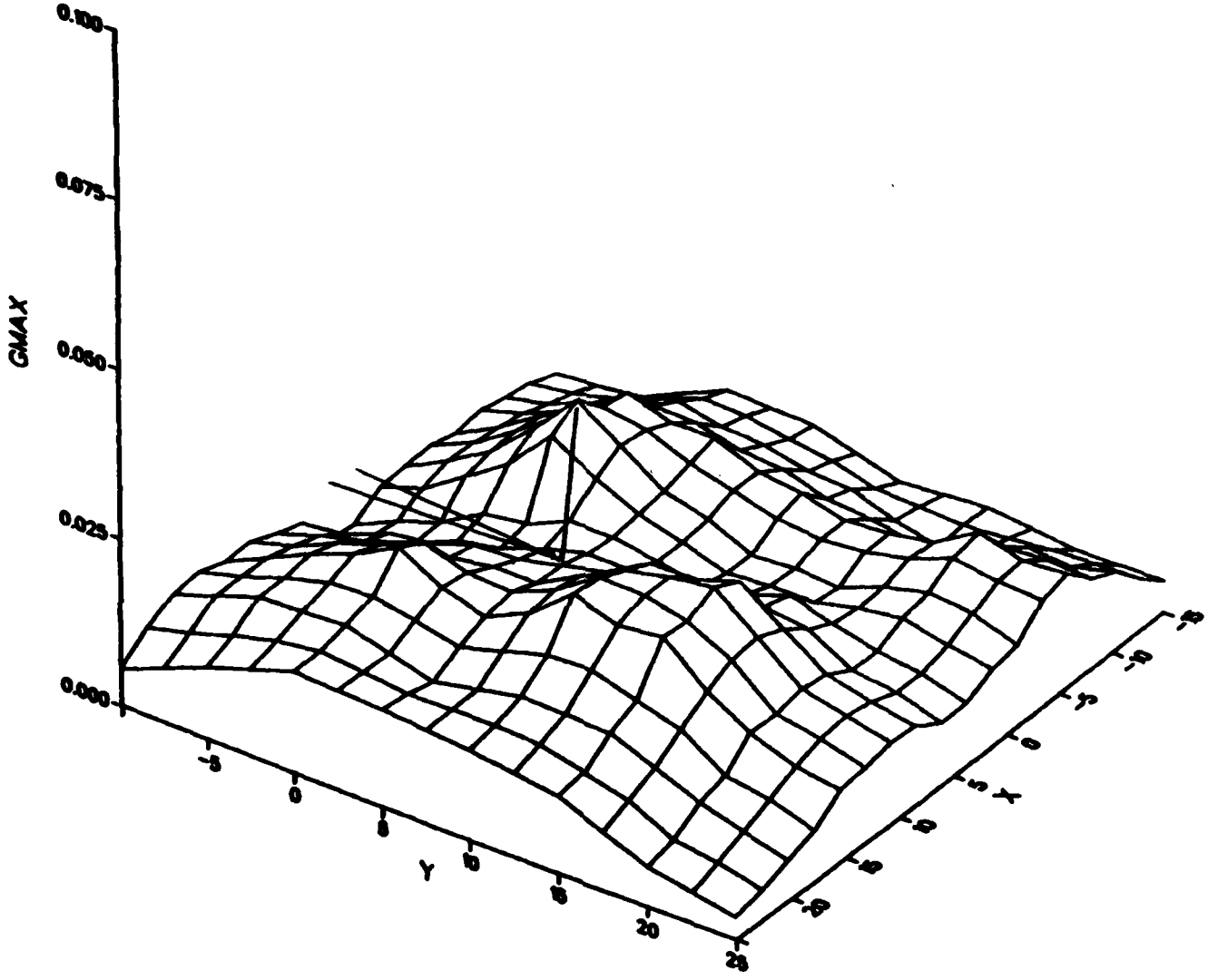

Figure A2. Set 38, ΔK = 6 $MN/m^{3/2}$, wet air environment.

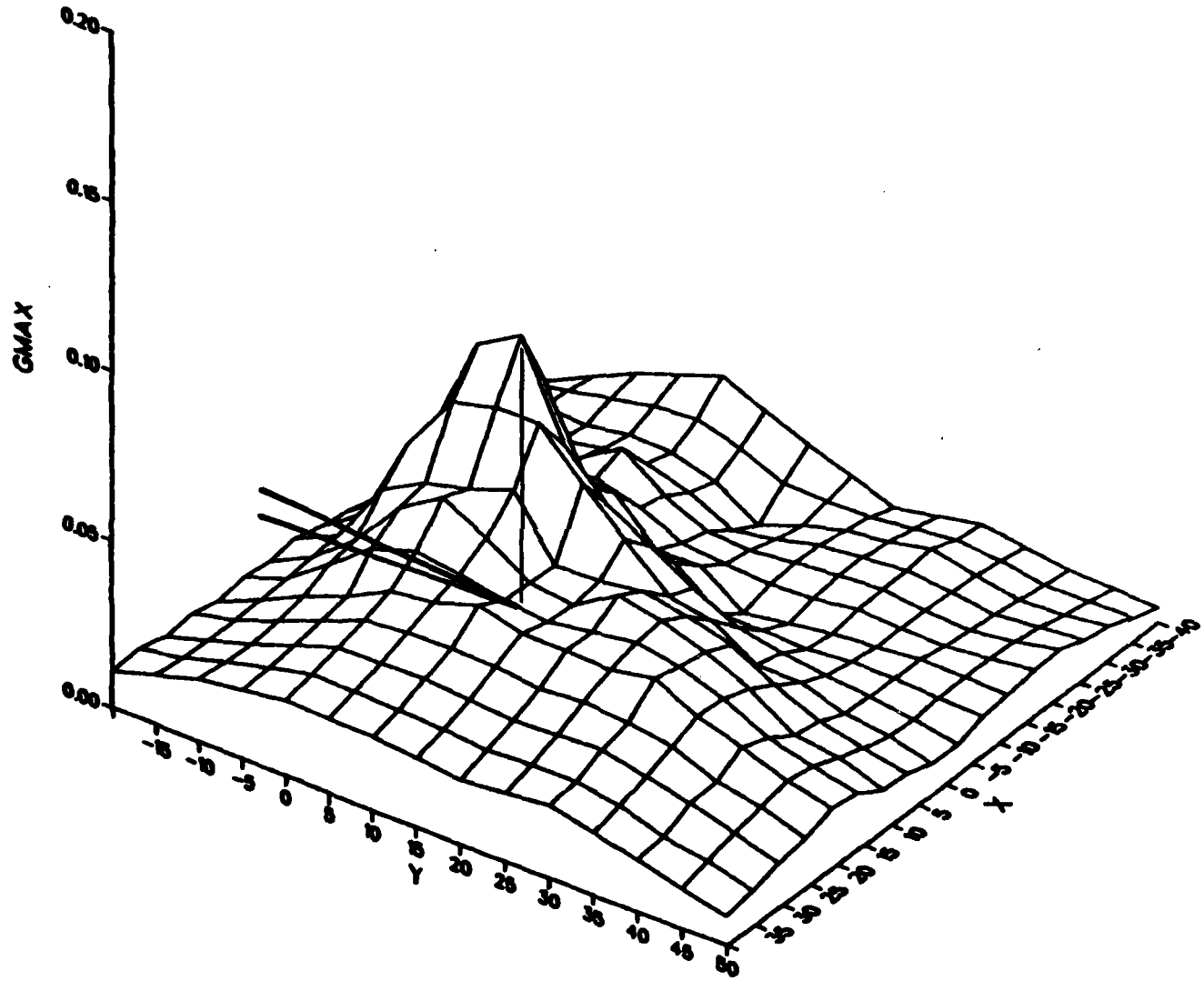

Figure A3. Set 41, ΔK = 8 $MN/m^{3/2}$, dry nitrogen environment.

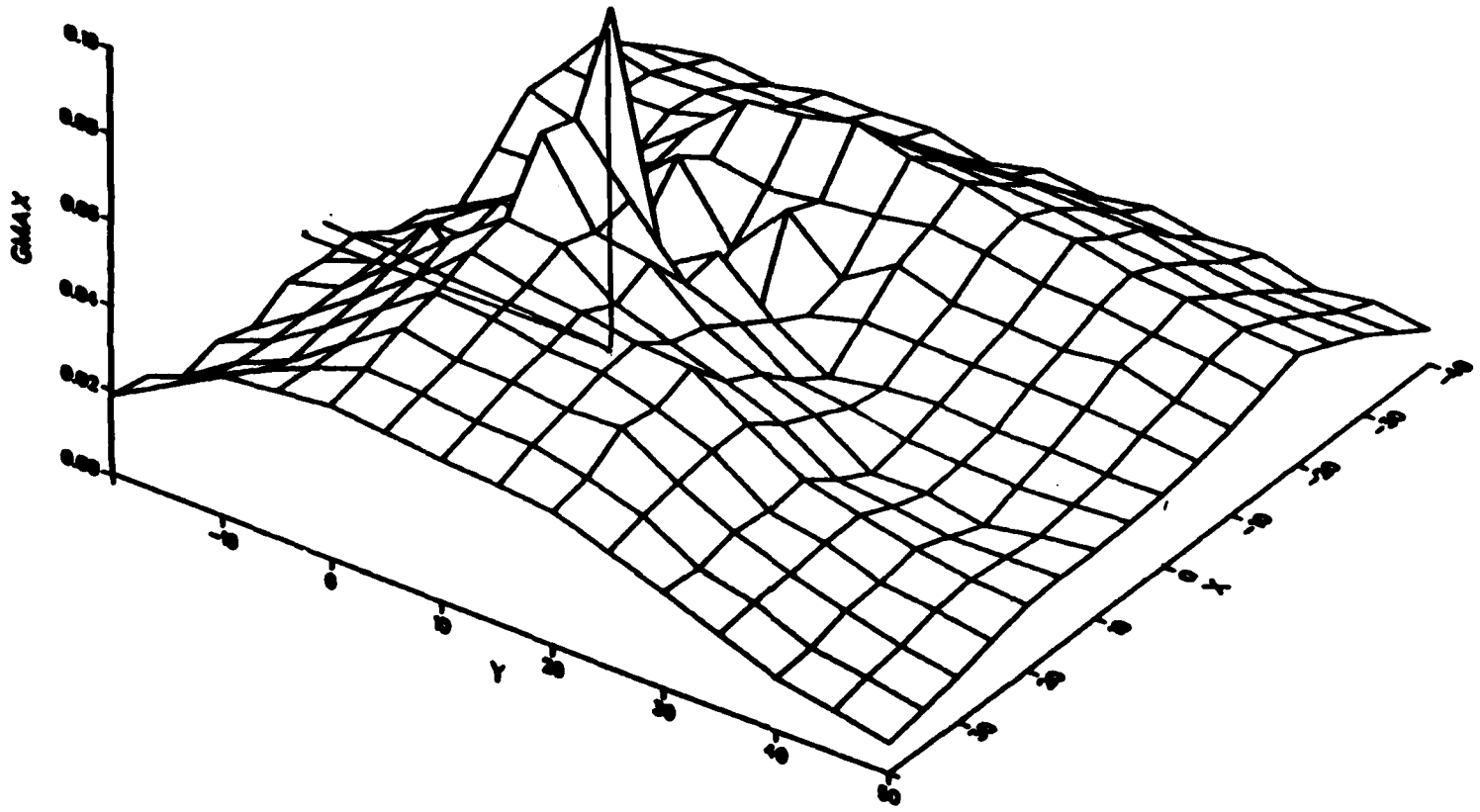

Figure A4. Set 42, ΔK = 8 $MN/m^{3/2}$, wet air environment.

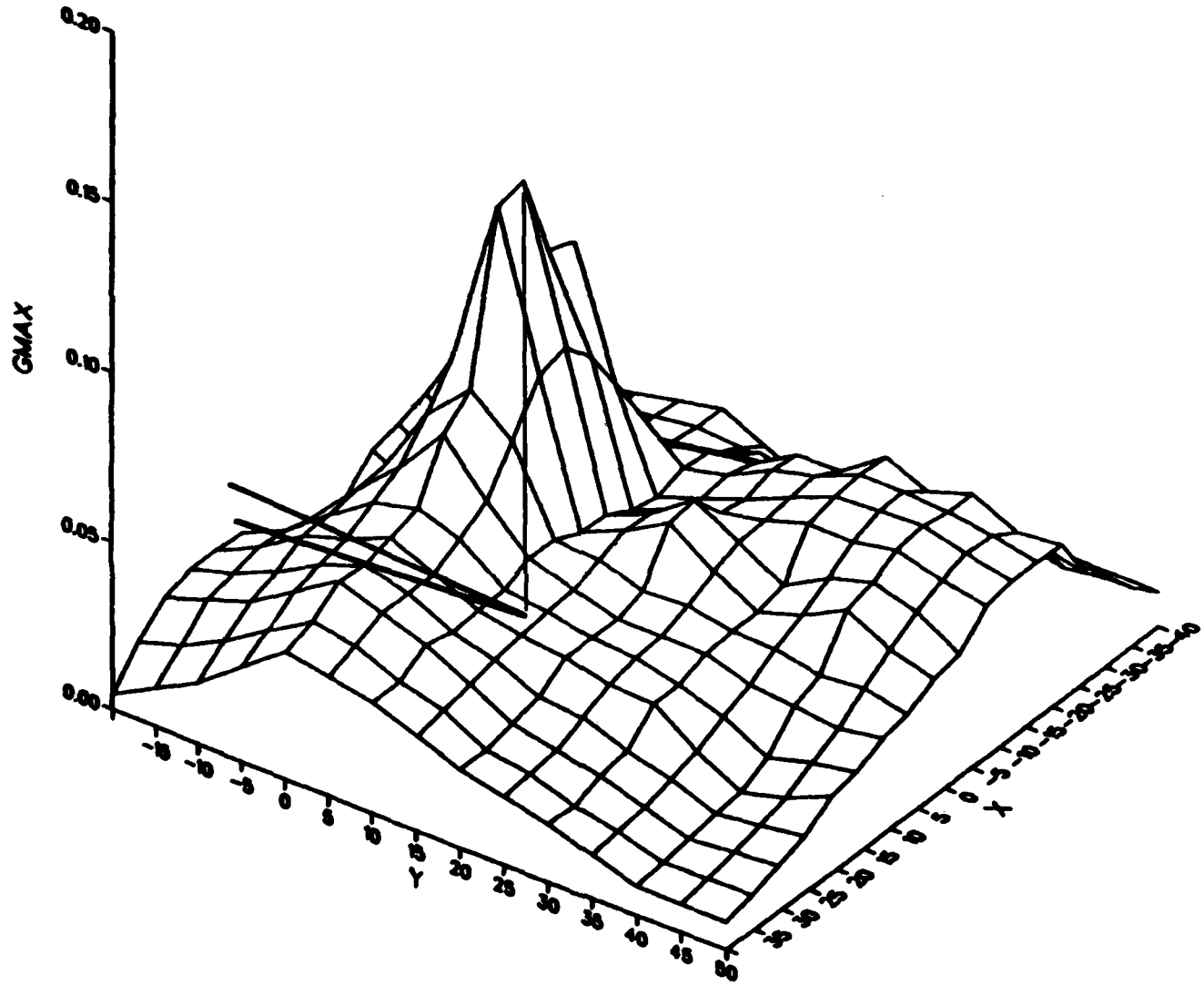

Figure A5. Set 44, ΔK = 10 $MN/m^{3/2}$, dry nitrogen environment.

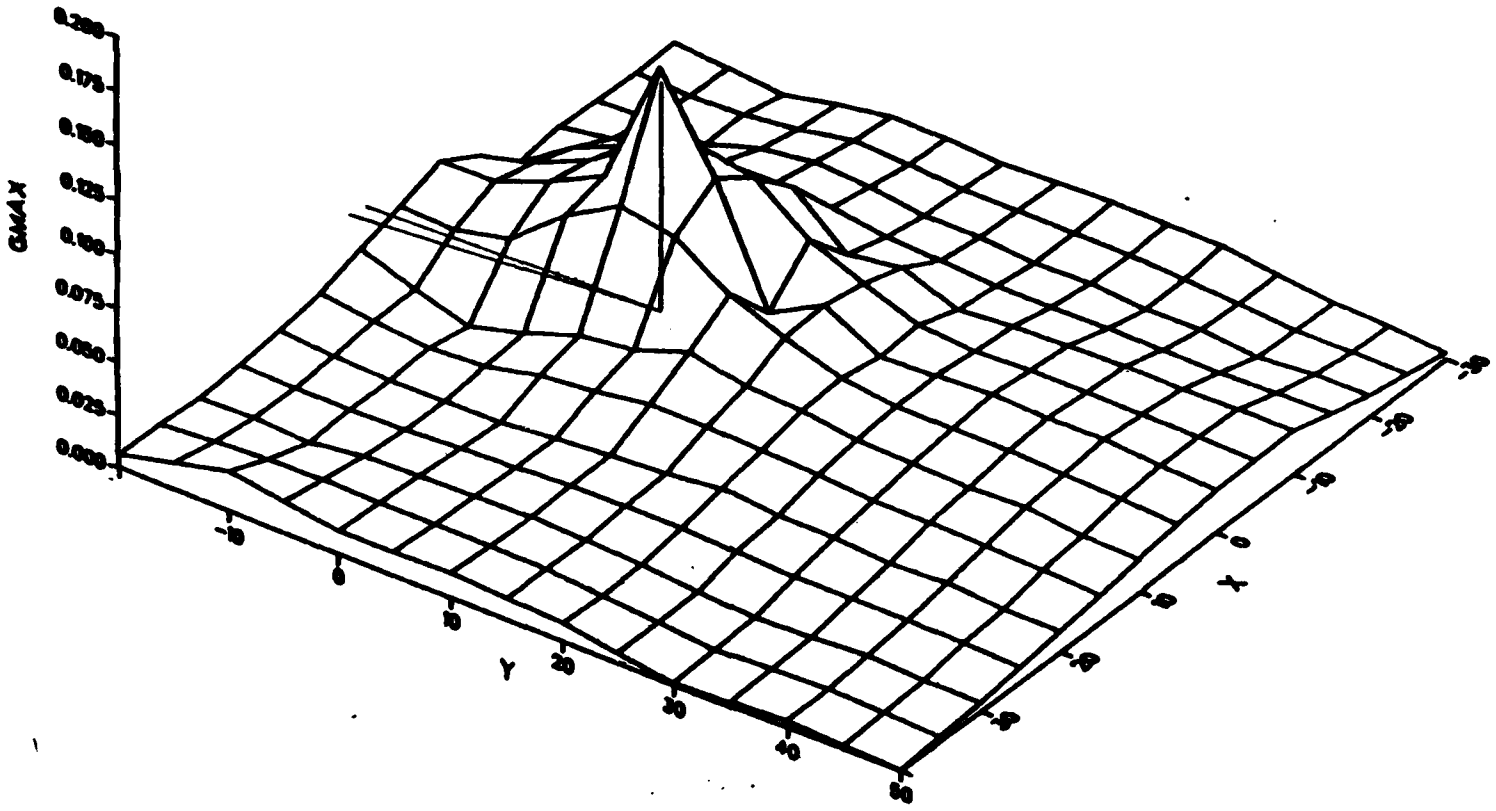

Figure A6. Set 55, ΔK = 11 $MN/m^{3/2}$, wet air environment.

[redacted]

FATIGUE CRACK TIP [redacted] OF A [redacted] ALUMINUM ALLOY IN VACUUM AND HUMID AIR

D. L. Davidson and R. Lankford

Abstract

Fatigue crack tip opening displacements and strains in the material very close to the crack tip have been determined from [redacted] measurements for cracks grown in both vacuum and humid air environments. The environment alters both the relations between crack tip opening displacement and crack tip strain, and the effect of cyclic stress intensity on these factors. Results of dynamic observation of intermittent crack growth are correlated with fractographic evidence. The relationships between crack tip parameters are used in a previously developed [redacted] mathematical model. The effect of wet air on fatigue crack growth is found to be a reduction in crack tip plasticity.

I. INTRODUCTION

This paper reports on the measurement of parameters which are needed to describe the mechanics of crack tips. Two recently developed tools are utilized in this study: a cyclic loading stage for the SEM[1] is used to view crack tips dynamically at high resolution, and the technique of stereoimaging[2] is used to determine crack opening displacements and strains at the crack tip and in the region nearby. These techniques have also been applied to fatigue cracks grown in 7075-T651 as formed by ingot metallurgical practice, and the results reported; thus, similar observations on a compositionally similar material which has been formed by a completely different technique offers the opportunity to assess the effect of metallurgical practice upon crack tip mechanics.

The powder metallurgy alloy chosen for this study has been reported to have markedly reduced sensitivity to stress corrosion cracking and exfoliation, as compared with 7075-T651. Thus, the alteration of crack tip mechanics by corrosion assisted fatigue seemed likely, and may be helpful in understanding the effect of metallurgical forming practice on fatigue crack growth.

Finally, the information reported here has been incorporated into a model similar to that previously used for 7075-T651.[3] A detailed comparison and interpretation of results for these two alloys will appear elsewhere.[4]

II. APPROACH

A. Material

The powder metallurgy alloy used for these experiments was obtained from Alcoa in 1977. It was part of an experimental batch being used in an alloy development program, and was at that time designated MA-87; substantially the same material is today produced in near-commercial quantities and designated X7091. Information on the manufacture of the material has been published elsewhere,[5] and is summarized below:

Material History

MA-87, Ingot 354877. Composition: Al-1.5Cu-2.5Mg-6.5Zn-.8Co. The compact was made from air-atomized powder, ABC-triple upset forged and extruded. Heat treatment: -T6 + 14 hrs at 162°C (Ref. 5). Tensile yield strength = 503 MPa.

The resulting microstructure, consisting of numerous alumina particles dispersed in a matrix of irregularly shaped grains, is shown in Fig. 5. Grain dimensions were in the range 5-30 μm and were elongated in the extrusion direction.

B. Experimental Technique

Specimens of gage section 21 x 3 mm thick were fabricated, and the fatigue crack was initiated from a single saw slit. Cracks were grown at ambient temperature in the range $5 < \Delta K < 11$ MN/m$^{3/2}$, $K_{min}/K_{max} = .11$-$.21$, in two environments: vacuum of 1 MPa (10^{-5} torr) and laboratory air of approximately 50% relative humidity (~12,000 ppm water vapor). Specimens

were transferred from the environment of interest to an especially constructed cyclic loading stage in the scanning electron microscope,[1] where they could be observed with high resolution while being loaded in the same way as done in the laboratory. Photographs and videotapes were made of the crack tip region. For cracks grown in laboratory air, observations were made only during the first few cycles, during which crack tip deformation remains unaffected by the vacuum of the SEM.

Fractography of typical fracture surfaces was done by SEM using a palladium coating to enhance resolution.

C. Analytical Techniques

Photographs were taken of the crack tip region at 1000 or 2000 magnification, at both minimum and maximum load. The displacements in the plane of the specimen surface due to the loading change could be both visualized and measured[2] using the stereoimaging technique. Gradients of these in-plane displacements were used to define[6] the strains in the loading axis (ε_{xx}) and perpendicular to it (ε_{yy}) and the shear strain (γ_{xy}). Measured displacements were also used to accurately determine crack opening both parallel and perpendicular to the loading axis.

D. Model

The crack tip quantities derived from these experiments will be examined in context of a model for fatigue crack growth developed previously by the authors.[7] This model is the modification of a similar one first developed by Antolovich, Saxena and Chanani.[8] The model includes the finding that crack growth is discontinuous and incorporates

the measured parameters of crack tip opening displacement and crack tip strain. The principal advantage of the model is that it allows determination of a stress intensity independent failure criterion.

A summary of the model is presented in the following: strain, which is considered to be the manifestation of "damage," is assumed to accumulate with each cycle, so that

$$\Delta N_c {}^{\beta} \Delta\varepsilon_p = \varepsilon_c \tag{1}$$

where $\Delta\varepsilon_p$ = the cyclic plastic strain range which occurs on each cycle in an element Δa just ahead of the crack tip, and ΔN_c = the number of cycles required for crack advance. The product, ε_c, is considered to represent the cumulative damage required for crack advance. If

$$\frac{da}{dN} = \frac{\Delta a}{\Delta N_c} \tag{2}$$

then Eqs. (1) and (2) may be combined to give

$$\frac{da}{dN} = \Delta a \left(\frac{\Delta\varepsilon_p}{\varepsilon_c} \right)^{1/\beta} \tag{3}$$

The per-cycle crack growth increment Δa will be determined from striation spacing, and will be assumed to be fundamentally dependent, either directly on ΔK_{eff}, or indirectly on ΔK_{eff} through the crack tip opening displacement (CTOD). The criteria for deciding whether Δa is CTOD or ΔK_{eff} dependent will depend on the relationships established between CTOD and ΔK_{eff} and between striation spacing and ΔK_{eff}. The appropriate

relationship is then incorporated into Eq. (3) along with the equation describing the change of $\Delta\varepsilon_p$ with ΔK_{eff}. From measured crack growth rates, and assuming that β and ε_c are independent of ΔK_{eff}, it is then possible to derive them. Table I lists the equations required for these calculations.

TABLE I

MA-87
Functions Used in the Fatigue Crack Growth Model
$\Delta K_{eff} = \Delta K - \Delta K_{TH}$

Equation Number	$\Delta a \propto \Delta K_{eff}$	$a \propto CTOD$
(4)	$\Delta a = A_o \Delta K_{eff}^n$	
(5)		$\Delta a = \alpha C_o$
(6)		$C_o = C\Delta K_{eff}^q$
(7)	$\Delta\varepsilon_p = K_o \Delta K_{eff}^r$	$\Delta\varepsilon_p = K_o \Delta K_{eff}^r$
(8)	$\frac{da}{dN} = B\Delta K_{eff}^s$	$\frac{da}{dN} = B\Delta K_{eff}^s$
(9)	$\beta = \frac{r}{s-n}$	
(10)		$\beta = \frac{r}{s-q}$
(11)	$\varepsilon_c = \left(\frac{A_o}{B}\right)^{\beta} K_o$	
		$\varepsilon_c = \left(\frac{\alpha C}{B}\right)^{\beta} K_o$

III. EXPERIMENTAL RESULTS

A. Crack Tip Measurements

Crack opening displacement vs distance y behind the crack tip is plotted in Figure 1. The value shown is the total (or resultant) COD which is defined as

$$COD = \left(COD_x^2 + COD_y^2 \right)^{1/2} \tag{12}$$

For both environments, these data fit the relation

$$COD = C_o |y|^p \tag{13}$$

Values of C_o and p are listed in Table II along with the plastic strain increment at the crack tip, $\Delta\varepsilon_p(0)$, where the latter is defined in terms of the total effective strain increment at the crack tip, so that $\Delta\varepsilon_p(0) = \Delta\varepsilon_t^{eff}(0) - .0069$, and

$$\Delta\varepsilon_t^{eff} = \left(\frac{2}{\sqrt{3}} \Delta\varepsilon_1^2 + \Delta\varepsilon_1 \Delta\varepsilon_2 + \Delta\varepsilon_2^2 \right)^{1/2} \tag{14}$$

$\Delta\varepsilon_1$ and $\Delta\varepsilon_2$ are the maximum and minimum principal strains, and .0069 is approximately twice the shear strain at yield.

The COD has a very large Mode II crack opening component. The ratio of COD_y/COD is 0.6-0.95 at 3 μm behind the crack tip for both environments and all ΔK. CTOD is defined as the opening 1 μm behind the crack tip, and is equal to C_o.

TABLE II

MA-87
Crack Tip Opening and Strain Data

ΔK $MN/m^{3/2}$	Environment	C_o (1 μm)	p	$\Delta\varepsilon_p(0)$	R	Data Set
5.5	Vac	.5	.315	.1461	.21	51
5.5	Wet	.68	.19	.1253	.21	67
7.8	Wet	.86	.23	.1205	.12	68
8.8	Wet	1.1	.295	.2076	.12	69
8	Vac	1.17	.30	.1925	.17	70
10	Vac	1.66	.20	.2011	.23	1A
11	Wet	1.09	.318	.2529	.11	71
11	Wet	1.0	.35	.2342	.11	72
11	Vac	1.6	.260	.2194	.12	73
11	Vac	1.75	.306	.2213	.12	74

The data of Table II are plotted in Figures 2-4. Lines shown on the figures have been determined by the method of least squares. Parameters describing these regression lines are given in Table III. In addition, the correlation relating $\Delta\varepsilon_p(0)$ and C_o is shown in Figure 4, and is described by the equation

$$\Delta\varepsilon_p(0) = A\, C_o^{\,x} \tag{15}$$

Combining Eqs. (4) and (6) also allows the derivation of this equation, where $K_o = AC^x$ and $r = qx$. This provides both an internal check on the computation of the quantities in Table II and a fundamental relationship between crack tip strain and crack tip opening displacement.

B. Direct Observation of Crack Growth

Evidence for noncontinuous crack growth is found from dynamic observation of crack growth in the scanning electron microscope and from fracture surface examination. A sequence of photographs of the crack tip region is shown in Figure 5. Starting with a sharp crack, Figure 5(c), cycling causes the crack tip to progressively blunt, Figure 5(e), until a new increment of growth occurs, Figure 5(f), which leaves the crack sharp again. This sequence shows that the crack does not grow on each cycle, and for $\Delta K \leq 6$ MN/m$^{3/2}$, 100 cycles or more may be required for crack advance in vacuum, although the number of cycles has not been established on a statistical basis. Although this process has been observed dynamically numerous times in several materials, the detailed sequence of events actually accompanying crack advance are not yet known, and may be different in different materials.

TABLE III

MA-87
Constants for Parameters in Various Equations
as Derived by Least-Squares-Fit Through the Data

$\Delta K_{eff} = MN/m^{3/2}$ CTOD = m

Variable	Equation Number	Vacuum	Wet
ΔK_{TH}		3.5	1.7
A_o	4	3.28×10^{-7}	1.3×10^{-7}
n		0.354	0.358
C	6	2.6×10^{-7}	3.8×10^{-7}
q		0.94	0.476
K_o	7	.1176	3.9×10^{-2}
r		.315	.792
B	8	7.37×10^{-10}	4.8×10^{-10}
s		2.18	3
A	15	14.1	1.6×10^{8}
x		.315	1.486

C. Fractography

Striations are associated with fatigue crack growth over the entire ΔK range studied, for both vacuum and air. In the air environment, striations appear fairly straight and clean-edged (Figure 6), while in vacuum, they have more of a "ripple" to their profile (Figure 7). Macroscopically, the fracture surfaces in these two environments are startlingly dissimilar. The vacuum surface looks much smoother, although close inspection at high magnification shows that the surface is covered with uniformly distributed fine striations. As concluded elsewhere,[9] striation spacings are the increment of crack growth Δa, and they were measured and correlated with ΔK_{eff} through Eq. (4) of Table I. Values of A_o and n in that equation are given in Table III.

D. Crack Growth Rate

Average crack growth rate, CTOD, and striation spacing are shown in Figures 8 and 9 for the two environments. The individual data have been presented elsewhere;[9] the equations for the various relationships are found in Table I and the parameters are given in Table III. Threshold ΔK was determined from crack growth data as that value of ΔK_{TH} which minimized the sum of the least-squares deviations.

IV. DISCUSSION

No clear alterations are made to crack tip strain range $\Delta\varepsilon_p(0)$ and CTOD by changing environment. However, there does appear to be a basic difference in the effect of water vapor on the relation between CTOD and strain, Figure 4, although unfortunately CTOD covers only a narrow range.

Fractography indicates that striation spacing greatly exceeds crack growth rate at low ΔK. This indicates that many cycles are required for crack advance, and is in agreement with dynamic observations of crack growth. For 7075-T651 it has been established by TEM that creation of striations is a two-step process, and crack tip blunting, accompanied by increasing strain, is implied. TEM work has not been done for MA-87, but due to similarities between dynamic observations and crack tip measurements, this material is assumed to undergo a similar cycle of progressive crack tip blunting which precedes growth. Thus, variations in crack tip strain and CTOD at various ΔK are not considered to be due to statistical variability or inaccuracies in measurement technique, but rather are due to strain analyses which were made at various points in the cumulative strain cycle.

Striation spacing and CTOD are dependent on ΔK_{eff} for the air environment, but not for vacuum. Since striation spacing is assumed to equal the increment of crack advance, Δa in vacuum is assumed to be directly proportional to ΔK_{eff}, Eq. (4), Δa in air is assumed to be proportional to CTOD, Eq. (5), which is, in turn, proportional to ΔK_{eff}, Eq. (6). In Eq. (5), α is determined by dividing striation spacing, Eq. (4) by CTOD, Eq. (6). For the air environment, $\alpha = 0.34$.

Knowing the functional dependencies of Δa, the other equations in Table I are used to compute β and ε_c (Table IV). These values are relatively insensitive to the crack growth rate curves used. For example, the crack growth data of Langenbeck[10] for X7091 in air give nearly the same values for β and ε_c, as do the crack growth data of McEvily,[11] also for X7091. In addition, McEvily has found $K_{TH} \cong 2$ MN/m$^{3/2}$, which is in good agreement with the present value of 1.7 MN/m$^{3/2}$. The values of β and ε_c in Table IV can be compared to values derived from low-cycle fatigue experiments[12] on this alloy: $\beta = 0.7$ and $\varepsilon_c = 0.8$.

TABLE IV

MA-87
Computed β and ε_c

Environment	β	ε_c
Vac	.172	.336
Air	.313	.225

By knowing β and ε_c, the number of cycles required for crack advance may be computed using Eq. (1), Table V. The large number of cycles required for crack advance at low ΔK in vacuum is in general agreement with dynamic observation of crack growth in the SEM. There are two effects of wet air: (1) to greatly decrease the number of cycles needed before crack growth, and (2) to decrease the magnitude of the crack advance. These changes act together to increase the crack growth rate.

TABLE V

MA-87
Computed Number of Cycles for Crack Extension

Environment	ΔK	ΔK_{eff}	$\Delta\varepsilon_p$	$\frac{\Delta a}{10^{-7}}$	ΔN_c
Vac	5	1.5	.134	3.8	188
	7	4.5	.174	5.1	43
	10	6.5	.212	6.4	14
	14	10.5	.247	7.5	6
Air	4	2.3	.075	1.8	34
	6	4.3	.124	2.2	7
	8	6.3	.168	2.5	3
	10	8.3	.208	2.8	1
	14	12.3	.285	3.2	.4

The lower value of ε_c in air indicates that water vapor decreases the plasticity associated with crack growth, and is in agreement with the decrease in $\Delta\varepsilon_p(0)$ in air, Figure 2. Hydrogen, which is released catalytically from H_2O at the newly created crack tip surface, is thought to be responsible for this decrease in crack tip plasticity. Whether the hydrogen acts on the surface of the crack, or is transported ahead of the tip by dislocations or diffusion is not known, but the hydrogen need not act over a distance in excess of Δa, the increment of crack advance, which is only about 0.3 μm.

V. SUMMARY AND CONCLUSIONS

Crack tip opening displacement and strain, striation spacing, and crack growth rate have been determined in vacuum and wet air environments at $5 < \Delta K < 12$ MN/m$^{3/2}$. The findings include:

1) Crack tip strain increment is proportional to crack tip opening displacement, but environment alters the proportionality.

2) In vacuum, the increment of crack growth, which is the average striation spacing, correlates with effective ΔK, while in air it correlates with CTOD.

3) Dynamic observation indicates that crack growth is intermittent, and that the crack tip becomes increasingly blunt prior to growth.

4) A model which treats the material just ahead of the crack tip as a tiny low-cycle fatigue specimen is utilized. Parameters are derived from the crack tip and fractographic measurements which describe the low-cycle fatigue behavior experienced by the material at the crack tip. Correlation of these parameters with those measured in laboratory low-cycle fatigue experiments is poor.

5) The model indicates that an increasingly large number of cycles are expended between increments of crack growth as ΔK is decreased, in agreement with experimental findings.

ACKNOWLEDGEMENT

This work was sponsored by the Office of Naval Research, Contract Number N00014-75-C-1038. The authors appreciate the encouragement of Dr. P. A. Clarkin, contract monitor.

REFERENCES

1. Davidson, D. L. and Nagy, A. 'A Low Frequency Cyclic Loading Stage for the SEM' Journ. of Physics E 1978 11, 207-210.
2. Davidson, D. L. 'The Observation and Measurement of Displacements and Strain by Stereoimaging' Scanning Electron Microscopy/1979/II, 79-86.
3. Davidson, D. L. and Lankford, J. 'The Effect of Water Vapor on Fatigue Crack Tip Mechanics in 7075-T651 Aluminum Alloy' Fat. of Engng. Mater. and Struct. 1982 (submitted).
4. Davidson, D. L. and Lankford, J. 'The Effect of Metallurgical Structure, Environment, and Stress Intensity on Fatigue Crack Tip Plasticity in Al-Zn-Mg-Cu Alloys' Fat. of Engng. Mater. and Struct. (to appear).
5. Otto, W. L. 'Metallurgical Factors Controlling Structure in High Strength P/M Products' Air Force Materials Laboratory Technical Report AFML-TR-76-60, 1975.
6. Williams, D. R., Davidson, D. L., and Lankford, J. 'Fatigue-Crack-Tip Plastic Strains by the Stereoimaging Technique' Exp. Mech. 1980 20, 134-139.
7. Davidson, D. L. and Lankford, J. 'Fatigue Crack Tip Strains in 7075-T6 by Stereoimaging and Their Use in Crack Growth Models' ASTM, Dearborn 1982 (in press).
8. Antolovich, S. D., Saxena, A., and Chanani, G. R. 'A Model for Fatigue Crack Propagation' Engng. Fract. Mech. 1975 7, 649-652.

9. Lankford, J. and Davidson, D. L. 'Fatigue Crack Micromechanics in Ingot and Powder Metallurgy 7XXX Aluminum Alloys in Air and Vacuum' Acta Met. 1982 (submitted).

10. Langenbeck, S. L. 'Investigation of the Fatigue and Crack Propagation Properties of X7091-T7E69 Extrusion' in "High Performance Aluminum Powder Metallurgy Alloys," The Metallurgical Society-AIME 1982 (in press).

11. McEvily, A. J. 'The Fatigue of Powder Metallurgy Alloys' Annual Report to the Air Force Office of Scientific Research, Grant 81-0046, 1982.

12. Lawley, A. and Koczak, M. J. 'A Fundamental Study of Fatigue in Powder Metallurgy Aluminum Alloys' in "High Performance Aluminum Powder Metallurgy Alloys," The Metallurgical Society-AIME 1982 (in press).

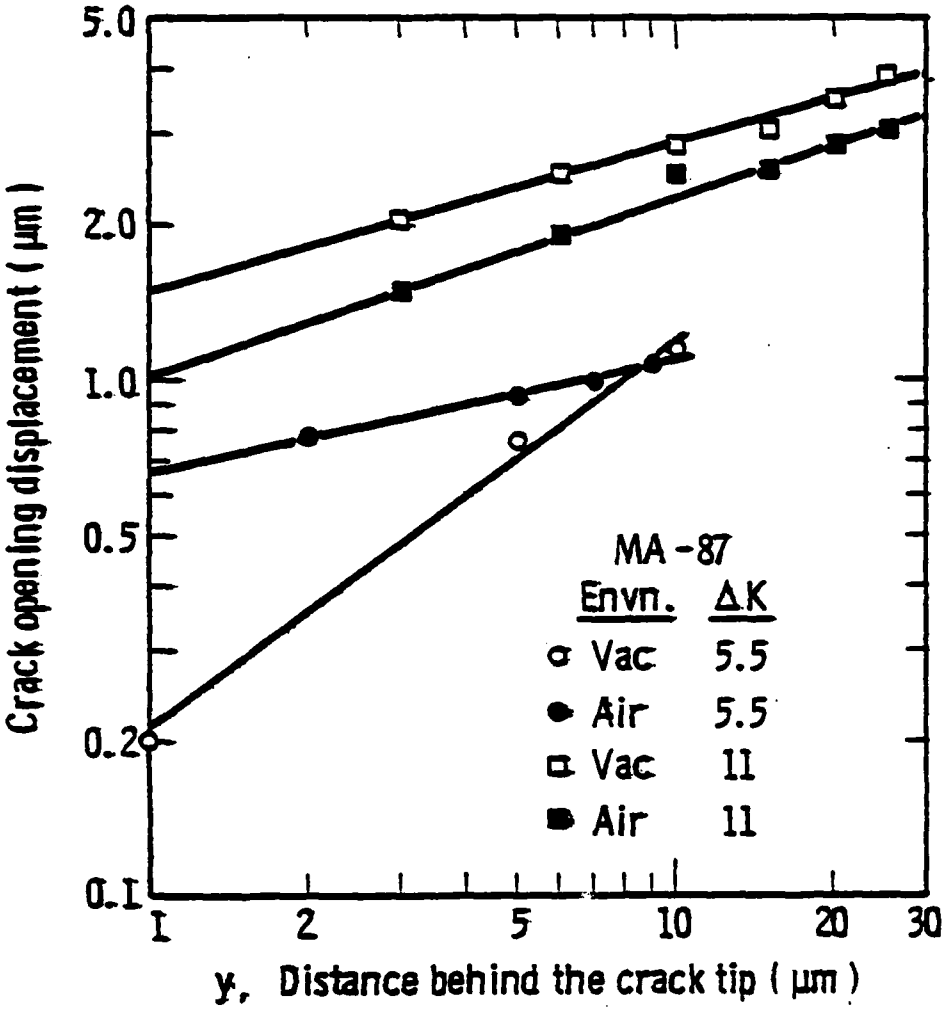

Figure 1. Total crack opening displacement as a function of distance behind the crack tip. Lines shown are least-square fits. $\Delta K = MN/m^{3/2}$.

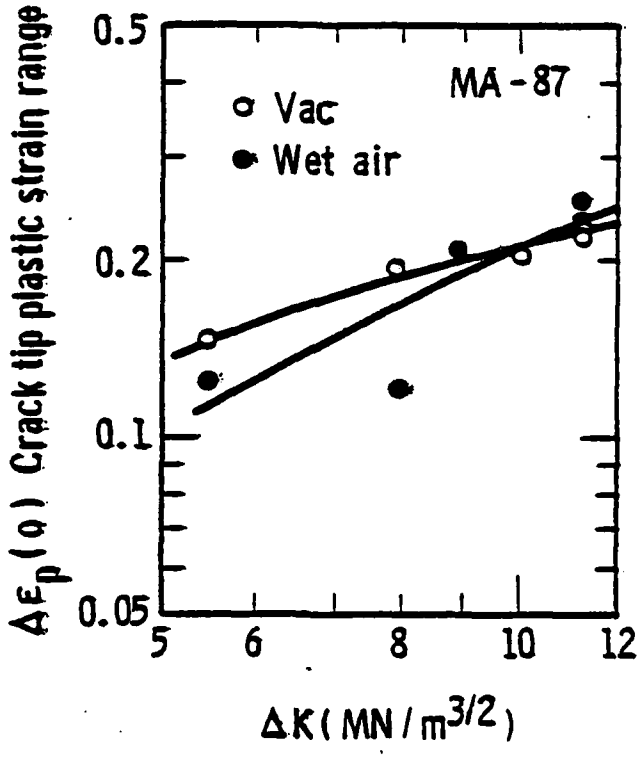

Figure 2. Crack tip plastic strain range vs cyclic stress intensity factor. Lines shown are least-square fits with ΔK_{TH} given in the text.

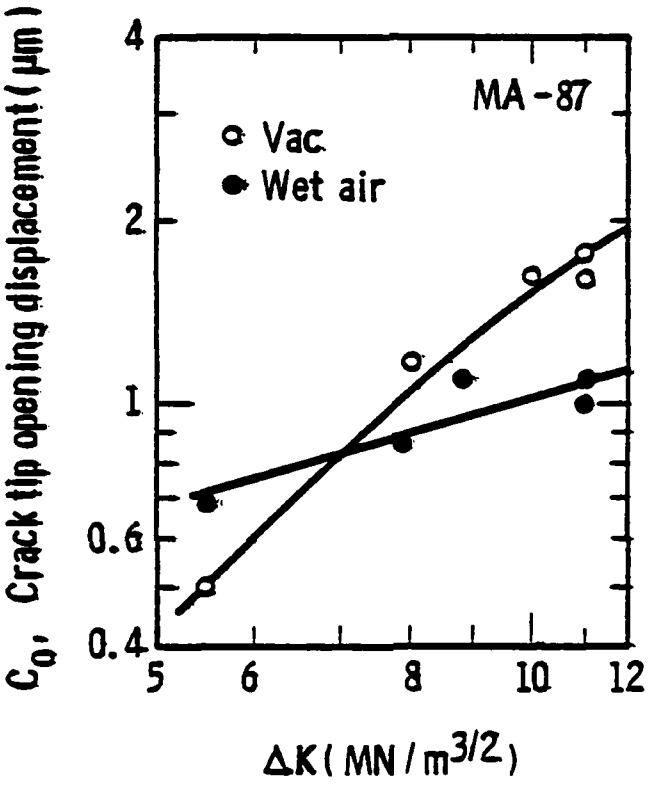

Figure 3. Total crack opening displacement 1 μm behind the tip vs cyclic stress intensity factor. Lines shown are least-square fits with ΔK_{TH} given in the text.

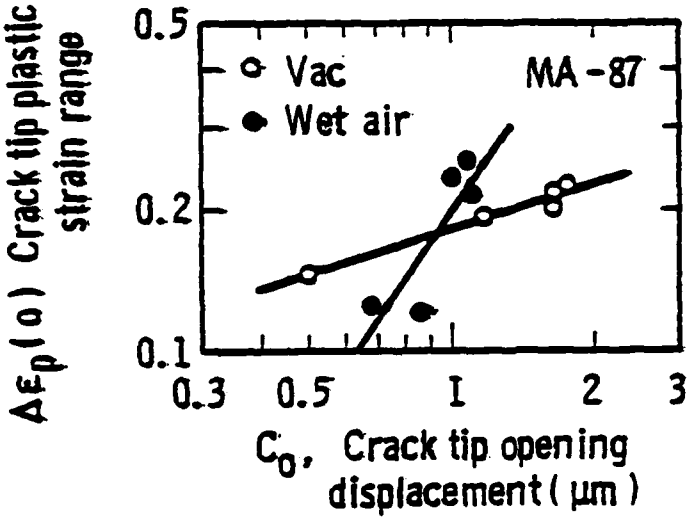

Figure 4. The correlation between crack tip opening displacement and strain range. Lines shown are least-square fits.

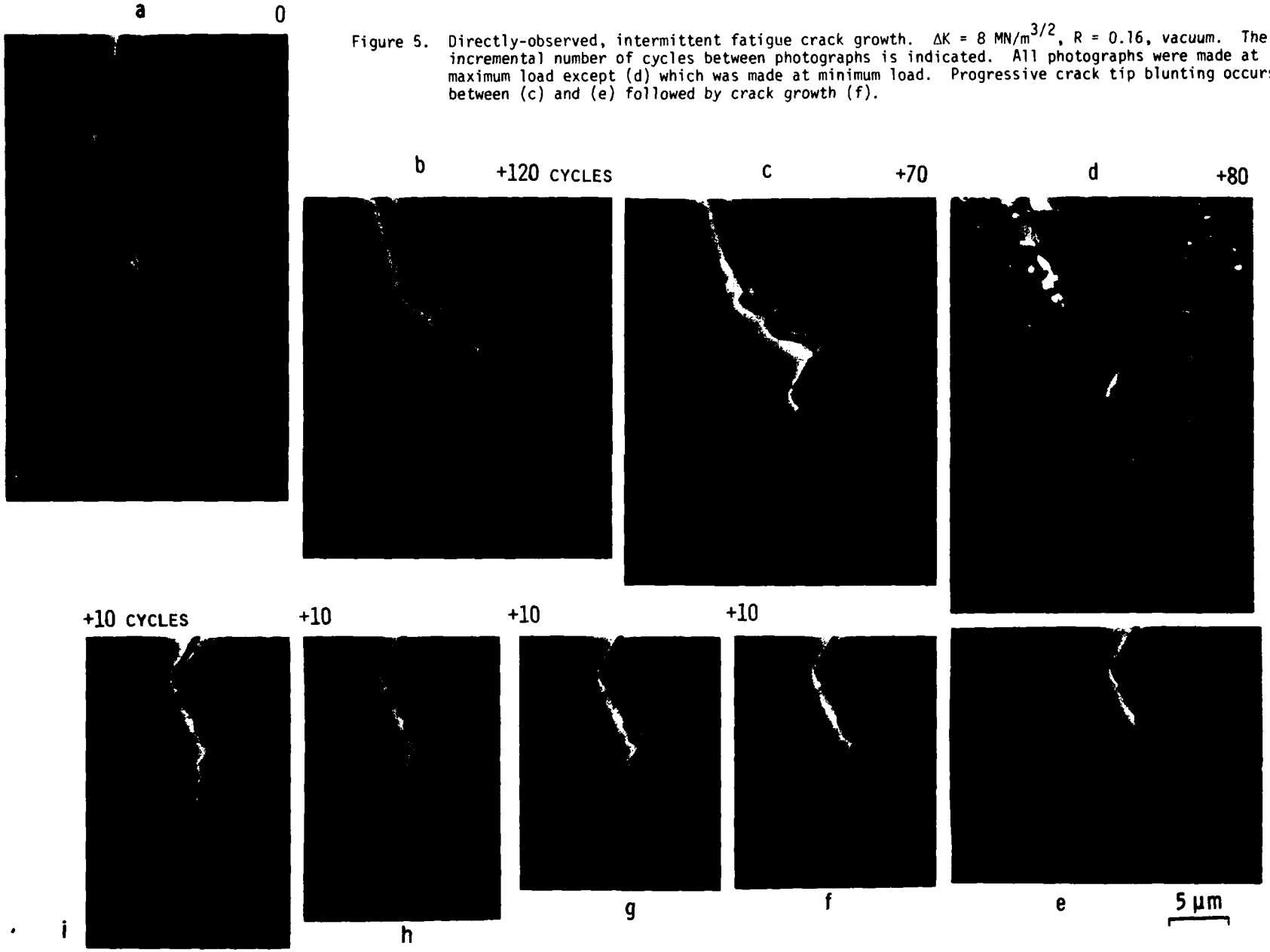

Figure 5. Directly-observed, intermittent fatigue crack growth. ΔK = 8 $MN/m^{3/2}$, R = 0.16, vacuum. The incremental number of cycles between photographs is indicated. All photographs were made at maximum load except (d) which was made at minimum load. Progressive crack tip blunting occurs between (c) and (e) followed by crack growth (f).

Figure 6. Fatigue striations from specimen cycled in wet air, $\Delta K = 7\ MN/m^{3/2}$.

Figure 7. Fatigue striations from specimen cycled in vacuum, $\Delta K = 10\ MN/m^{3/2}$.

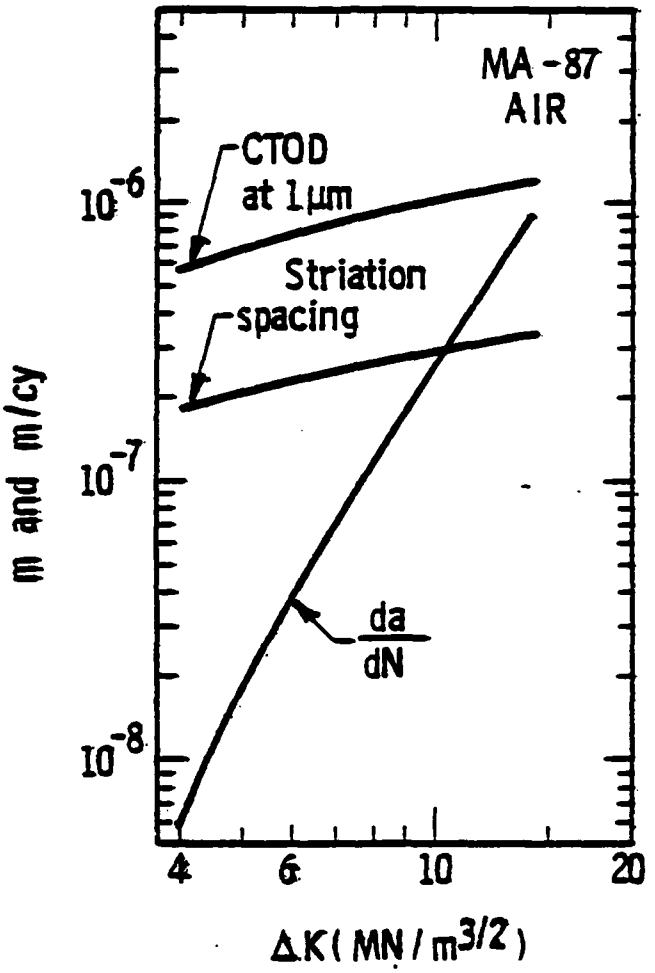

Figure 8. Measured crack growth rate, crack tip opening displacement, and striation spacing vs ΔK in moist air. Lines shown are least-square fits with ΔK_{TH} = 1.7 MN/m$^{3/2}$.

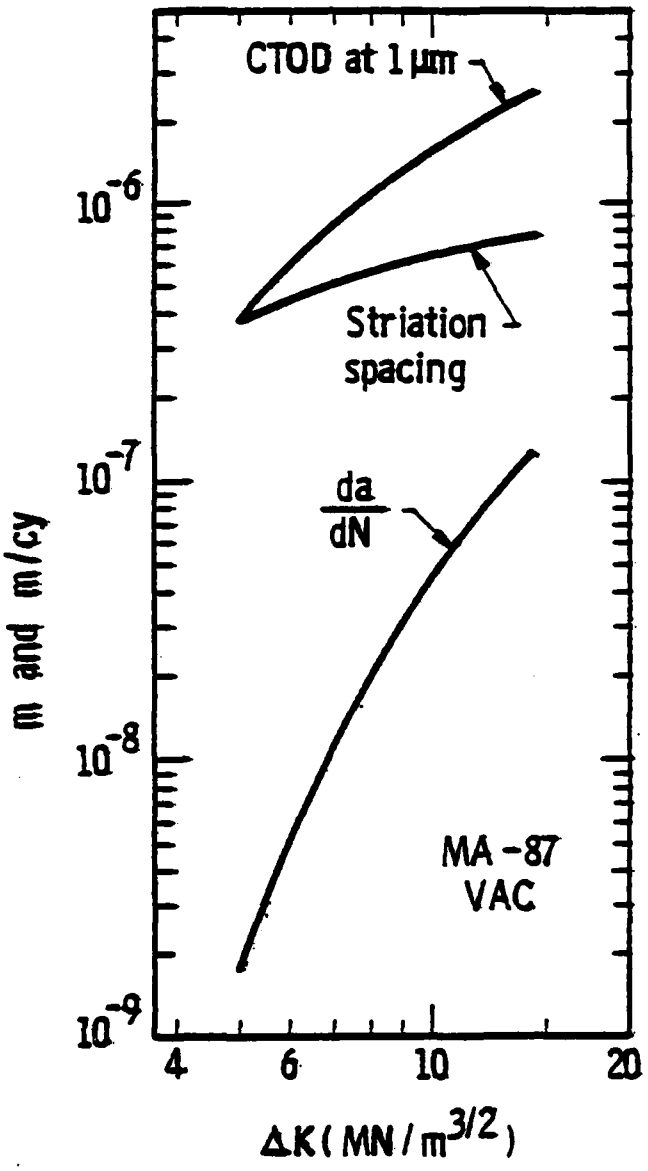

Figure 9 Measured crack growth rate, crack tip opening displacement, and striation spacing vs ΔK in vacuum. Lines shown are least-square fits with $\Delta K_{TH} = 3.5$ MN/m$^{3/2}$.

APPENDIX B

MA-87

Additional data are presented in this appendix to that found in the foregoing manuscript. Plots of displacements and Mohr's circles are shown because these have not been previously given. Data set numbers are the same as those given in Table II of the manuscript. On the displacement diagrams, the dot represents the position of the point before load is applied; the end of the line is the displacement which has occurred due to the loading. The cross is the crack tip.

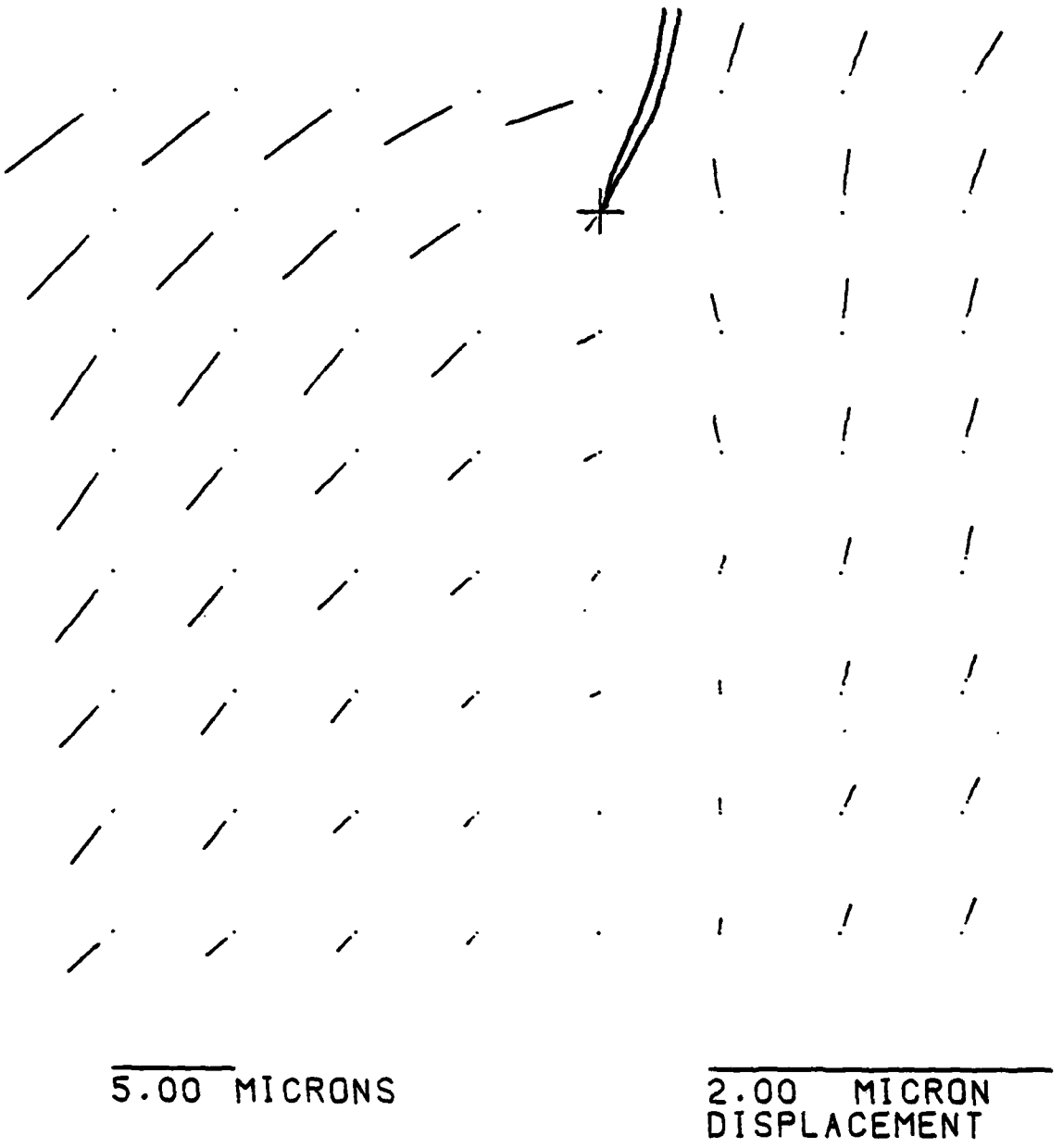

Figure B1. Set 67, $\Delta K = 5.5\ MN/m^{3/2}$, wet air environment.

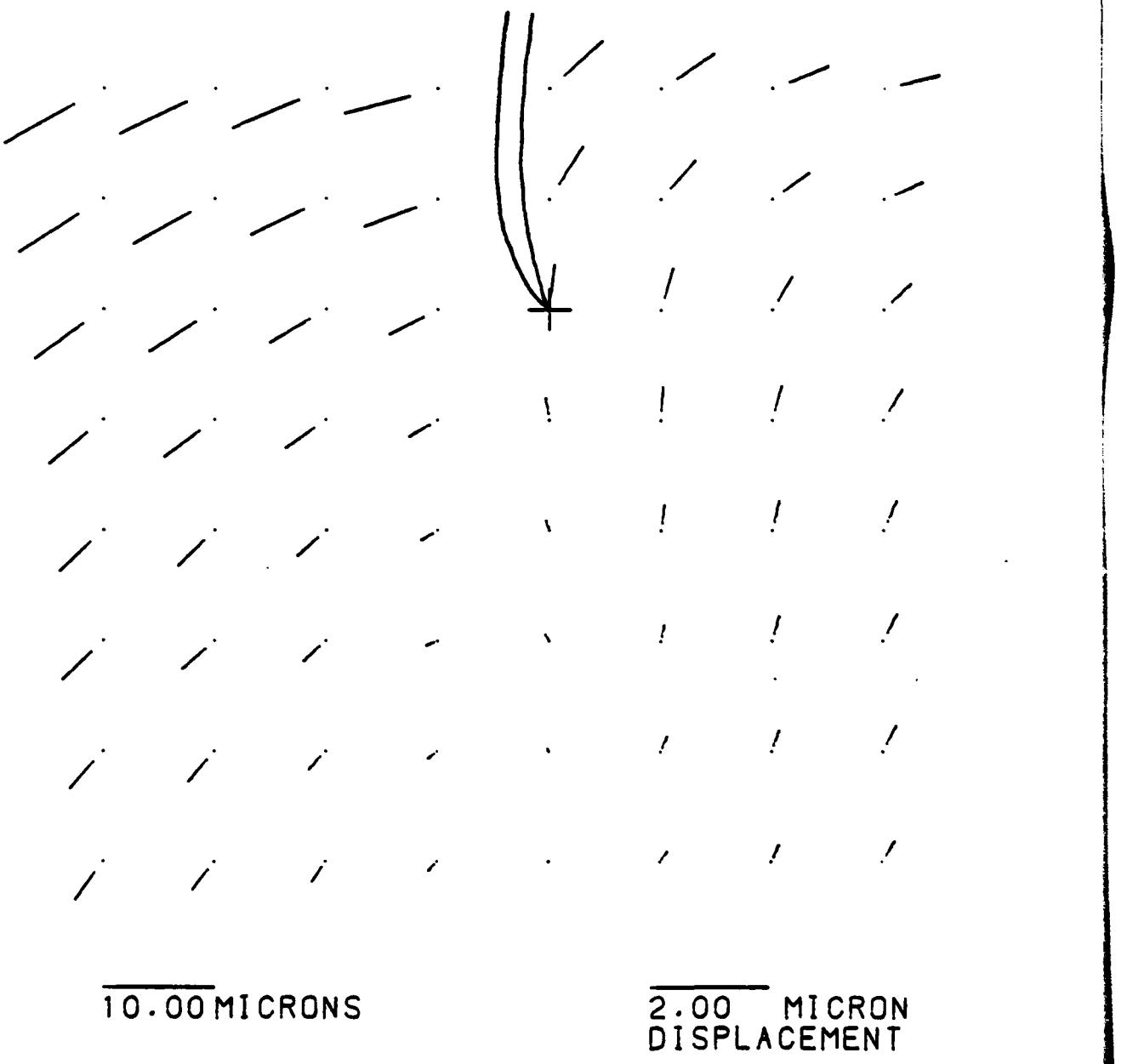

Figure B2. Set 70, $\Delta K = 8\ MN/m^{3/2}$, vacuum environment.

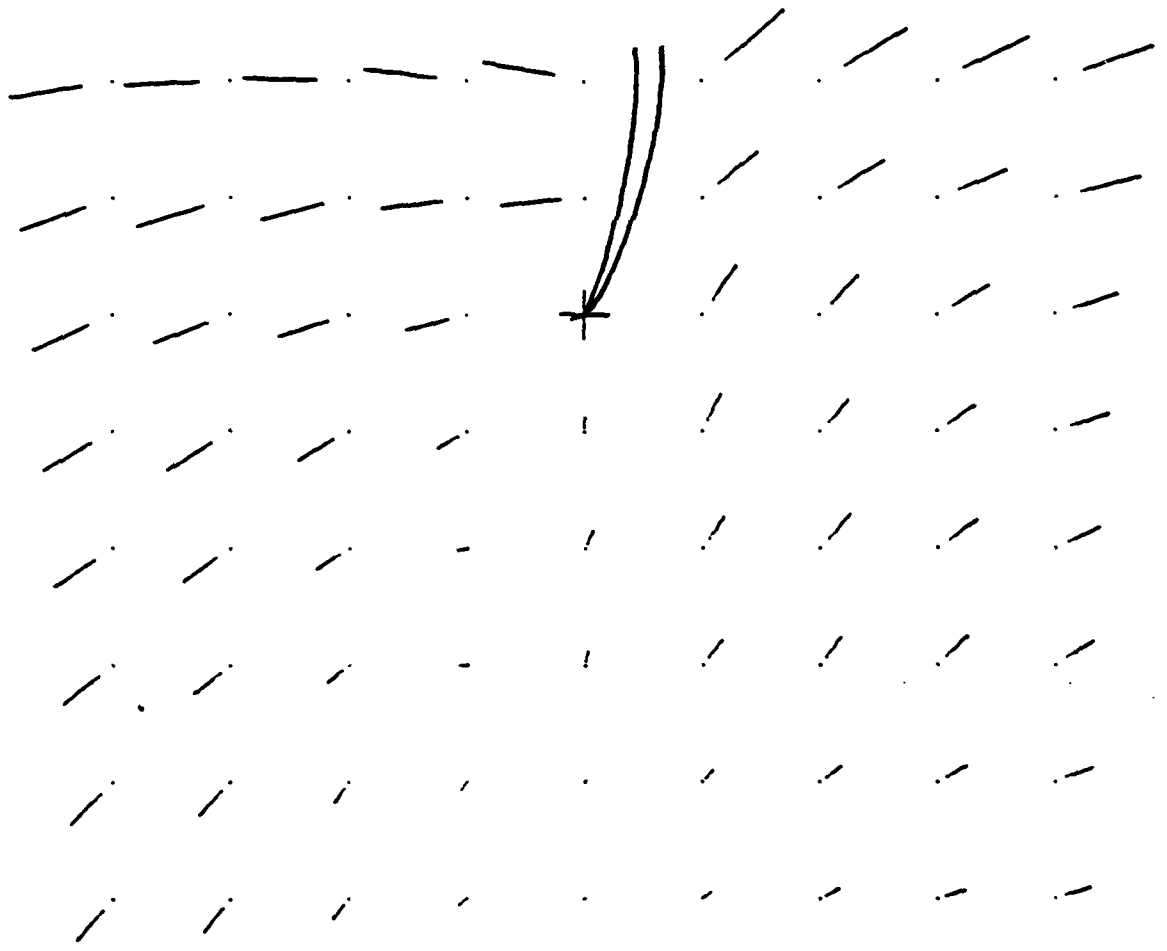

Figure B3. Set 73, ΔK = 11 $MN/m^{3/2}$, vacuum environment.

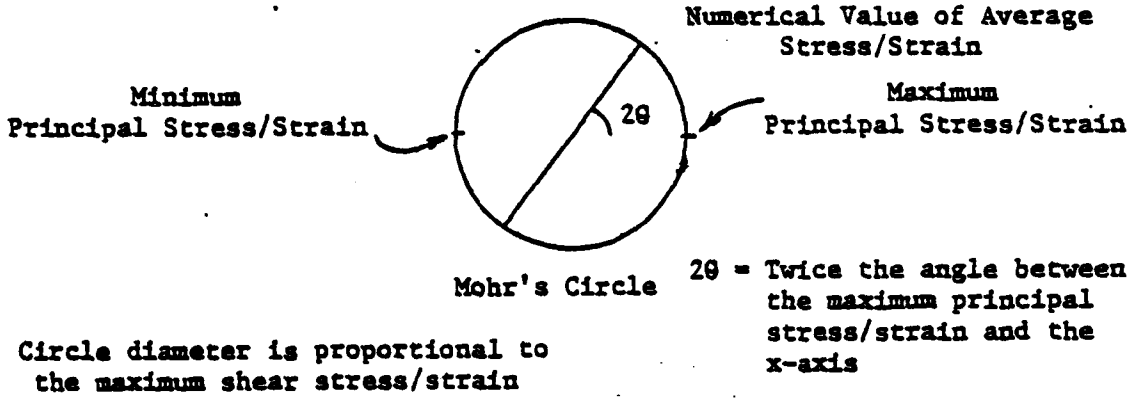

Figure B4. Interpretation of Mohr's circles on the following diagrams.

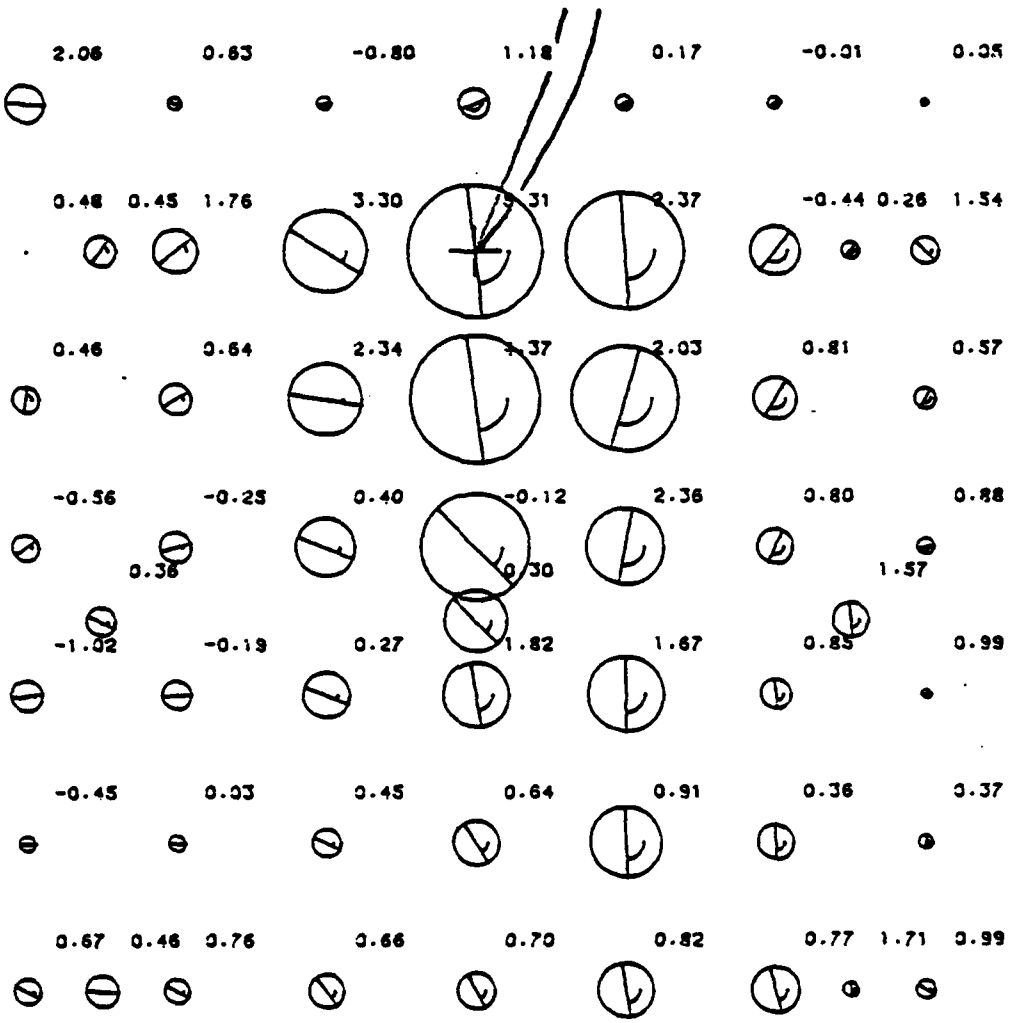

Figure B5. Set 67, $\Delta K = 5.5\ MN/m^{3/2}$, wet air environment.

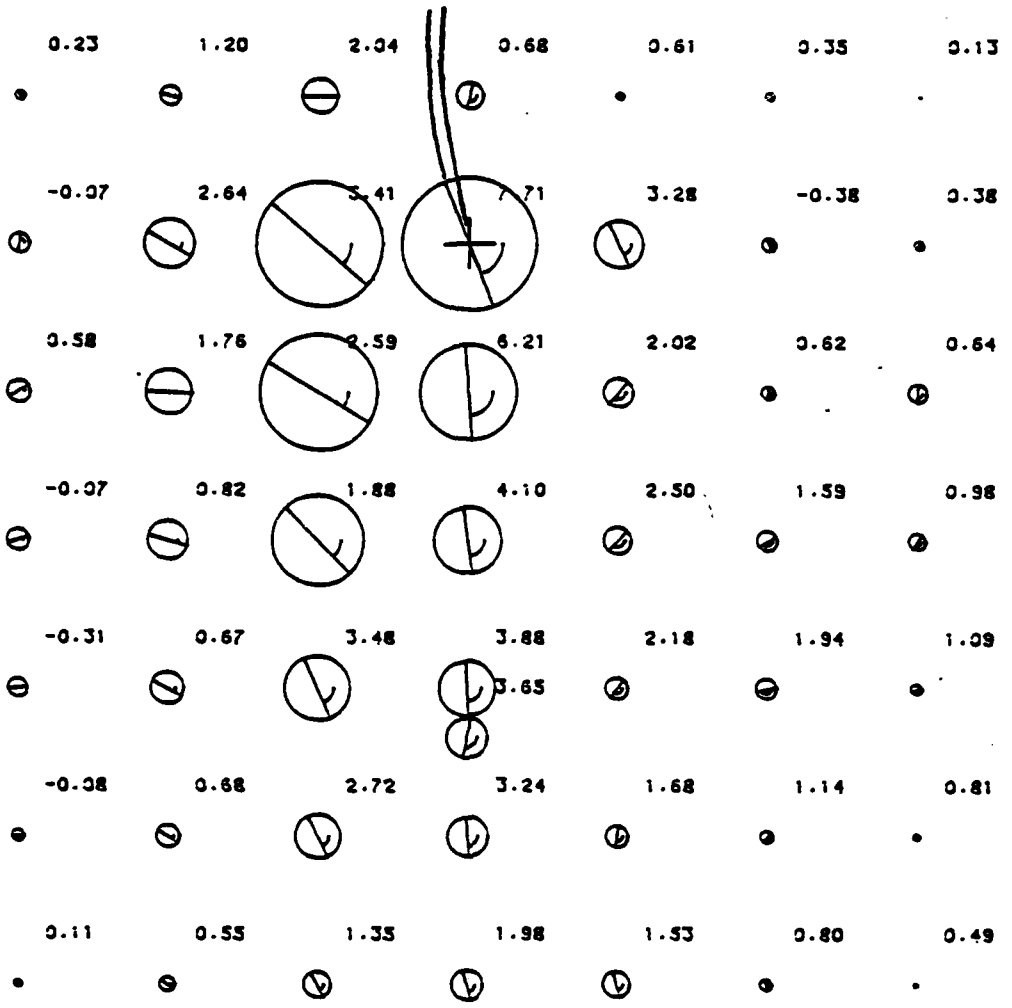

Figure B6. Set 70, ΔK = 8 $MN/m^{3/2}$, vacuum environment.

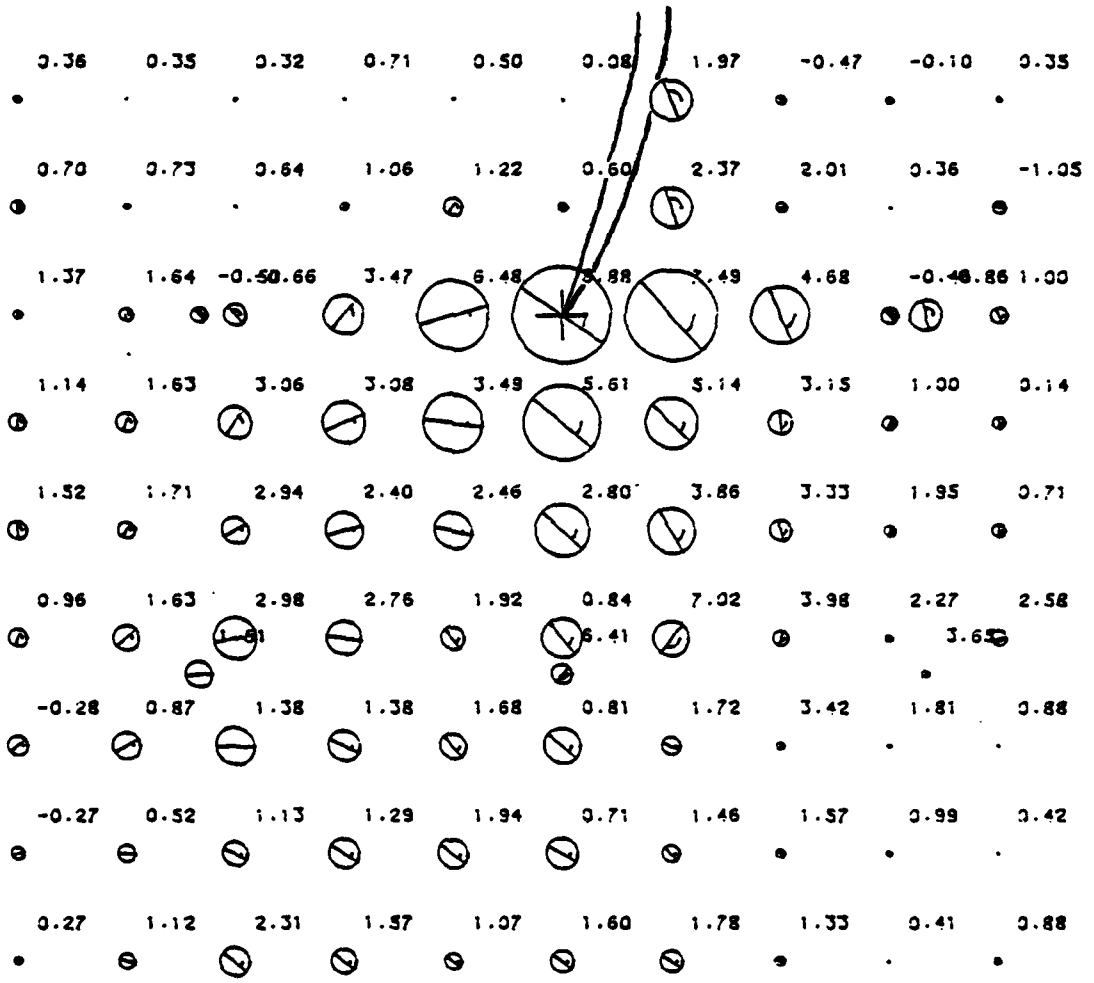

Figure B7. Set 73, ΔK = 11 $MN/m^{3/2}$, vacuum environment.

[redacted]

[redacted]

by

J. Lankford and D. L. Davidson

ABSTRACT

Fractographic analysis of fatigue crack growth in 7075-T6 ingot and MA-87 powder metallurgy aluminum alloys is combined with high resolution, dynamic observation of crack tip deformation and opening. It is found that below the Paris regime, in both moist air and vacuum, crack growth does not proceed cycle-by-cycle, but is incremental. Crack extension is a two-stage process which produces a striation, but only after a number of cycles during which the crack blunts and accumulates local strain damage near the tip, followed by an increment of "brittle" crack extension. The effect of moist air is to reduce the plasticity required for an increment of crack extension, hence the number of blunting cycles preceding crack extension. Implications for analytical crack growth models based on crack tip micromechanics are discussed.

INTRODUCTION

The growth of fatigue cracks in aluminum alloys has been a subject of research for several decades. Despite this concerted effort, the precise set of circumstances corresponding to incremental crack extension remains something of a mystery. This is unfortunate, since knowledge of these circumstances is required in order to fashion valid predictive crack growth models. Thus, the many different models which have been developed are all based on varying assumptions regarding the criteria for, and micromechanism of, crack advance. Most of what is known about crack advance has derived from the interpretation of fatigue fracture markings, observed either by means of scanning electron microscopy (SEM), or by transmission electron microscopy (TEM) of carbon replicas. In addition, a few experimentalists have carried out TEM studies of thin foils containing both the fatigue fracture surface and its adjoining deformed substrate.

The authors have recently begun to study crack advance at high resolution under dynamic conditions, by use of a special servo-controlled, hydraulically-actuated cyclic loading machine which fits inside the SEM specimen chamber [1]. The results of investigations carried out on wrought 7075-T651 aluminum alloy [2] and MA-87 [3], a powder metallurgy alloy of nearly the same chemical composition, have indicated that crack advance takes place intermittently. That is, the crack tip will tend to open and close for a number of cycles, and then extend a small distance on the next cycle. Repetition of this process causes incremental crack advance requiring multiple cycles, the number of cycles decreasing with increasing cyclic stress intensity ΔK.

In order to model this process quantitatively, it is necessary to specify the conditions at the crack tip at the time the crack advances, and to determine the distance by which the crack extends. Furthermore, any required assumptions should be compatible with the fractographic evidence. Therefore, an SEM fractographic analysis of fatigue crack growth in 7075-T651 and MA-87 alloys has been carried out. This study was supplemented by correlation with the results of other investigators who have employed thin foil TEM, and SEM and TEM replica fractography. In addition, crack tip opening displacement and crack tip opening mode were established with the aid of the SEM cycling stage. All of these factors were utilized in constructing a basic scenario of crack advance.

The present study provides a physical basis for quantitative models, presented elsewhere [2,3], of fatigue crack growth in 7075-T651 and MA-87. A valuable companion to this series of papers is the recent Air Force Materials Laboratory report [4] by Doerr, which provides an extensive, detailed comparison of the microstructures and material properties of the two alloys.

II. MATERIALS

Both materials were fabricated by Alcoa; the 7075 alloy was obtained commercially as a rolled, 6 mm-thick plate in the T651 condition, while the MA-87 was received directly from Alcoa as part of an ingot from an experimental heat. Nominal compositions and yield strengths are shown in Table I. The microstructure of the 7075-T651 plate consisted of pancake grains approximately 130 x 60 x 18 μm, with the longest grain dimension in the rolling direction. Material characterization of MA-87 is more

TABLE I

MATERIAL CHARACTERIZATION

Alloy	Heat Treatment	Composition	Yield Strength (MPa)
7075	T651	Al-5.6Zn-2.5Mg-1.6Cu	508
MA-87	T6 + 14 hrs. @ 162C	Al-6.5Zn-2.5Mg-1.5Cu-.8Co	503

complicated. When the present material was obtained in 1977, it was called MA-87; the current Alcoa X7091 is essentially the same alloy. The initial compact, made from air-atomized powder, was ABC-triple upset-forged and extruded. The resulting microstructure consists of irregularly shaped grains in the size range 5-30 μm, elongated in the extrusion direction.

III. EXPERIMENTAL PROCEDURE

Cracks oriented normal to the rolling (7075-T651) and extrusion (MA-87) directions were nucleated in single-edge-notch specimens of gage section 3-mm thick x 21-mm wide. Load shedding in small load increments was used to reach near-threshold rates of growth, and subsequent crack growth was carried out at a stress ratio of approximately 0.15. Test environments consisted of laboratory air at a relative humidity of approximately 50%, and vacuum of $<10^{-5}$ torr. Crack growth was monitored optically with a 100X microscope.

Observation of the tips of cracks grown in the moist environment was performed within the SEM cycling stage only during the first few cycles following transfer from the laboratory fatigue machine to the SEM. Fractographic observations of striations have shown [5] that during these first few cycles, crack tip extension is essentially unaffected by the vacuum of the SEM.

In order to fully characterize crack tip yielding, high magnification photographs were taken of the tips at both minimum and maximum load. These photographs were analyzed by the stereoimaging technique [6,7], to yield local material displacements within the plane of the specimen surface

both normal and parallel to the loading axis, which in turn provided accurate values for crack tip strains, crack tip opening displacements (CTOD), and opening modes. The strain and CTOD data have been reported in detail elsewhere [2,3]; the present work will use only the best-fit relationships.

Following crack growth tests, the specimens were broken open, and their fatigue fracture surfaces characterized using the SEM. In order to optimize resolution, the surfaces were palladium coated.

IV. RESULTS

A. Fractography

All of the microfractographic features described below were observed uniformly over the entire fracture surface. This suggests that the same mechanisms of fatigue fracture are characteristic of both the surface and interior regions of the specimen, and that surface observations of crack tip behavior should be relevant in the interior as well.

1. 7075-T651

The fractography of 7075-T651 was found to be surprisingly complex. The fracture surface formed in air is characterized by periodic structures (Figure 1; in this, and subsequent photos, the large arrow indicates the direction of crack growth), which are present at all stress intensities, and whose average spacing increases with ΔK. However, these features cover only part of the fracture surface, most of which, for $\Delta K \gtrsim 6\ MNm^{-3/2}$, is composed of much finer micro-striations (Figure 2). These striations are not easily resolved in the SEM, and it is necessary to tilt the specimen about in order to bring them into view. Some evidence of fine striations lying upon the coarser periodic structures was seen, but

their resolution was more difficult than in the surrounding regions. For ΔK less than about 6 $MNm^{-3/2}$, striations were basically unresolvable, and the surface consisted of what appear to be cyclic cleavage facets (Figure 3).

Changing the environment from air to vacuum in this low stress intensity regime produces the fractographic profile shown in Figure 4. On the vacuum side of the transition, sharply angled facets are superimposed upon a predominant, uniform field of what might be termed "coarse" striations. The facets disapper above $\Delta K \approx 7$ $MN^{-3/2}$, and subsequent fatigue crack growth is characterized primarily by coarse striations (Figure 5). The striations are considered coarse because of the fact that they actually are made up of still finer striations, as shown in Figures 6 and 7. Frequently, the coarse striations do not form at all, and regions of the fracture surface are composed entirely of the fine striations (lower portion of Figure 7). Since the fine striations seem to serve as subunits of the coarse ones, and can form in their absence, they are considered to be more directly related to incremental crack advance.

2. MA-87

Striations are associated with fatigue crack growth in MA-87 over the entire ΔK range studied, for both vacuum and air. In the air environment, striations appear fairly straight and clean-edged (Figure 8), while in vacuum, they have more of a "ripple" to their profile (Figure 9). Macroscopically, the fracture surfaces in these two environments are startlingly dissimilar, as shown in Figure 10. The vacuum surface looks much smoother, although close inspection at high magnification shows that the surface is covered with uniformly distributed fine striations. Also present is a dispersion of fine particles, ranging from irregularly shaped, ~0.1 μm in size (Figure 9), to smooth and almost

spherical, ~ 1.5 μm in diameter. Some of these larger particles are found in clusters (Figure 11); close examination of these provides information regarding their origin, since the particles obviously exist in various stages of evolution. In Figure 11, several smooth, flat platelets (arrow, P) can be seen. From one of these, a spherical particle (a) has detached itself, and other, similar particles are separating at b and c.

Particles such as those described here also were observed on the MA-87 air fracture surface. However, they were never found in clusters, and usually were seen as rather widely separated, discrete entities.

B. Correlation of Crack Extension Parameters

1. 7075-T651, Air

Parameters which may be relevant to crack extension in 7075-T651 in air are shown in Figure 12. The "periodic" structures described earlier are several orders of magnitude larger than the average per cycle crack extension $^{da}/dN$, and increase more gradually with ΔK than does $^{da}/dN$. Also shown are data derived from SEM observations by Kirby and Beevers [8], for 7075-T651. The latter termed the periodic features which they observed striations but, as was noted earlier, SEM resolution of the small microstriations in 7075-T651 is fairly difficult. This conclusion is supported by TEM replica observations by Wanhill [9], Broek [5], and Vogelesang [10], each of whom studied 7075-T6* air-environment fatigue fractography, and obtained results in agreement with the present microstriation spacings shown in

*Within the present context, 7075-T6 and 7075-T651 are essentially identical.

Figure 12. Included for comparison is the line which fits the extensive TEM striation measurements by Broek [5].

A limited amount of relevant thin foil transmission electron microscopy has been carried out by Wanhill [9], who published the spacings of periodic dislocation substructure bands located just beneath the fracture surface; these data, for ΔK = 7-7.8 $MNm^{-3/2}$, are included in Figure 12. It is evident that the dislocation band spacings correspond quite closely to the fine-striation spacings, and at ΔK = 8 $MNm^{-3/2}$, exceed only slightly the average crack growth rate. However, as ΔK decreases, so does the margin by which the striations and, presumably, the dislocation band spacings, surpass da/dN.

To determine the CTOD-ΔK relationship, the opening displacements parallel and perpendicular to the loading axis, COD_x and COD_y, respectively, were accurately measured using stereoimaging [6,7]. The total crack opening, COD, is the vector sum of the two individual components. In this paper, the crack tip opening displacement (CTOD) is defined as the value of COD 1 μm behind the crack tip.

As shown in Figure 12, there is reasonably good agreement between striation and dislocation band spacing and CTOD, but the values do not agree with corresponding average crack growth rates. At low stress intensities in particular, striation spacings exceed da/dN by approximately an order of magnitude. Measurements [2] of $CTOD_x$ and $CTOD_y$ show that the Mode I component dominates, accounting for roughly 0.9 of the CTOD.

2. 7075-T651, Vacuum

The coarse striations behave similarly (Figure 13) to the periodic structures characteristic of air. However, the fine striations display very little sensitivity to ΔK, certainly much less than that found in air. At ΔK = 7-7.8 $MNm^{-3/2}$, there again is good agreement between striation spacing and the underlying dislocation band spacing established independently by Wanhill [5]. Below $\Delta K \approx 20$ $MNm^{-3/2}$, the striation spacing exceeds the average crack growth rate by from one to three orders of magnitude.

Crack tip opening displacement is found to be quite sensitive to ΔK in vacuum, as shown in Figure 13. Moreover, unlike the situation which prevails in air, CTOD does not correlate with striation spacing. It was found [2] that Mode I opening still predominates, being roughly 80% of the total, although this represents a slightly greater tendency to shear than that found in air.

3. MA-87, Air

For the powder metallurgy alloy, CTOD and striation spacing in air follow similar ΔK dependencies (Figure 14), as they did for 7075-T651. However, contrary to the case for the ingot alloy, the MA-87 curves no longer coincide, but are displaced, with the CTOD exceeding the corresponding striation spacing by a factor of about four. Striation spacing and $\frac{da}{dN}$ coincide at $\Delta K \approx 10$ $MNm^{-3/2}$, but diverge rapidly at lower cyclic stress intensities. Crack tip openings are much large in air for MA-87 than for 7075-T651 (compare the CTOD curves in Figures 12 and 14), and the Mode II component of CTOD is much greater, accounting for roughly 48% of the total crack tip opening [3].

4. MA-87, Vacuum

In vacuum, CTOD and striation spacing have a different ΔK-dependency (Figure 15) than for air, behavior which is similar to that of 7075-T651, even to the extent that CTOD is more sensitively dependent on ΔK. For $\Delta K < 10$ $MNm^{-3/2}$, striation spacing and CTOD exceed the average crack growth rate by several orders of magnitude, and the crack opening mode mix is similar to that in air [3].

V. DISCUSSION

To facilitate discussion, the relationships between fractography, substructure, crack tip opening, and crack growth rate have been drawn to scale for each alloy and environment combination at $\Delta K = 7.5$ $MNm^{-3/2}$, this being the only stress intensity for which substructure data [9] are available. The specific relevance of these parameters to the crack extension process is developed, followed by a general discussion of certain other aspects of parametric behavior, and their implications.

A. Interpretation of Fractography

1. 7075-T651, Air

The two types of fractographic features found for 7075-T651 in air are shown in Figure 16, in which the average crack growth rate is compared with (a) the periodic structures, and also with (b) the fine-striation and dislocation substructural spacings. As noted earlier, striations are found over the entire fracture surface, including the ledges which make up the coarse periodic structures, although the striations on the ledges are more difficult to resolve than elsewhere. The physical reason for the formation of the periodic structures is not evident, but this detail is probably not very relevant to crack advance,

since the overwhelming implication is that an increment of crack growth consists of one striation, or dislocation substructure, spacing. Further, since this spacing is twice the macroscopic crack growth rate, evidently an average of two cycles are required to cause crack extension over a distance of approximately one CTOD (Figure 16c).

Earlier, Bowles and Broek [11] performed transmission electron diffraction pattern analysis of the orientation of the fracture plane in striated regions of 7075-T6 fatigued in air. Their study showed that in every case, the planes were of the {110} type; it is assumed that the same situation prevails in the present study. This being the case, the results of the recent fatigue study of 7010-T76 in moist air by Nix and Flower [12] should be relevant, since in this work, it was likewise found that the striated fracture plane was {110}. In particular, it was firmly established that the heavily dislocated regions constitute the leading edges of striations, while the dislocation-free regions corresponding to the trailing edges were {110}. The formation of each was thus a two-step process, involving first plastic flow and blunting, followed by brittle separation {110}. Here the term brittle means simply that few dislocations remain after crack passage [12].

This description of crack advance also should be applicable to 7075-T651 in air, with the exception that more than two cycles generally are required for crack advance. For the selected stress intensity, 7-8 $MNm^{-3/2}$, the process apparently is, in fact, just as envisaged by Nix and Flower: one cycle to blunt plus one cycle to extend. However, at lower cyclic stress intensities, for example, $\Delta K = 5\ MNm^{-3/2}$,

the striation spacing is approximately 0.1 μm, or about 5 times the corresponding crack growth rate of 0.02 μm. This implies that the crack blunts for at least 4 cycles before extending. The proposed concept of intermittent, rather than continuous, crack extension, is supported even more strongly by the results of crack growth tests in vacuum.

2. 7075-T651, Vacuum

In vacuum, fine striations, with their corresponding substructures, are superimposed upon coarser ones (Figure 17). Observation of crack growth within the SEM suggests that the coarse striations may be related to crack branching (Figure 18), or to local changes in crack direction. Incremental extension, however, is observed only on a much finer scale.

As for crack growth in air, it is apparent that the primary elements of crack extension in vacuum are the fine striations and their associated substructures. These striations, however, unlike those formed in air, probably are not crystallographic. Nix and Flower [12] could not resolve striations in vacuum for 7010-T76, but were able to determine that the fracture surface was non-crystallographic. In the present case, stereophotographs of the fine striations formed in vacuum showed that they are not flat; rather, the striations are rounded in profile, suggesting a non-crystallographic process of formation.

The striation and dislocation substructure spacings (Figure 17a) again show excellent agreement, and are equal to approximately twice the CTOD (Figure 17b). However, all three of these factors are greatly in excess of the average macroscopic crack growth rate, the striation/dislocation substructure spacings exceeding $^{da}/_{dN}$ by a factor

of 43. This implies that 43 cycles were required to produce 0.3 μm of crack extension, a discrete event which probably occurred on the forty-third cycle. It was observed during dynamic cycling in the SEM that the crack tip was usually increasingly blunt at the peak loading (K_{max}) with each successive cycle. Thus, it appears that the crack spends most of the imposed stress cycles in blunting, with crack growth finally taking place when the material in the immediate vicinity of the tip has either become unstable, or has exhausted its ability to blunt. The foregoing analysis suggests, for example, that at $\Delta K = 5$ MNm$^{-3/2}$, as many as 1000 blunting cycles would be required in order to extend the crack, on the next cycle, by 0.25 μm.

3. MA-87-Air

At $\Delta K = 7.5$ MNm$^{-3/2}$, the powder metallurgy material seems to behave similarly to the ingot 7075-T651 alloy, in that the striation spacing exceeds the average crack growth rate by a factor of 2, while $CTOD_x$ is about 1.9 times the average striation spacing (Figure 19a). On the other hand, there are no large-scale periodic structures, and the CTOD (Figure 19b) is both larger, and has a much larger Mode II shear component, than is the case for the ingot alloy. The MA-87 striations have a profile similar to that characteristic of the 7075-T651 in air, suggesting that fatigue microfracture likewise might be crystallographic on {110}. However, this has not been verified. Although for $\Delta K = 7.5$ MNm$^{-3/2}$, crack extension again requires at least two cycles, in accord with the concept of Nix and Flower, many cycles obviously would be required at lower stresses

AD-A122 960 CRACK TIP PLASTICITY ASSOCIATED WITH CORROSION ASSISTED FATIGUE(U) SOUTHWEST RESEARCH INST SAN ANTONIO TX D L DAVIDSON ET AL. 15 NOV 82 N00014-75-C-1038 2/2

UNCLASSIFIED F/G 11/6 NL

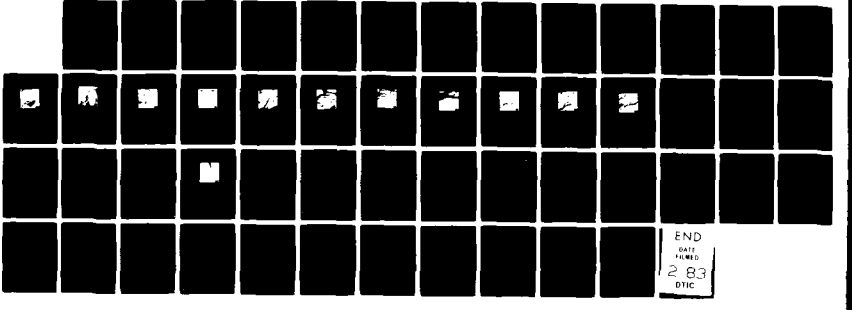

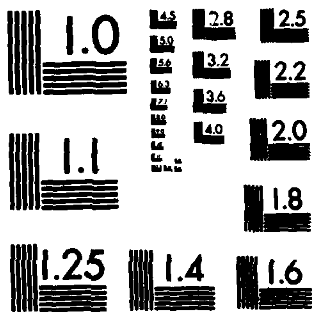

MICROCOPY RESOLUTION TEST CHART
NATIONAL BUREAU OF STANDARDS-1963-A

intensities. In the latter ΔK-range, observation of crack tips loaded in the SEM shows that on a typical cycle, the crack tip is blunt, in accordance with the multiple cycle blunting-brittle extension sequence discussed previously.

4. MA-87, Vacuum

In vacuum, the MA-87 crack tip opening displacement is nearly identical to that found in air, but the striation spacings are twice as large, and the macroscopic crack growth rate is lower by a factor of almost 10 (Figure 20), than the corresponding parameters in air. At a cyclic stress intensity of 7.5 $MNm^{-3/2}$, 37 cycles would be required to achieve a crack growth increment equal to one striation. Observation of crack growth in the SEM again shows that generally, the crack tip is blunt, and that numerous cycles of blunting precede an increment of crack extension.

B. General Discussion

The major implication of the preceding discussion is that fatigue crack growth is intermittent, rather than continuous. This is an extremely important concept in terms of the analytical modeling of crack advance, since nearly all existing models share the critical assumption that crack advance occurs on each cycle. The present work suggests, on the contrary, that within the threshold-to-Paris law transition region, the crack tip blunts, but does not extend, for many consecutive cycles. Since blunting requires significant plastic strain at the tip, it seems reasonable to suppose that crack extension corresponds to the inability of the material at the crack tip to yield one more time without fracturing. Several crack tip models [13-19] do require a critical crack tip strain

for extension. However, the present results suggest that for the regime $\Delta K_{Threshold} < \Delta K \lesssim 10\ MNm^{-3/2}$, the only relevant models are those [17-19] which account for the accumulation of damage at a temporarily stationary crack tip. These models all can be written in the form

$$da/dN = \frac{\Delta a}{\Delta N} \qquad (1)$$

where Δa is an increment of extension which the present results suggest is equal to a striation spacing, and ΔN is the number of low cycle fatigue cycles required to fail the material over the distance Δa. The problem of the modeler is to somehow determine the forms which Δa and ΔN should take. This is not the same as incorporating damage which occurs cumulatively within material elements ahead of a steadily advancing crack tip [13-16].

As an alternative to the proposed concept of intermittent crack growth, one might suggest that crack growth is actually continuous, but on too small a scale to be resolved. However, this is contrary to the experimental evidence in several regards. First, the intermittent crack growth process has been clearly observed (unpublished work) in the SEM for several aluminum alloys such as 6061-T6 and IN 9052, for which the increment of crack advance was found to be fairly large, hence readily discernible. Secondly, continuous advance would require that the brittle second step in the crack extension process take place over many cycles. Hence, on any such cycle when the crack is observed, the tip would be sharp. Yet, the general SEM observation, cycle after cycle, was that the crack tip was blunt. Finally, if crack advance does occur on a substriation level, how does one account for the striation and its underlying dislocation structure?

It is interesting to observe that most, if not all, existing models of crack growth do not include the effect of environment. Strictly speaking, the models are most relevant to crack growth in a vacuum. Ironically, however, the present results indicate that the fundamental assumption of more-or-less continuous crack advance is satisfied only in moist air, and then only for $\Delta K \gtrsim 8$ MNm$^{-3/2}$. The "embrittling" effect of hydrogen [20] in the moisture entrained in the air apparently derives from its reduction of the critical strain for crack tip advancement [2,3], hence the number of cycles required to achieve the condition for crack advance. Under the above stress intensity/environmental conditions, striation spacings and the average crack growth rate approach 1:1 correspondence. On the other hand, since the models do not explicitly include the effect of hydrogen, any agreement between experiment and theory seems rather fortuitous.

The authors have combined the concept of intermittent crack advance with detailed measurements of local crack tip strains to develop an analytical model, presented elsewhere [2,3]. The latter analysis incorporates into its extension criterion the concept of a number of cycles being required to achieve the condition for an increment of crack advance. The model will not be developed here, but certain additional factors derived from the present work are relevant to the modeling effort, and will be discussed briefly.

For uniaxial tensile loading, it is assumed that the crack tip opens in Mode I; an analysis by Broek for this situation yields [21]

$$\text{CTOD} = 4(1+\nu)\left(\frac{K_I}{E}\right)\sqrt{r/2\pi}\,\sin\frac{\theta}{2}\left[2-2\nu-\cos^2\frac{\theta}{2}\right] \qquad (2)$$

where K_I is the Mode I stress intensity factor, E is Young's modulus, ν is Poisson's ratio, θ is the angle between the crack plane and the point being analyzed with the crack tip as the vertex, and r is the distance to the point being analyzed. For the loading conditions used in our experiments, $K_I = K_{max}$, $\theta = \pi$, and $r = 1$ μm; using the appropriate values for E and ν, the theoretical opening mode CTOD for $\Delta K = 7.5$ $MNm^{-3/2}$ turns out to be 0.29 μm for both materials.

As shown in Table II, this prediction is fairly realistic for 7075-T651, with $CTOD_x^{Theory}$ somewhat exceeding $CTOD_x^{Exp}$ for both air and vacuum. Since the Mode II crack opening component is relatively small (Figure 16c), Equation (2) is also a fairly good representation of the total crack tip opening displacement $CTOD^{Exp}$. The agreement between the theoretical and experimental crack tip opening displacements is not surprising, considering the basis for the calculation, and the actual deformation conditions at the crack tip. In deriving Equation (1), it was assumed that crack tip plasticity makes a negligible contribution to crack opening, so that the predicted displacement is based on elastic response. This is not a bad approximation to experimental findings at low ΔK; strain measurements reported elsewhere [2] indicate that for 7075-T651 in both air and vacuum, the maximum crack tip shear strain at $\Delta K = 7.5$ $MNm^{-3/2}$ is only .02-.04.

On the other hand, maximum shear strains at the tips of MA-87 cracks in air and vacuum reach nearly 0.2 at $\Delta K = 7.5$ $MNm^{-3/2}$[3] and, as noted earlier (Figures 16b and 20b), the cracks open in mixed Modes I and II, with a very large Mode II component. This apparently destroys the

TABLE II

CRACK TIP OPENING 1 μm FROM CRACK TIP,
$\Delta K = 7.5\ MNm^{-3/2}$

Material	Environment	$CTOD_x^{Exp(\dagger)}$	$CTOD_{Eq\ (2)}^{Theory}$	$CTOD^{Exp(\dagger\dagger)}$
7075-T6	Air	0.238	0.29	0.25
7075-T6	Vacuum	0.17	0.29	0.2
MA-87	Air	0.47	0.29	0.9
MA-87	Vacuum	0.54	0.29	0.9

† $CTOD_x^{Exp}$ = the measured value of CTOD in the loading direction.

†† $CTOD^{Exp}$ = the combined x and y CTOD measurements.

validity of the Mode I CTOD correlations, and the relatively large-scale crack tip plasticity invalidates the linear elastic approximation implicit in Equation (2). Thus, $CTOD^{Theory}$ underestimates $CTOD_x^{Exp}$ in MA-87 by about a factor of 3 (Table II).

The magnitude of the CTOD may be important, because of its use in models to predict crack advance. For example, several recent micromechanical models [2,3,18] are based on the premise that an increment of crack extension is proportional to CTOD, i.e., that

$$\Delta a = \alpha CTOD \tag{3}$$

where α is an alloy- and environment-sensitive, but ΔK-insensitive, constant. The validity of this concept can be investigated as follows.

The preceding fractographic analysis, as well as direct observation, suggest that crack growth is intermittent, and that when the crack extends, it creates a striation; thus, Δa = striation spacing, and

$$\alpha = \frac{\text{striation spacing}}{CTOD} \tag{4}$$

Since both striation spacing and CTOD are known as functions of ΔK (Figures 12-15), these relationships can be used in Equation (4) to determine $\alpha(\Delta K)$. Results of this calculation for the two alloys are shown in Figure 21. It is evident that in air, α is independent of ΔK, and is equal to .65 and .26 for 7075-T6 and MA-87, respectively. However, in vacuum, α is inversely proportional to ΔK, with an average value, for 6 $MNm^{-3/2} < \Delta K \leq 10$ $MNm^{-3/2}$, of ~1.5 for 7075-T6, and .55 for

MA-87. It is not known why this difference between air and vacuum environments exists. However, it should be noted that values of α in excess of unity do not mean that the crack is actually extending an especially large distance. This regime, for 7075-T6 at $\Delta K \gtrsim 9$ $MNm^{-3/2}$, corresponds to such very small crack tip opening displacements that, despite the relatively large values of α, the crack growth increments (striation spacings) are correspondingly small.

It should be emphasized that Equation (3) is only an hypothesis. The true physical determinant of the crack extension distance may well be related to the development of a region of material instability just ahead of the crack tip, or to the dimensions of a critically strained region at the crack tip. Exactly how the crack lengthens is still not known. Continued efforts to measure crack tip parameters, and to characterize near crack tip material behavior,may lead to a more fundamental understanding of the crack advance mechanism.

Finally, it is interesting to briefly consider the unusual behavior of MA-87 crack tips in vacuum. The fracture surfaces, although striated, exhibit evidence of extensive Mode II motion, especially in terms of the spherical particles. To the knowledge of the authors, these have previously been observed only in situations involving either fretting fatigue [22], rolling contact wear [23], or pure Mode II fatigue crack growth [24]. It is interesting that the spheres were not observed in air to the same extent that they were in vacuum. Since the crack tip opening in air also possesses a large Mode II component, it appears that continuous oxidation may alter the mechanism of sphere formation. Specifically, it may impede the formation of the sphere nuclei, the smooth,

flat platelets labeled (P) in Figure 11. These flakes resemble microscopic Beilby layers, mirror-like regions which have been cold worked in the extreme, thereby becoming almost amorphous, while still retaining the chemical composition of the parent material. Such layers have been identified [24] as the nuclei of spherical wear debris in both fretting fatigue and rolling contact. In air, smaller particles are generated on the crack surface, and are even pushed out of the crack by Mode III motion [26]. Although intrinsically interesting, it is not evident that these processes are major factors in controlling macroscopic crack growth rate, since the air versus vacuum crack growth rate differential for MA-87 is roughly the same as that for 7075-T651, which does not develop wear particles.

VI. CONCLUSIONS

The preceding results and interpretation support the following conclusions regarding fatigue crack growth in 7075-T651 and MA-87 aluminum alloys:

1. Fatigue crack growth is intermittent.
2. Crack growth proceeds by a process of repetitive crack tip deformation and blunting, culminating in an increment of crack extension requiring very little additional deformation.
3. A striation corresponds to a single increment of fatigue crack growth.

4. More crack tip loading cycles are required for incremental crack extension in vacuum than in air, and more are required at lower than higher cyclic stress intensities.
5. An increment of crack extension is equal to from 0.25 to 1.5 times the CTOD 1 μm behind the crack tip.
6. The effect of air is to reduce the plasticity required for an increment of crack extension.
7. Cracks loaded remotely in Mode I actually open in mixed Modes I and II, and for MA-87, the Mode II component predominates in both air and vacuum.
8. If the Mode II crack opening component is sufficiently large, fracture face rubbing can be so extensive as to produce spherical wear debris, particularly in vacuum.

VII. ACKNOWLEDGEMENTS

The authors are grateful to the Office of Naval Research for financial support under Contract Number N00014-75-C-1038, and to Dr. Philip Clarkin, Contract Monitor, for his encouragement.

REFERENCES

1. D. L. Davidson and A. Nagy, J. Phys. E 11, 207 (1978).
2. D. L. Davidson and J. Lankford, Fat. Eng. Mat. Struct. (submitted).
3. Ibid.
4. S. H. Doerr, "A Comparison of Microstructure and Properties of Equivalent Strength Ingot Metallurgy and Powder Metallurgy 7XXX Aluminum Alloys," AFWAL-TR-81-4068 (1981).
5. D. Broek, "Some Contributions of Electron Fractography to the Theory of Fracture," NLR-TR-72029U, National Aerospace Laboratory NLR, The Netherlands (1972).
6. D. L. Davidson, in Scanning Electron Microscopy/1979/II, SEM, Inc., AMF O'Hare, IL, 79 (1979).
7. D. R. William, D. L. Davidson, and J. Lankford, Exp. Mech. 20, 134 (1980).
8. B. R. Kirby and C. J. Beevers, Fat. Eng. Mat. Struct. 1, 203 (1979).
9. R. J. H. Wanhill, Met. Trans. 6A, 1587 (1975).
10. L. B. Vogesang, "Some Aspects of the Environmental Effect on the Fatigue Mechanism of a High Strength Aluminum Alloy," Delft University of Technology, Report VTH-200, Delft, The Netherlands (1975).
11. C. Q. Bowles and D. Broek, Int. J. Fract. Mech. 8, 75 (1972).
12. K. J. Nix and H. M. Flower, Acta Metall. 30, 1549 (1982).
13. B. Tomkins, Phil. Mag. 18, 1041 (1968).
14. H. W. Lin and N. Iino, in Fracture 1969, Chapman and Hall, N.Y., 812 (1969).

15. S. Majumdar and J. Morrow, in Fracture Toughness and Slow-Stable Cracking, ASTM STP 559, 159 (1974).

16. S. B. Chokraborty, Fat. Eng. Mat. Struct. 2, 331 (1979).

17. S. D. Antolovich, A. Saxena, and G. R. Chanani, Eng. Frac. Mech. 7, 649 (1975).

18. J. Lanteigue and J.-P. Bailon, Met. Trans. 12 A, 459 (1981).

19. G. Glinka, Int. J. Fat., 59 (1982).

20. R. P. Wei, P. S. Pao, R. G. Hart, T. W. Weir, and G. W. Simmons, Met. Trans. 11A, 151 (1980).

21. D. Broek, in Elementary Engineering Fracture Mechanics, Noordhoff International Publishing, Leyden, 72 (1974).

22. G. L. Goss and D. W. Hoeppner, Wear 24, 77 (1973).

23. D. Scott and G. H. Mills, Wear 24, 235 (1973).

24. M. C. Smith and R. A. Smith, Wear 76, 105 (1982).

25. D. Scott, W. W. Seifert, and V. C. Westcott, Sci. Amer. 230, 88 (1974).

26. J. Lankford and D. L. Davidson, Met. Trans. (submitted).

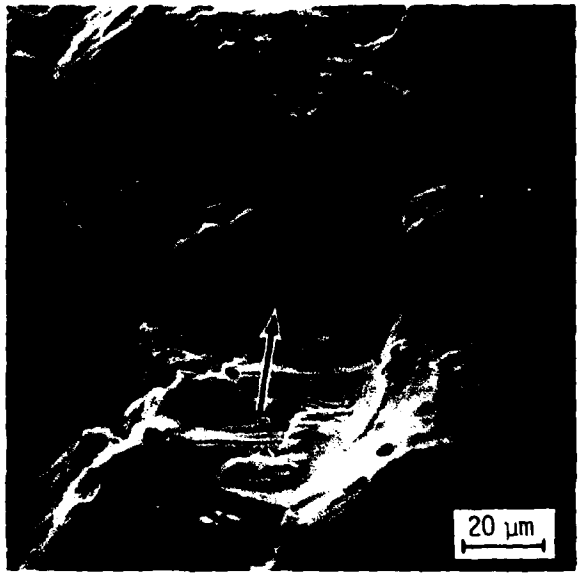

Figure 1. Periodic structures in 7075-T651 at $\Delta K \approx 10$ MNm$^{-3/2}$ in air. Note that structures extend to specimen edge at right.

Figure 2. Striations in 7075-T651 at $\Delta K \approx 7$ $MNm^{-3/2}$ in air.

Figure 3. Cyclic cleavage facets in 7075-T651 at $\Delta K \approx 5$ $MNm^{-3/2}$ in air.

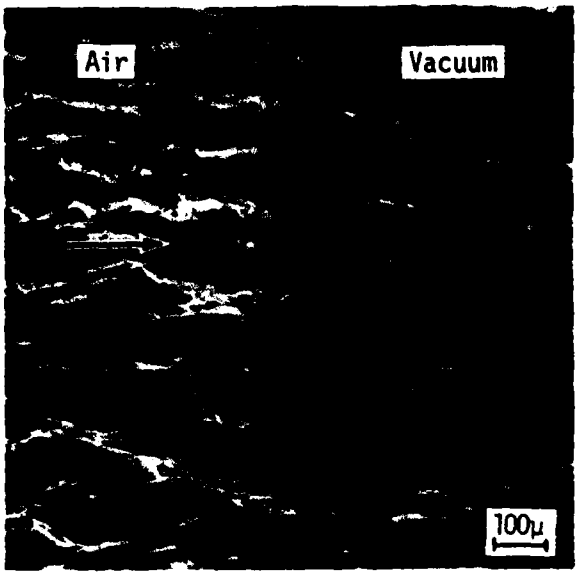

Figure 4. Macroscopic view of air to vacuum transition (dashed line) in 7075-T6 at $\Delta K = 4$ $MNm^{-3/2}$. Note sharply angled facets on the vacuum side of the transition.

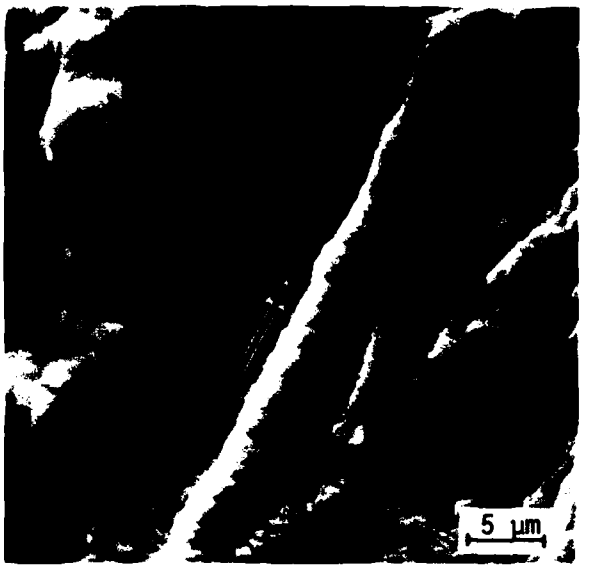

Figure 5. "Coarse" striations in 7075-T651 at $\Delta K = 8\ MNm^{-3/2}$ in vacuum.

Figure 6. Fine striations superimposed on coarse striations in 7075-T651 at $\Delta K \approx 14$ $MNm^{-3/2}$ in vacuum.

Figure 7. Coarse and fine striations in 7075-T651 at $\Delta K \approx 12$ MNm$^{-3/2}$ in vacuum.

Figure 8. Striations in MA-87 at $\Delta K \approx 10$ $MNm^{-3/2}$ in air.

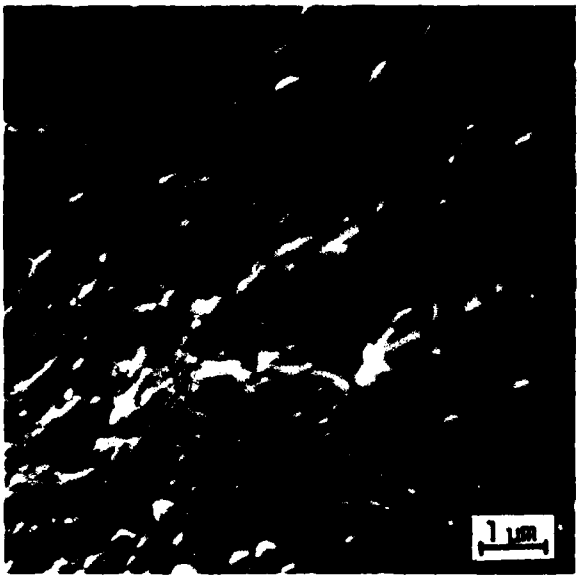

Figure 9. Striations in MA-87 at $\Delta K \approx 6.5$ $MNm^{-3/2}$ in vacuum. Note distribution of small particles on surface.

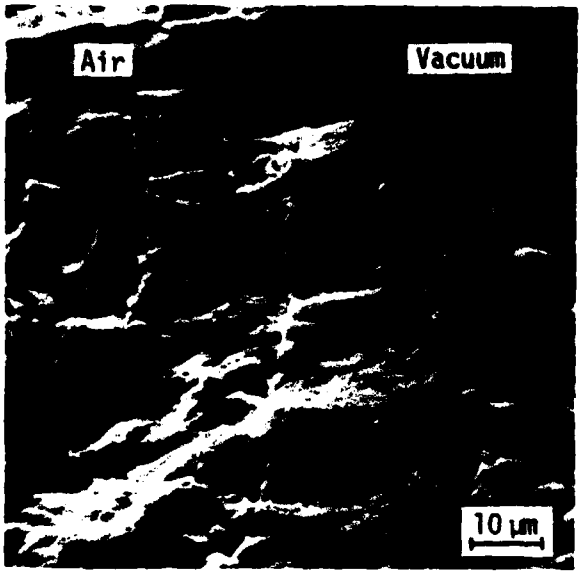

Figure 10. Air to vacuum transition in MA-87 at $\Delta K \approx 4$ MNm$^{-3/2}$.

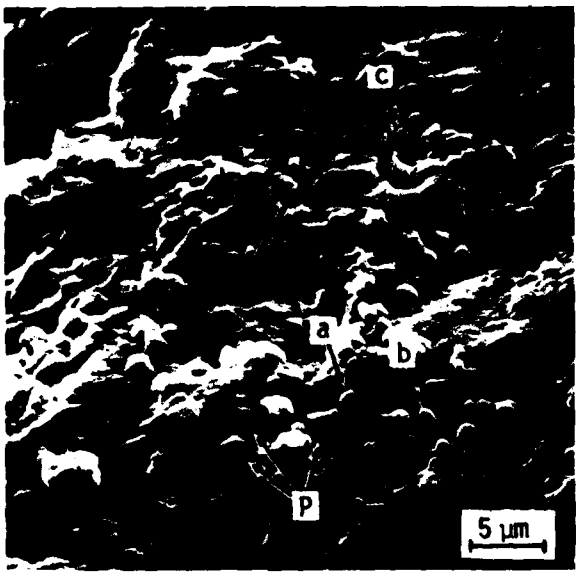

Figure 11. Spherical particles on MA-87 fracture surface at $\Delta K \approx 7$ MNm$^{-3/2}$ in vacuum. "P" indicates smooth, flat platelets, "a" denotes a particle which has detached from a platelet, and "b" and "c" represent particles in the process of forming.

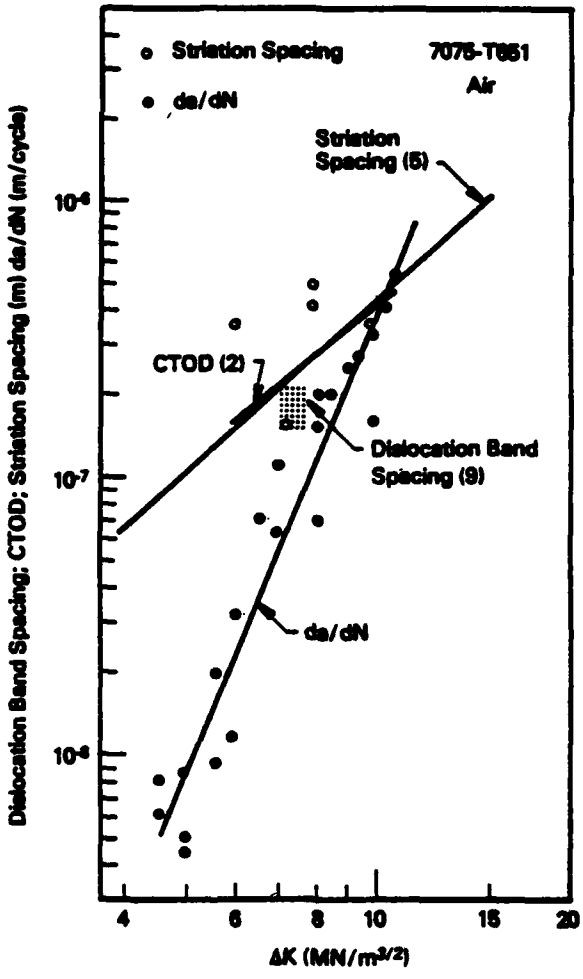

Figure 12. Crack Tip Parameters Versus ΔK for 7075-T651 in air.

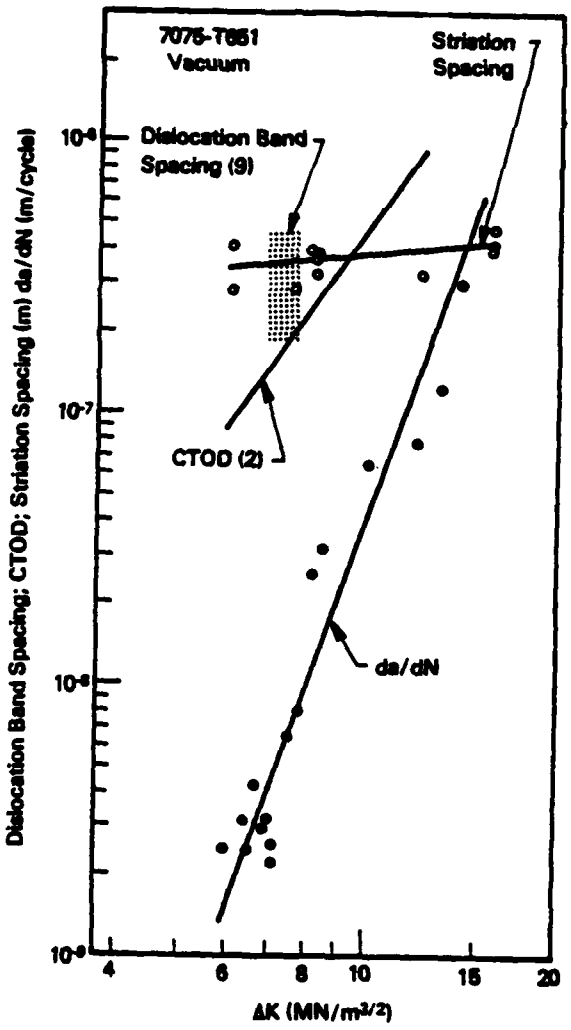

Figure 13. Crack Tip Parameters Versus ΔK for 7075-T651 in vacuum.

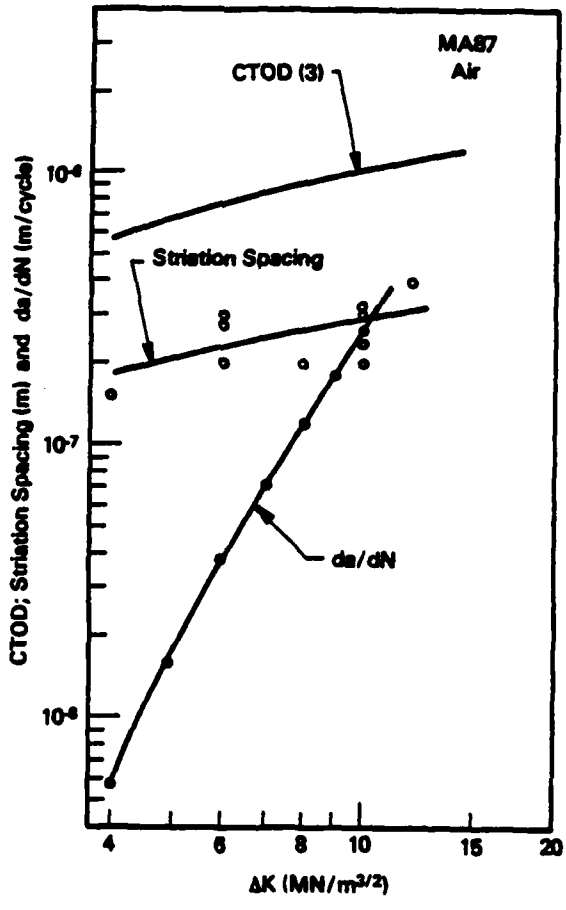

Figure 14. Crack Tip Parameters Versus ΔK for MA-87 in air.

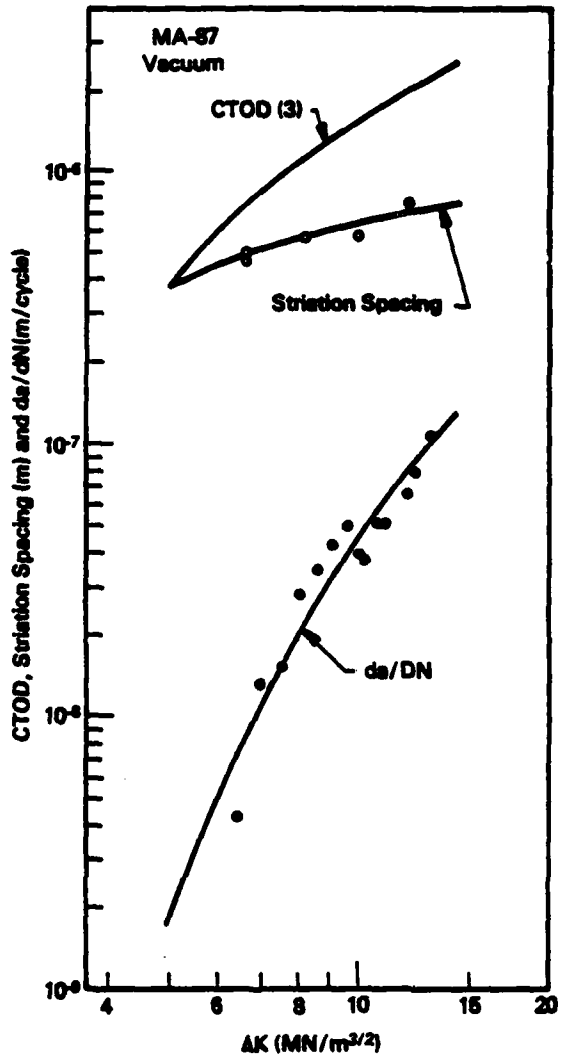

Figure 15. Crack Tip Parameters Versus ΔK for MA-87 in vacuum.

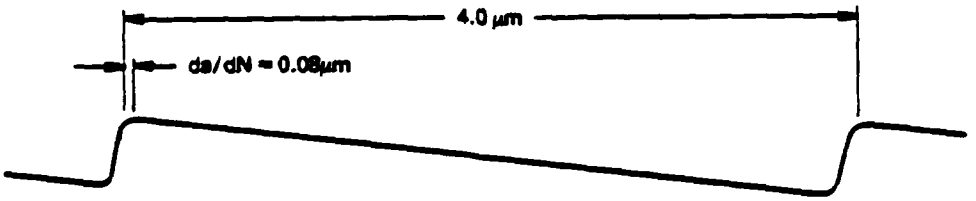

(a) Coarse Periodic Structures

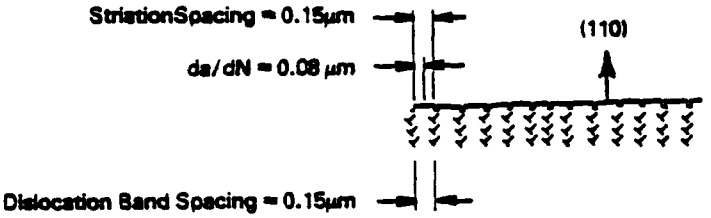

(b) Striations and Dislocation Bands

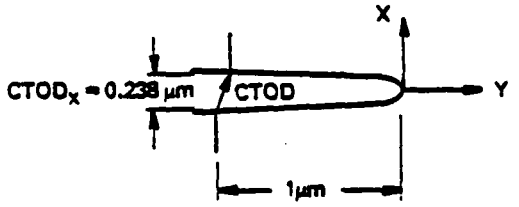

CTOD$_X$ ≈ 1.5x Striation Spacing

≈ 1.5x Dislocation Band Spacing

≈ 3x da/dN

(c) Crack tip opening displacement, showing relative motion of a reference scratch 1 μm behind the tip.

Figure 16. Scaled cross-sectional view of fractographic features for 7075-T651 at ΔK = 7.5 MNm$^{-3/2}$ in air.

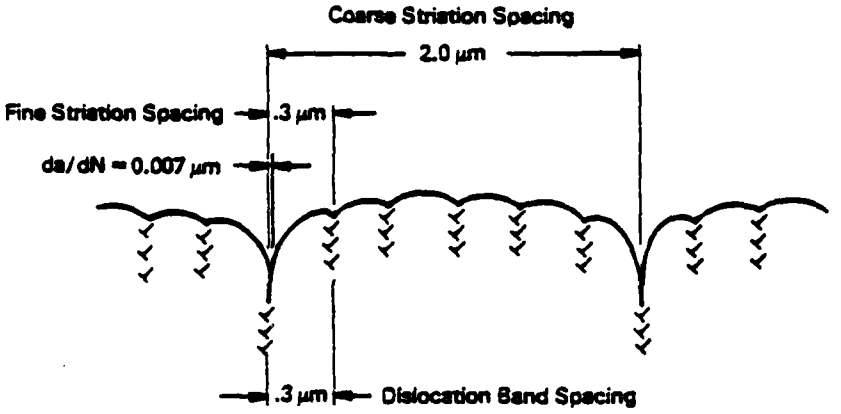

(a) Striations and dislocation bands

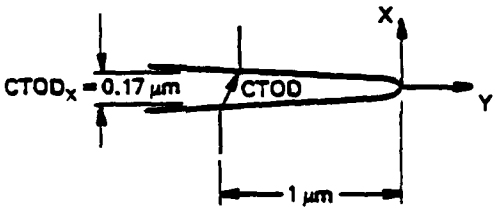

CTOD$_X$ ≈ 5x Striation Spacing

≈ .5x Dislocation Band Spacing

= 24x da/dN

(b) Crack tip opening displacement, showing relative motion of a reference scratch 1 μm behind the tip.

Figure 17. Scaled cross-sectional view of fractographic features for 7075-T651 at ΔK = 7.5 MNm$^{-3/2}$ in vacuum.

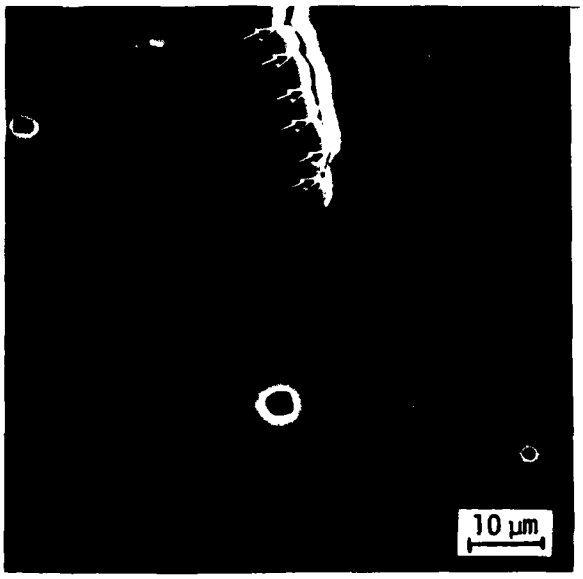

Figure 18. Side view of 7075-T651 crack tip at maximum load, ΔK = 11 $MNm^{-3/2}$, in vacuum. Cusps (arrows) in the crack profile correspond to the "coarse" striation spacing.

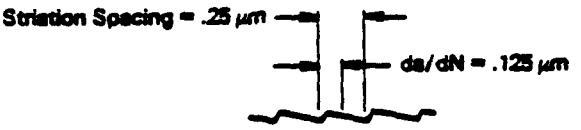

(a) Striations

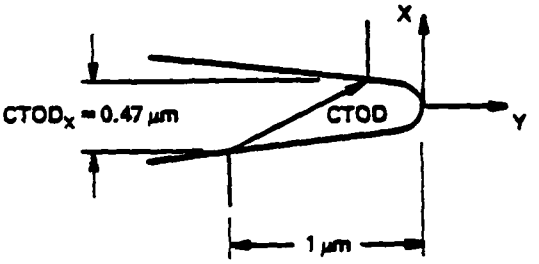

CTOD$_X$ ≈ 2x Striation Spacing

≈ 4x da/dN

(b) Crack tip opening displacement, showing relative motion of a reference scratch 1 μm behind the tip.

Figure 19. Scaled cross-sectional view of fractographic features for MA 87 at ΔK = 7.5 MNm$^{-3/2}$ in air.

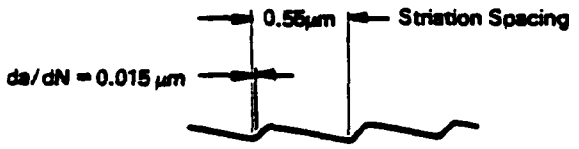

(a) Striations

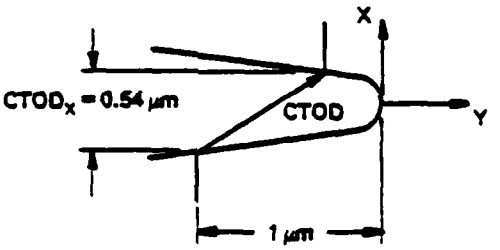

CTOD$_X$ = Striation Spacing

= 37 da/dN

(b) Crack tip opening displacement, showing relative motion of a reference scratch 1 μm behind the tip.

Figure 20. Scaled cross-sectional view of fractographic features for MA 87 at $\Delta K = 7.5$ MNm$^{-3/2}$ in vacuum.

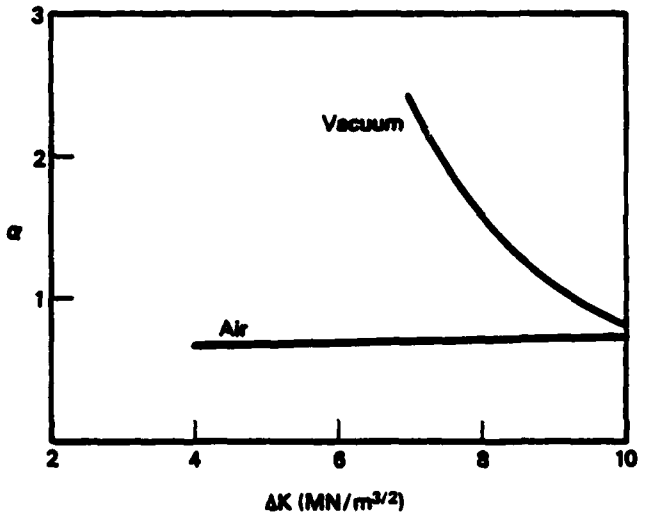

(a) 7075-T6

Figure 21. α versus ΔK for air and vacuum.

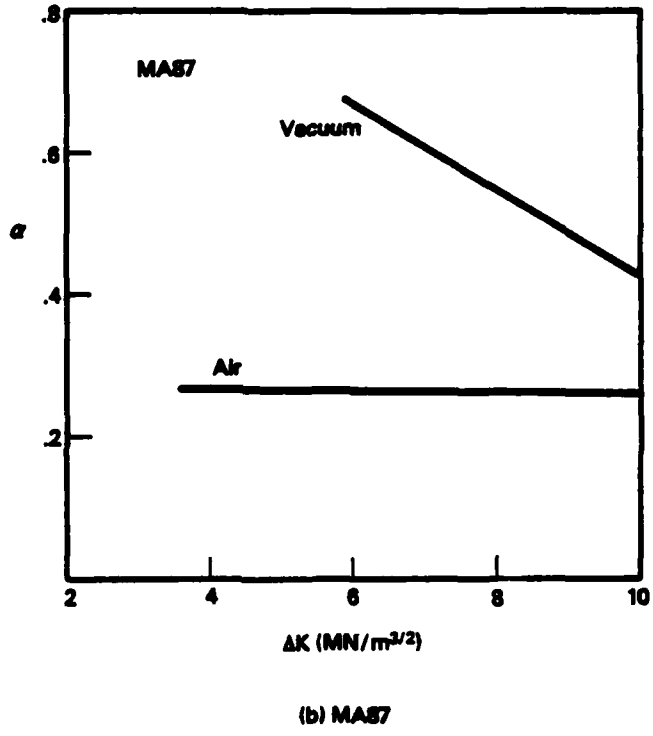

(b) MA87

Figure 21 (continued). α versus ΔK for air and vacuum.

[redacted]

[redacted]

[redacted]

[redacted]

ABSTRACT

Crack opening displacement at distances in the range of from 1 to 30 μm behind the crack tip have been measured in Mode I (parallel to the loading axis) and in Mode II for the ingot alloy 7075-T651 and the similar powder metallurgy aluminum alloy MA-87 using the stereoimaging technique. A substantial Mode II opening was found for both alloys, but for MA-87 the Mode II opening exceeded Mode I at the crack tip. Crack openings were found to be greater in a very dry environment than in moist air.

INTRODUCTION

A crack opens in response to the load applied to the body containing it. The magnitude of the opening depends on the geometric relationship between the body and the crack, the applied load, and the distance from the tip at which the opening is measured. In fatigue, crack tip opening magnitude is thought to be related to the increment of growth; thus, attempts have been made to (1) measure crack tip opening displacement (CTOD), and (2) compute its magnitude. Previously, successful measurements have been made only at higher values of cyclic stress intensity factor (ΔK), where crack growth rates are 0.1 to 1 mm/cycle, because of limited resolution of measurement techniques.[1] This paper reports on direct measurements of crack opening displacements which have been made to within 1 μm of the crack tip of fatigue cracks growing in aluminum alloys in the near-threshold region of cyclic stress intensity factor (ΔK). Crack opening in moist and dry environments was measured both parallel (Mode I) and perpendicular (Mode II) to the loading axis.

MATERIALS AND EXPERIMENTAL METHODS

The measurements reported in this paper were part of a much larger effort to study and quantify fatigue crack growth in 7075-T651, manufactured by conventional ingot metallurgical practice, and in MA-87 (now designated X7091), which was manufactured by powder metallurgy techniques. Both materials were obtained from Alcoa; the MA-87 was part of an experimental heat and was obtained directly from Alcoa Research Laboratory, the

7075-T651 was obtained commercially. More information on the manufacturing technology and metallurgical characterization of these materials may be found in our results of fatigue crack growth in these alloys.[2,3] Likewise, a detailed account of the experimental techniques and procedures may be found in those references; thus, they will only be summarized here.

Fatigue cracks were grown in a single-edge notched specimen with a 21 mm by 3 mm thick gage section in either 1 MPa (10^{-5} torr) vacuum or very dry nitrogen (less than 5 ppm water vapor) and in moist laboratory air, at 1 to 5 Hz. Pin loading of the specimen was used to minimize any effects of grip or fatigue machine misalignment and to assure pure Mode I loading. Specimens were then transferred to a cyclic loading stage which operates within the scanning electron microscope,[4] and photographed at both maximum and minimum load. Displacements were then measured using the stereoimaging technique.[5] The accuracy of these measurements has been estimated at $\pm$ 0.044 mm.[6] For $\Delta K \geq 8$ MN/m$^{3/2}$, photographs were taken at 1000X, and for $\Delta K \leq 8$ MN/m$^{3/2}$ photographs were made at 2000X; therefore, the expected accuracy of the measured displacements is $\pm$ 0.044 μm for $\Delta K \geq 8$ MN/m$^{3/2}$ and $\pm$ 0.022 μm for $\Delta K < 8$ MN/m$^{3/2}$.

RESULTS

Measurements in both the direction of the loading axis (x) and perpendicular to it (y) are required because in all cases, crack opening was observed along both axes. Figures 1 through 4 display the results on linear axes in terms of COD_x and COD_y, for both environments. Although no measurements exist closer to the crack tip than are shown, it is assumed that $COD_x = 0$ at $y = 0$; however, this is not necessarily true for COD_y.

The trends exhibited by the data may be generalized as follows:

1) For 7075-T651, COD_x and COD_y both approach zero as the crack tip is approached. At $-y = 3\,\mu m$, COD_y (Mode II opening) is 20 to 60% of COD_x (Mode I).

2) For MA-87, COD_x (Mode I) is zero at the crack tip, but not COD_y (Mode II), which begins to exceed the magnitude of Mode I at 3 to 6 μm behind the crack tip. Displacements of similar magnitude in the y-direction extend well into the plastic zone ahead of the crack tip.

If COD_x and COD_y are combined as

$$COD = (COD_x^2 + COD_y^2)^{1/2} \tag{1}$$

then these same data for both alloys give the following relation[2,3]

$$COD = C_o|-y|^p \tag{2}$$

Values of C_o and p have been derived and tabulated for both alloys.[2,3] Figure 5 correlates p with ΔK; even though considerable scatter exists, general trends in these data are given by

$$p = p_o + v\Delta K_{eff} \tag{3}$$

The factor C_o correlates with ΔK[2,3]

$$C_o = C\Delta K_{eff}^{q} \qquad (4)$$

Table I tabulates values of the constants in Eqs. (3) and (4) which have been determined by the method of least-squares minimization.

TABLE I

Constants for Eqs. (3) and (4)

	7075-T651		MA-87	
	Dry/Vac	Wet Air	Vac	Wet Air
ΔK_{TH} ($MN/m^{3/2}$)	0	0	3.5	1.7
p_o	0.994	0.364	0.362	0.037
v	-4.9×10^{-2}	$+3.36\times10^{-2}$	-9.4×10^{-3}	2.71×10^{-2}
C	1.4×10^{-10}	4×10^{-9}	2.6×10^{-7}	3.8×10^{-7}
q	3.6	1.4	0.94	0.476

Although loading was macroscopically in pure Mode I, microscopic deviation of the crack path from a direction perpendicular to the loading direction might cause a significant magnitude of Mode II opening. Accordingly, the deviation of the crack path was measured for all the cases analyzed, and was found to average 25° for both alloys. Since there is no difference between the degree of deviation between the two alloys, it is not reasonable to attribute the large difference in degree of Mode II to this factor.

DISCUSSION

The large component of Mode II opening (COD_y) evident from these results is surprising, in that there is no theoretical continuum mechanics treatment which predicts this phenomenon. This suggests that the presence of Mode II crack opening is due to the influence of metallurgical factors on crack opening. If this concept is correct, it is possible to rationalize crack opening differences between these two microstructurally dissimilar aluminum alloys. There are two principal differences: (1) for 7075-T651 COD_y approaches zero at the crack tip, while for MA-87, COD_y remains approximately constant along the crack flank, so that at the crack tip there is still a large component of Mode II; (2) the magnitude of crack opening for MA-87 exceeds that for 7075-T651, at distances greater than 2 μm from the crack tip. How microstructure might cause such differences is not clear. The macroscopic yield stress and work hardening characteristics of both materials are similar, even though the grain size of MA-87 is 5-10 μm, as compared to 100-200 μm for 7075-T651. The principal difference in the alloys is in the composition, size, and distribution of the dispersoids, and since dispersoids affect slip, the alloys may have different slip characteristics, which could contribute to the differences in opening mode magnitude and mix in a not yet understood way. Differences in texture between the two materials may also be important.

The measurements presented here are the only known crack opening values which have been made for both Modes I and II, and the only data known closer than 200 μm to the crack tip. Thus, comparison with other experiments is not possible.

The theoretical and numerical treatment by Dean and Hutchinson[7] for cracks in a work hardening material should provide results comparable with the present measurements. By choosing a work hardening coefficient of N = 10 (their notation), the cyclic hardening characteristics of these aluminum alloys are approximated. The comparable COD values thus computed are shown on Figures 1-3 for ΔK = 6, 8 and 10 $MN/m^{3/2}$. The comparison with measured results is good for ΔK = 6 $MN/m^{3/2}$, for both alloys, but not nearly so good for ΔK = 8 and 10 $MN/m^{3/2}$. The reasons for the degree of agreement are not apparent. Analysis of the crack flank opening slope, the coefficient p in Eq. (2), may provide one clue, in that a value of p = 0.74 is predicted from the analysis of Dean and Hutchinson, and only at lower ΔK does this agree with measured values. However, this line of reasoning would lead to the expectation of better agreement at ΔK = 8 $MN/m^{3/2}$ than was achieved.

The effect of environment on the two materials is similar: The Mode I opening (COD_x) is larger in the dry environment than for wet air. This trend is most apparent for MA-87. Also, CTOD is larger for MA-87 than for 7075-T651, at the same ΔK. Another similarity is the effect of environment on p, the coefficient in Eq. (2). In both cases, p increases as ΔK increases in wet air, which is opposite of the effect in the dry environment. For 7075-T651, this means that the slope of the crack opening approaches that of an elastic crack (p = 0.5) at low ΔK in wet air, while for MA-87 p is less than half the elastic value, a curious result. The

lowering of COD and p by the wet air environment are manifestations of the embrittling effect of water vapor on the near crack tip material for these alloys, and agrees with crack tip strain measurements[2,3] and fractography.[8]

Measurement of COD_x at distances greater than 200 μm from the crack tip indicates that p should approach 0.5, the value for an elastic crack, and the data in Figures 1-4 indicate that the COD_y has decreased to a small value, or has stopped increasing, so that at large distances behind the crack tip, the magnitude of the Mode II opening is a negligible fraction of the COD. Therefore, continuum mechanics describes this portion of the crack adequately.

What the presence of a Mode II component means to fatigue crack growth is not entirely clear, but there are two effects which are immediately apparent:

1) Mode II component of opening at the crack tip increases the magnitude of the shear strain in the material immediately ahead of the tip, and since crystalline solids fail largely in shear, Mode II enhances the failure of the material at the crack tip.
2) A Mode II component results in rubbing between the two fracture surfaces.

The magnitude of shear strain at the crack tip has been measured for MA-87[3] and found to be larger than for 7075-T651,[2] which agrees with (1). Fracture surface rubbing is apparent in the fractography of MA-87,[9] where

there is considerable evidence of wear and fretting. The heat treatment of this material corresponds to an overaged (T7) condition, which is known to readily form thick oxides on the fracture surface, relative to the peak-aged (-T6) condition.[10] The Mode II component of opening causes so much rubbing that the growth of cracks in air results in debris being extruded out of the crack, Figure 6. This sliding and increased debris formation probably acts to wedge the crack somewhat, and decreases the crack growth rate by decreasing the range of strain at the crack tip. Lower crack tip strains have, in fact, been measured for MA-87 in air as compared to vacuum.[3]

CONCLUSIONS

1. Crack opening has been measured and found to be a combination of both Mode I and Mode II for the aluminum alloys 7075-T651 and MA-87.
2. The relative magnitudes of opening mode are dependent upon both material and environment, with MA-87 exhibiting the largest amount of Mode II at the crack tip.
3. Mode I opening is larger for both alloys in the dry environment than for wet air, and neither are in agreement with analytical results.

ACKNOWLEDGEMENT

This work was sponsored by The Office of Naval Research, Contract Number N00014-75-C-1038. The authors appreciate the encouragement of Dr. P. A. Clarkin, contract monitor.

REFERENCES

1. H. W. Liu and J. S. Ke 'Moire Method' in "Experimental Techniques in Fracture Mechanics, 2" A. S. Kobayashi, ed., Iowa State Univ. Press, 1975, pp. 111-165.
2. D. L. Davidson and J. Lankford "The Effect of Water Vapor on Fatigue Crack Tip Mechanics in 7075-T651 Aluminum Alloy" Fatigue of Engng. Mater. and Struct. (in review 11/82).
3. D. L. Davidson and J. Lankford "Fatigue Crack Tip Mechanics of a Powder Metallurgy Aluminum Alloy in Vacuum and Humid Air" Fatigue of Engng. Mater. and Struct. (in review 11/82).
4. D. L. Davidson and A. Nagy, J. Phys. E. 1978, Vol. 11, pp. 207-210.
5. D. L. Davidson, Scanning Electron Microscopy/1979/II, pp. 79-86.
6. D. R. Williams, D. L. Davidson and J. Lankford, Exper. Mech. 1980, Vol. 20, pp. 134-139.
7. R. H. Dean and J. W. Hutchinson, Fracture Mechanics: Twelfth Conference, ASTM STP-700, pp. 383-405, Amer. Soc. Testing, Mater., Philadelphia, 1980.
8. J. Lankford and D. L. Davidson "Fatigue Crack Micromechanics in Ingot and Powder Metallurgy 7XXX Aluminum Alloys in Air and Vacuum," Acta Met. (in review 11/82).
9. J. Lankford and D. L. Davidson "Spherical Wear Debris Formed During Nominal Mode I Fatigue Crack Growth" Mater. Science and Engng. (submitted 11/82).
10. A. K. Vasudevan and S. Suresh "Influence of Corrosion Deposits on Near-Threshold Fatigue Crack Growth Behavior in 2XXX and 7XXX Series Aluminum Alloys" Met. Trans. A (submitted 9/82).

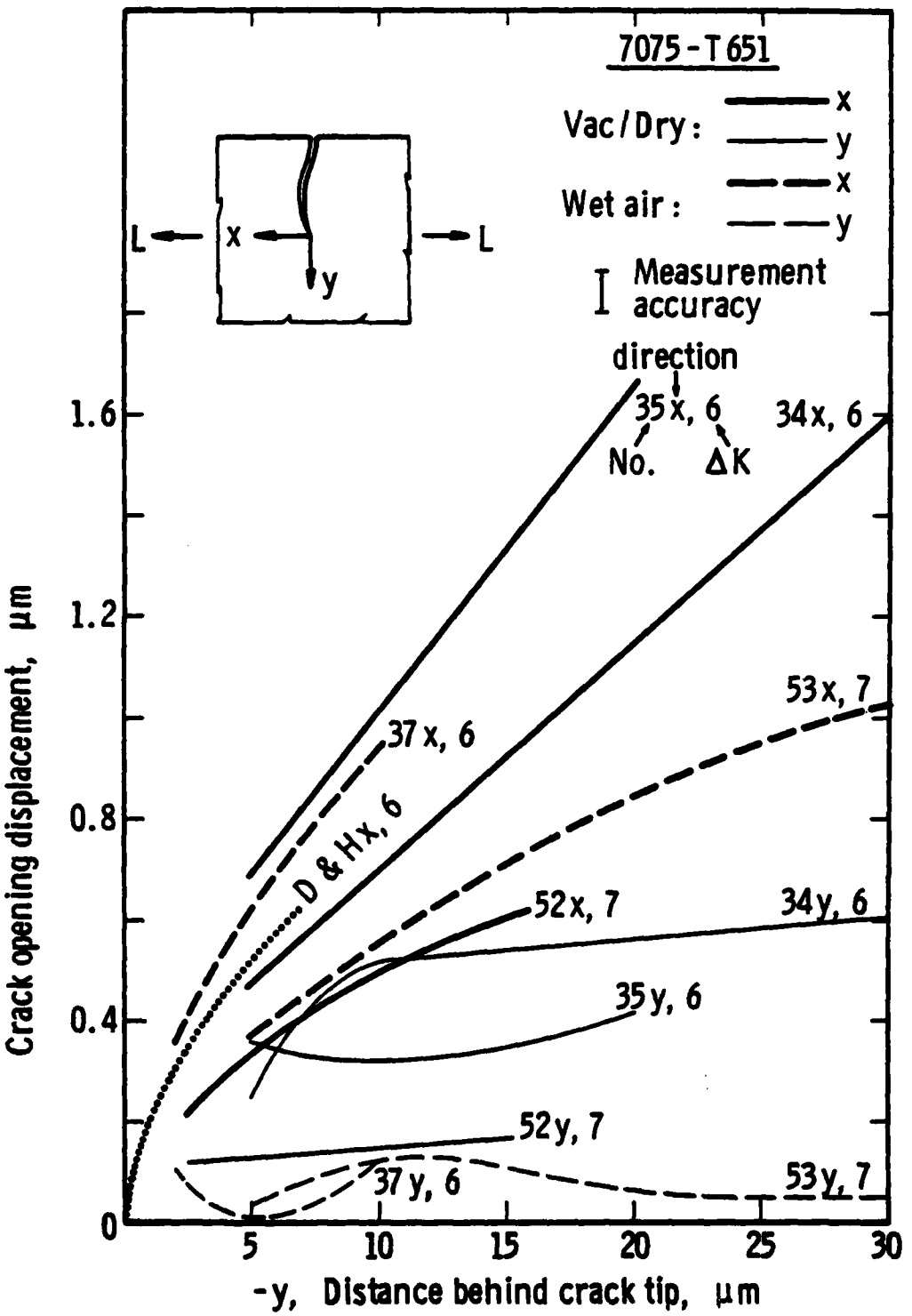

Figure 1. Crack opening measurements for $\Delta K = 6$ and 7 $MN/m^{3/2}$. The computed crack opening, COD_x, from Dean and Hutchinson[7] is shown as D & H. Measurement accuracy is determined from the accuracy of the stereoimaging measurement technique.

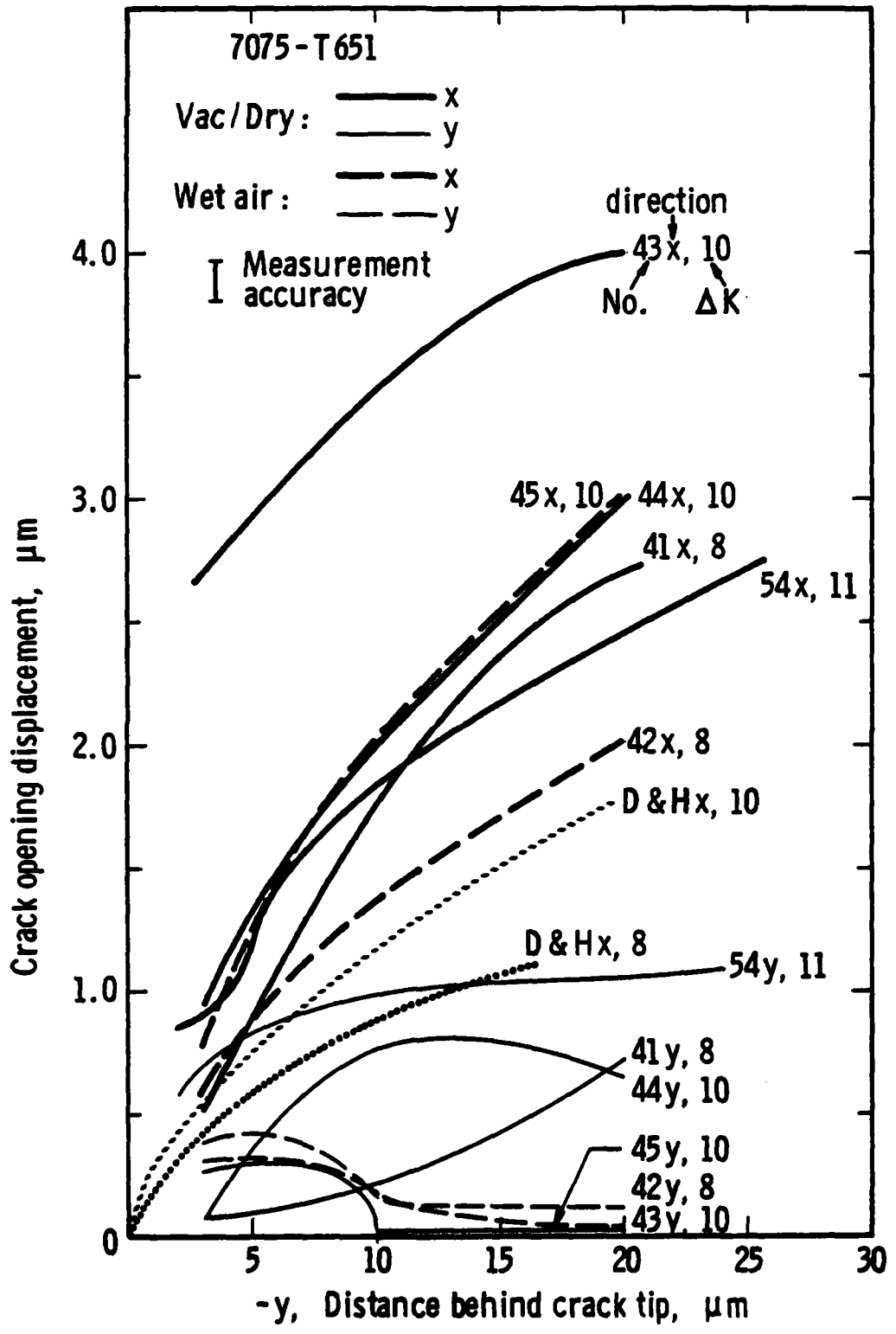

Figure 2. Crack opening measurements for $\Delta K \geq 8$ MN/m$^{3/2}$. Computed COD_x from Dean and Hutchinson[7] is shown as D & H.

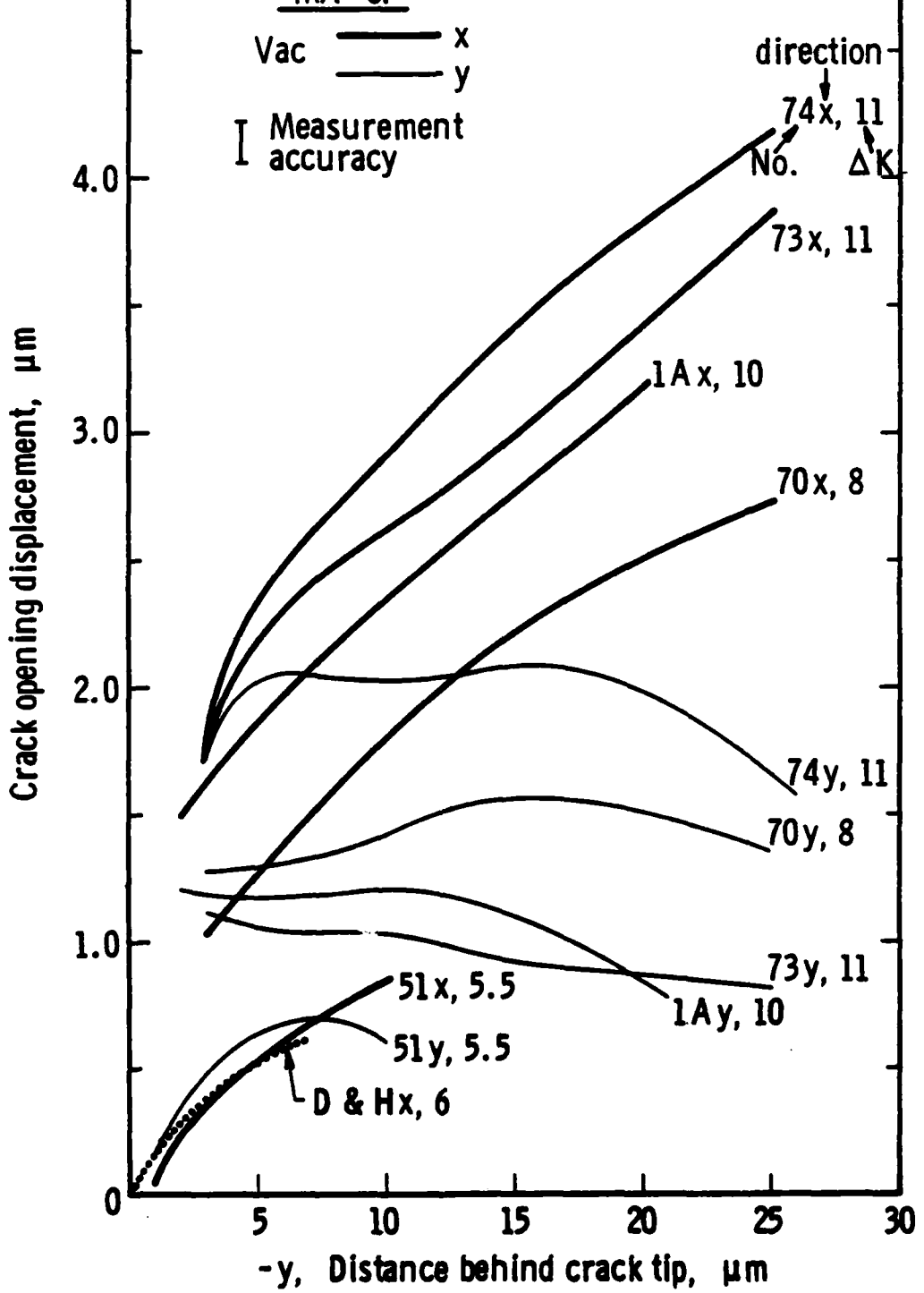

Figure 3. Crack opening measurements for the vacuum environment. Computed COD_X from Dean and Hutchinson[7] is shown as D & H.

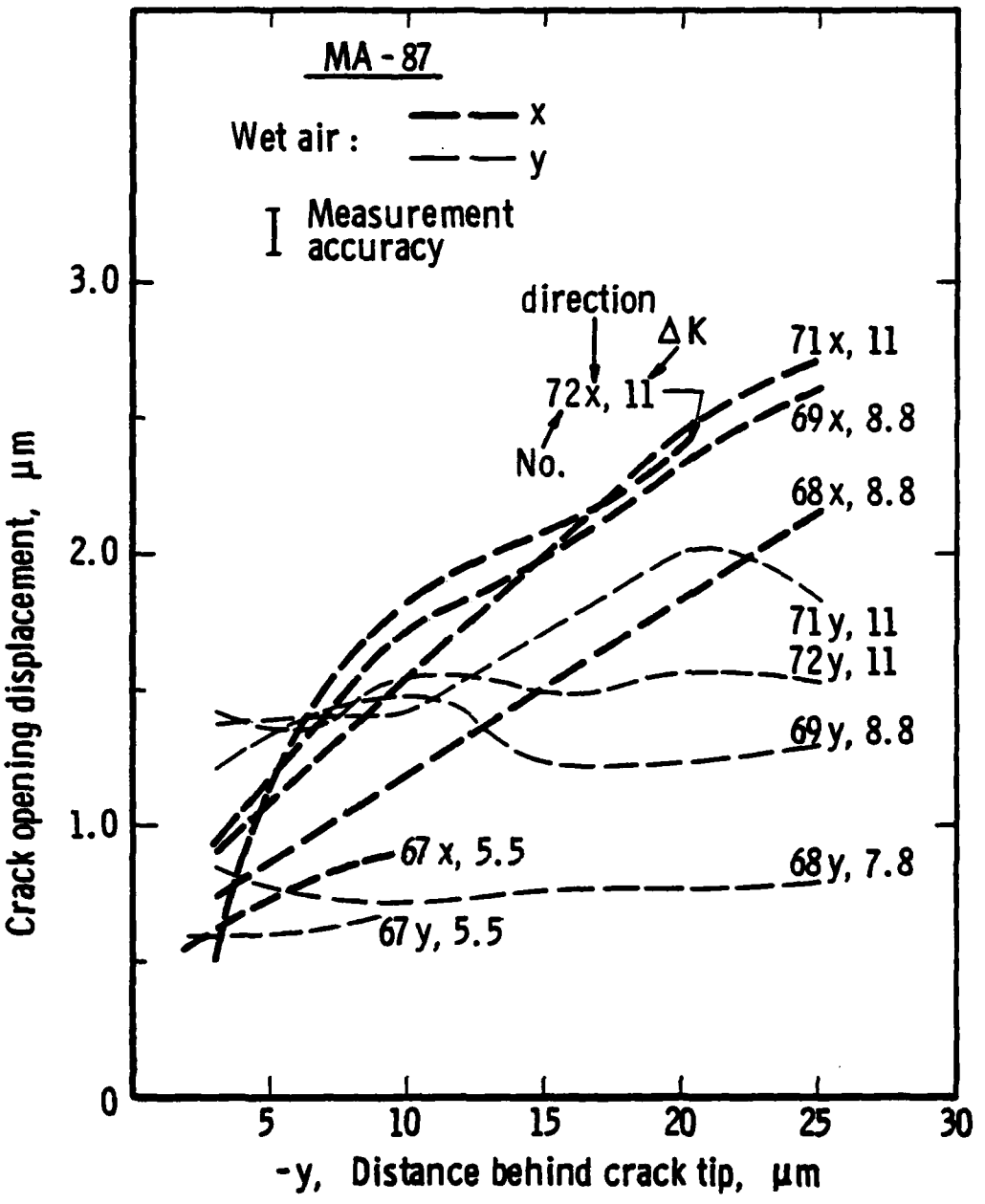

Figure 4. Crack opening measurements for the wet air environment.

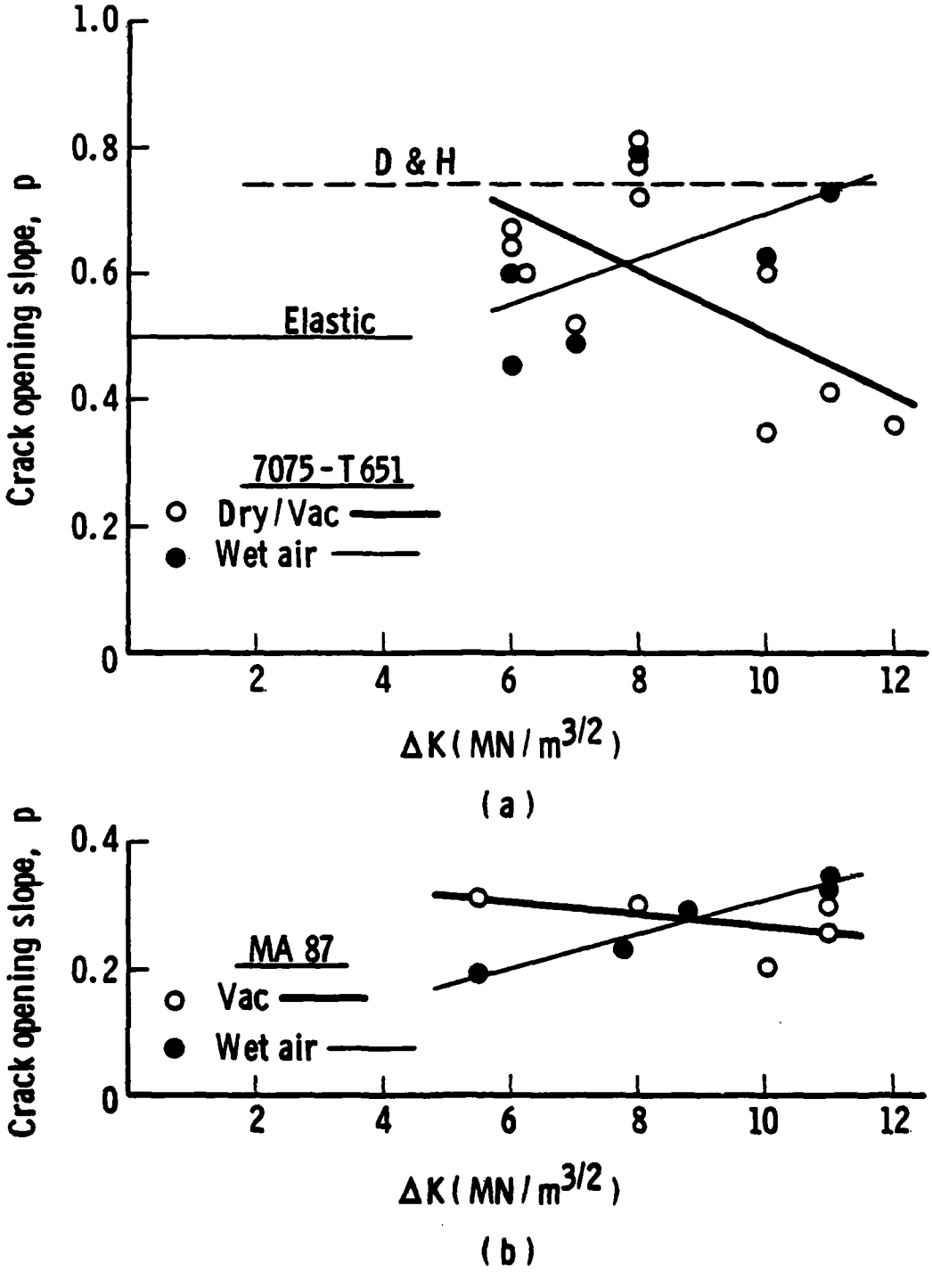

Figure 5. Variations of the coefficient p in Eq. (2) with ΔK. The value derived from Dean and Hutchinson[7] is shown as D & H.

UNCLASSIFIED

SECURITY CLASSIFICATION OF THIS PAGE (When Data Entered)

REPORT DOCUMENTATION PAGE		READ INSTRUCTIONS BEFORE COMPLETING FORM
1. REPORT NUMBER	2. GOVT ACCESSION NO. AD-A122 960	3. RECIPIENT'S CATALOG NUMBER
4. TITLE (and Subtitle) CRACK TIP PLASTICITY ASSOCIATED WITH CORROSION ASSISTED FATIGUE		5. TYPE OF REPORT & PERIOD COVERED Interim Report June 1981 - September 1982
		6. PERFORMING ORG. REPORT NUMBER 06-4268
7. AUTHOR(s) D. L. Davidson J. Lankford		8. CONTRACT OR GRANT NUMBER(s) N00014-75-C-1038
9. PERFORMING ORGANIZATION NAME AND ADDRESS Southwest Research Institute P. O. Drawer 28510 San Antonio, TX 78284		10. PROGRAM ELEMENT, PROJECT, TASK AREA & WORK UNIT NUMBERS NR 036-109/2-25/76(471)
11. CONTROLLING OFFICE NAME AND ADDRESS Office of Naval Research 800 North Quincy Street Arlington, VA 22217		12. REPORT DATE November 15, 1982
		13. NUMBER OF PAGES 141 + prelims.
14. MONITORING AGENCY NAME & ADDRESS(if different from Controlling Office)		15. SECURITY CLASS. (of this report) UNCLASSIFIED
		15a. DECLASSIFICATION/DOWNGRADING SCHEDULE

16. DISTRIBUTION STATEMENT (of this Report)

Reproduction in whole or in part is permitted for any purpose of the United States Government. Distribution is unlimited.

17. DISTRIBUTION STATEMENT (of the abstract entered in Block 20, if different from Report)

18. SUPPLEMENTARY NOTES

19. KEY WORDS (Continue on reverse side if necessary and identify by block number)

Corrosion fatigue
Crack tip plasticity
Fatigue-environment interaction
Fractography
Fatigue crack propagation
Crack tip strains
Aluminum alloys
Crack opening displacement

20. ABSTRACT (Continue on reverse side if necessary and identify by block number)

Crack tip opening displacements and strains have been measured for fatigue cracks grown in water vapor and very dry or vacuum environments in ingot formed 7075-T651 and powder metallurgy formed MA-87 (now X7091). Detailed analysis of the effect of environment on the crack tip parameters in each alloy has been performed. Dynamic observations of crack growth and an extensive fractographic study have been made. Models are presented which utilize the data derived from both static and dynamic analysis.

DD FORM JAN 73 1473 EDITION OF 1 NOV 65 IS OBSOLETE

UNCLASSIFIED

SECURITY CLASSIFICATION OF THIS PAGE (When Data Entered)

This report is in the form of four manuscripts which have been submitted to various journals for publication:

1. The Effect of Water Vapor on Fatigue Crack Tip Mechanics in 7075-T651 Aluminum Alloy

2. Fatigue Crack Tip Mechanics of a Powder Metallurgy Aluminum Alloy in Vacuum and Humid Air

3. Fatigue Crack Micromechanisms in Ingot and Powder Metallurgy 7XXX Aluminum Alloys in Air and Vacuum

4. Mixed Mode Crack Opening in Fatigue

Data in the manuscripts are supplemented by appendices.

Water vapor is found to have a considerable effect on crack tip parameters and on fractographic features for both alloys. Crack opening displacement is found to be mixed mode, with the magnitude being sensitive to both alloy and environment.